ITBS 2007

4th International Conference on

Imaging Technologies in Biomedical Sciences

From Medical Images to Clinical Information
Bridging the Gap

22 - 28 September 2007

Milos Conference Center *George Eliopoulos*
Milos Island, Greece

Pre-Conference Workshop on Brain Imaging
22nd September 2007
University Mental Health Research Institute (UMHRI, Athens)

Book of Abstracts

Sponsored by
S&B Industrial Minerals S.A. and the Greek Ministry of National Education and Religious Affairs

ITBS07 PROGRAM

Athens, 22 September, 2007
&
George Eliopoulos Conference Centre
Milos Island, Greece
23-28 September, 2007

	Sat 22-SEP	Sun 23-SEP	Mon 24-SEP	Tue 25-SEP	Wed 26-SEP	Thu 27-SEP	Fri 28-SEP
09:00 - 10:30	"Brain Imaging" Workshop in Athens		Session I Clinical Imaging	Session III Small Animal Imaging	Session V Clinical Imaging	Session VI Multimodalities, Image Reconstruction & Visualization	Session IX Radiotherapy, Dosimetry
	Coffee Break		Coffee Break	Coffee Break	Coffee Break	Coffee Break	Coffee Break
11:00 - 13:00	"Brain Imaging" Workshop in Athens		Clinical Imaging	Small Animal Imaging	Clinical Imaging	Multimodalities, Image Reconstruction & Visualization	Brain Perfusion **CLOSING**
16:30 - 19:30	**Afternoon Free**	**Registration & Welcome Reception**	Session II Development in Imaging Technologies	Session IV **POSTER Session**	**EXCURSION**	Session VII Simulation Techniques Session VIII Invited Speakers from Industry	
						BANQUET	

Workshop in Athens: **"Brain Imaging"** (Conveners: C. Stefanis, A. Georgopoulos)

	Saturday, 22nd September 2007
	Co-Chairmen : **Prof. Costas Stefanis,** University Mental Health Research Institute (UMHRI), Athens **Prof. Apostolos Georgopoulos,** Brain Sciences Center, Univ. of Minnesota, USA
08:30-09:00	**Registration**
	Session I
09:00-09:15	Welcome **Prof. Costas Stefanis,** University Mental Health Research Institute (UMHRI), Athens **Prof. Costas Papanicolas,** Institute of Accelerating Systems & Applications (IASA), Athens
09:15-10:00	**Prof. Kamil Ugurbil,** Center for Magnetic Resonance Research, Univ. of Minnesota, USA *"Advances in High Field Imaging of the Brain; New Frontiers at 7 and 9.4T Human Brain Imaging"*
10:00-10:15	Discussion
10:30-11:00	**Coffee Break**
11:00-11:45	**Prof. Christer Halldin,** Karolinska Intituet, SE *"PET in Neuroscience and Drug Development"*
11:45-12:00	Discussion
12:00-12:45	**Prof. Apostolos Georgopoulos,** Brain Sciences Center, Univ. of Minnesota, USA *"Multidisciplinary Studies of Brain Function"*
12:45-13:00	Discussion
	Session II Chairman : Prof. Costas Stefanis
13:00-13:45	**Round Table Discussion**

Registration & Welcome Reception

Sunday, 23 September 2007 (afternoon)
17:30-19:30 *George Eliopoulos* Conference Center, Milos Island

Session I: Clinical Imaging

Monday, 24 September 2007 (morning)

Time	Speaker	Title
09:00-09:15	E. Stiliaris (UoA & IASA)	WELCOME
09:15-10:00	M. Hofmann (Bern)	Opening Talk
10:00-10:45	A. Todd-Pokropek (UCL)	From Nuclear Medicine to Molecular Imaging
10:45-11:15	Coffee Break	
11:15-11:35	C. Houzard	Influence of Tumor Mean Atomic Number and Density on CT Attenuation Corrected PET: Phantom Studies.
11:35-11:55	J. Carney	Post-Injection Transmission Imaging for Attenuation Correction on a MicroPET Scanner.
11:55-12:15	C. Houzard	Feasibility of Iodine Contrast Enhanced CT-Scan during a 18F-Fluorodeoxyglucose (18FDG) Positron Emission Tomography (PET-CT) Study.
12:15-12:35	C. Maintas	The Metabolic Activity of High Density Tissue in PET is Influenced by CT Attenuation Correction? A Phantom Simulation Study.
12:35-12:55	F. Kalantari	Scatter Correction in SPECT Imaging of Heart Using Deconvolution Method: A Simulation Study.
12:55-13:15	H. Taleshi Ahangari	A New Method for Attenuation Correction in SPECT Using Dual Energy Acquisition.

Session II: Development in Imaging Technologies

Monday, 24 September 2007 (afternoon)

Time	Speaker	Title
16:30-17:00	B. Knoop (Hannover)	*Quo Vadis* Quantitative PET/CT?
17:00-17:20	A. Kerek	Ectomography – Tomographic Technique for Mobile Imaging System.
17:20-17:40	T. Weitzel	Impact of Statistical Region Growing on the Recovery of Standard Uptake Values (SUV) for Small Lesions by using Fourier-Transform-Interpolation, Deconvolution and Statistical Region Growing ("FIDES") to determine SUV.
17:40-18:00	I. Kantemiris	On the Feasibility of Real Time Imaging in Radiotherapy Using Antiproton Beams.
18:00-18:20	J. Verhaeghe	Use of a Stereo-Vision System for Head Motion Correction for PET Acquisitions.

18:20-18:40	K. Karathanasis	A FEM Simulation Study of the Optimization of the Imaging Attributes of a Microwave Radiometry System with Possible Functional Imaging Capabilities.
18:40-19:00	A. Oikonomou	Potential Brain Imaging Using Near Field Radiometry.
19:00-19:20	M. Giamalaki	Focused Microwave Radiometry from a Possible Functional Imaging Perspective: Theoretical Optimization of the Properties of a Microwave Radiometry System.
19:20-19:40	M. Ozdemir	Quantitative Proton Magnetic Resonance Spectroscopy without Water Suppression.

Back

Session III: Small Animal Imaging
Tuesday, 25 September 2007 (morning)

Time	Speaker	Title
09:00-09:30	Alain Le Pape (Orleans)	Potential and Limits of Small Animal Imaging for the Translational Approach in Biomedical Research and Drug Discovery
09:30-09:50	Y. Tekabe	Imaging Atherosclerotic Plaque Biology using Radionuclides.
09:50-10:10	A. Munar	Firsts Results of a New High Resolution PET System for Small Animals using Large Continuous Scintillating Crystals.
10:10-10:30	D. Thanasas	A Correction Method of the Spatial Distortion in Planar Images from Gamma Camera Systems.
10:30-11:00	Coffee Break	
11:00-11:20	F. Cassol Brunner	Simulation of PIXSCAN, a photon counting micro-CT for small animal imaging.
11:20-11:40	A. Bonissent	A Calibration Method for the PIXSCAN Small Animal X-ray CT Scanner.
11:40-12:00	Zhou Rong	Calibration of Pinhole MicroSPECT Using a Single Point Source.
12:00-12:20	Ing-Tsung Hsiao	Fast Iterative Reconstructions: Simulation and Application for Animal CT.

Session IV: POSTER Session
Tuesday, 25 September 2007 (afternoon)

Back

Session V: Clinical Imaging

Wednesday, 26 September 2007 (morning)

Time	Speaker	Title
09:00-09:45	C. Degenhard (Philips)	Time-of-Flight PET: Technical Challenge and Clinical Impact
09:45-10:05	N. Arikidis	Integrating Multiscale Active Contours and Region Growing for Microcalcifications Segmentation in Mammography.
10:05-10:25	E. Kokkinou	Monitoring of Bone Regeneration Process by means of Texture Analysis.
10:25-10:45	F. Kalantari	Energy Window Setting for Optimum Tl-201 Heart Imaging.
10:45-11:15	Coffee Break	
11:15-12:00	A. Hengerer (Siemens)	PET/MRI Molecular Imaging of the Future
12:00-12:20	F. Kalantari	Compensation of Cross-contamination in Simultaneous ^{201}Tl/^{99m}Tc Myocardial Perfusion SPECT Imaging.
12:20-12:40	I. Boniatis	Grading and Quantification of Hip Osteoarthritis Severity by Analyzing the Spectral Energy Distribution of Radiographic Hip Joint Space.
12:40-13:00	P. Korfiatis	Exploiting Unsupervised and Supervised Classification for Segmentation of the Pathological Lung in CT.

Back

Session VI: Multimodalities, Image Reconstruction and Visualization

Thursday, 27 September 2007 (morning)

Time	Speaker	Title
09:00-09:30	TBC	PET/MRI Animal and Human
09:30-09:50	M. Goris	Analytical Fusion of Different Modality Images based on Prior Knowledge.
09:50-10:10	E. Rault	Improving the Reconstruction of Yttrium-90 Bremsstrahlung Images using Monte Carlo based Reconstruction.
10:10-10:30	V. Pedash	Sinogram Correction Technique for Non-Parallel Projection SPECT Imaging.
10:30-11:00	Coffee Break	
11:00-11:20	T. Weitzel	Contrast Improvement of Anatomical and Metabolic Features in PET Imaging by using Principal Component Analysis of Dynamic PET Data to Generate Multimodal Images.
11:20-11:40	G. Kagadis	An Automated Methodology for the Segmentation of *in vivo* Acquired DSA Images: Application in the New Zealand Hindlimb Ischemia Model.
11:40-12:00	S. Michopoulou	Computer Assisted Characterization of Cervical Intervertebral Disc Degeneration in MRI.

Session VII: Simulation Techniques

Thursday, 27 September 2007 (afternoon)

Time	Speaker	Title
16:30-16:50	R. Van Holen	Reducing High Energy Contamination in SPECT using a Rotating Slat Collimator.
16:50-17:10	K. Gorji	Reducing of the Respiratory Motion Artifacts in PET Cardiology: A Simulation Study.
17:10-17:30	J. Lagares	The MIRaS (Medical Image Radiotherapy and Simulation) Project.
17:30-17:50	T. Sakellaris	Photon and Primary Electron Arithmetics in Photoconductors for Digital Mammography: Monte Carlo Simulation Studies

Session VIII: Invited Speakers from Industry

Thursday, 27 September 2007 (afternoon)

Time	Speaker	Title
18:00-19:30	M. Bergstroem, M. Lusser, H. Newiger, M. Schmand	**INVITED SPEAKERS from INDUSTRY** **Round Table Discussion**

Back

Session IX: Radiotherapy, Dosimetry, Brain Perfusion

Friday, 28 September 2007 (morning)

Time	Speaker	Title
09:00-09:30	Boen L. Kam (Erasmus MC)	Radiopeptide Therapy
09:30-09:50	P. Bouziotis	Labelling of Bevacizumab with Technetium-99m: Initial *in vitro* and *in vivo* Studies.
09:50-10:10	A. Moutsatsos	On the Use of High Field Strength and Parallel Imaging Techniques for MRI-based Polymer Gel Dosimetry of Radio-Surgical Beams.
10:10-10:30	Hsiu-Ling Chen	Three-Dimensional Imaging for Dose Distribution and Mapping in Intraoral and Panoramic Radiographies.
10:30-10:50	L. Petrokokkinos	Characterization of a New Polymer Gel for Radiosurgery Dosimetry using Magnetic Resonance Imaging.
10:50-11:20	Coffee Break	
11:20-11:40	P. Georgoulias	Evaluation of Brain Perfusion in Specific Brodmann Areas in Frontotemporal Dementia and Alzheimer Disease using Automated 3-D Voxel based Analysis.
11:40:12:00	Bang-Hung Yang	Changes of Regional Cerebral Flow when Playing a 3D Platform Video Game using Voxel-by-Voxel Analysis.

Closing Talk

Time	Speaker	Title
12:15-13:00	R. Itti (Lyon)	Closing Talk
13:00-13:30		Closing

Back

Version 1.08 (updated on 20-SEP-2007, 13:00 EEST)

ITBS 2007

Index of Abstracts

5	104_Sakellaris	T Sakellaris , G Spyrou , G Tzanakos and G Panayiotakis **Photon and primary electron arithmetics in photoconductors for digital mammography: Monte Carlo simulation studies**	Taxiarchis Sakellaris University of Patras, School of Medicine, Department of Medical Physics, 265 00 Patras, Greece msakellar@gmail.com	**ORAL** **S_VII**
7	105_Koutalonis	M. Koutalonis, H. Delis, G. Spyrou, L. Costaridou, G. Tzanakos and G. Panayiotakis **Monte Carlo simulation studies of spatial resolution in magnification mammography using the edge method**	Manthos Koutalonis University of Patras, Department of Medical Physics, 265 00 Patras, Greece mkoutalonis@med.upatras.gr	**POSTER**
8	106_Yeh	Mai-Yu Yeh, Tsong-Hai Lee, Tzuu-Kang Chyi, Ho-Ling Liu **Automated detection of arterial input function in DSC perfusion MRI in a stroke rat model**	Mai-Yu Yeh Graduate Institute of Medical Physics and Imaging Science, Chang Gung University, Taoyuan, Taiwan; MRI Center, Chang Gung Memorial Hospital, Taoyuan, Taiwan maiyu730521@mail.cgu.edu.tw	**POSTER**
9	107_Kagadis	George C. Kagadis, Panagiota Spyridonos, Dimitris Karnabatidis, Athanassios Diamantopoulos, Konstantinos Katsanos, Antonis Daskalakis, Nikolaos Samaras, John Maroulis, Efrosini Sourgiadaki, Dionisios Cavouras, Dimitris Siablis, George C. Nikiforidis **An automated methodology for the segmentation of in vivo acquired DSA images: application in the New Zealand hindlimb ischemia model**	George C. Kagadis, PhD School of Medicine, University of Patras, GR 26500 Rion, Greece kagadis@med.upatras.gr	**ORAL** **S_VI**

11	108_Bonissent	R. Khoury, A. Bonissent, JC. Clemens, C. Messeen, E. Vigeolas, M. Billault, C. Morel **A Calibration Method for the PIXSCAN Small Animal X-ray CT Scanner**	Alain Bonissent Centre de Physique des Particules de Marseille (CPPM), IN2P3/CNRS and Université de la Méditerranée Aix-Marseille II, France bonissen@cppm.in2p3.fr	**ORAL** **S_III**
12	109_Korfiatis	P. Korfiatis, C. Kalogeropoulou, D. Daoussis, T. Petsas, A. Antonopoulos, and Lena Costaridou **Exploiting Unsupervised and Supervised Classification for Segmentation of the Pathological Lung in CT**	Panayiotis Korfiatis Department of Medical Physics, School of Medicine, University of Patras, 265 00 Patras, Greece korfp@upatras.gr	**ORAL** **S_V**
13	110_Tekabe	Yared Tekabe, Qing Li, Marija Sedlar, Stan Majewski, Ann Marie Schmidt, Lynne L Johnson **Imaging atherosclerotic plaque biology using radionuclides**	Yared Tekabe Columbia University, New York, NY yt2166@columbia.edu	**ORAL** **S_III**
14	111_Wagenknecht	Gudrun Wagenknecht and Markus Losacker **Combined live wire and active surface approach for volume-of-interest segmentation**	Gudrun Wagenknecht Central Institute for Electronics, Research Center Juelich, D-52425 Juelich, Germany g.wagenknecht@fz-juelich.de	**POSTER**

15	112_Georgoulias	V. Valotassiou, J. Papatriantafyllou, N. Sifakis, P. Georgoulias, C. Karageorgiou, C. Zerva **Evaluation of brain perfusion in specific Brodmann areas in Frontotemporal dementia and Alzheimer disease using automated 3-d voxel based analysis**	Panagiotis Georgoulias, MD, PhD Nuclear Medicine Dpt, University Hospital of Larissa, Larissa, Greece georgoulias@hotmail.com	**ORAL** **S_IX**
16	113_Michopoulou	S. Michopoulou, I. Boniatis, L. Costaridou, D. Cavouras, E. Panagiotopoulos, G. Panayiotakis **COMPUTER ASSISTED CHARACTERIZATION OF CERVICAL INTERVERTEBRAL DISC DEGENERATION IN MRI**	Sofia Michopoulou University of Patras, School of Medicine, Department of Medical Physics, 26500 Patras, Greece smichopoul@upatras.gr	**ORAL** **S_VI**
17	114_Gouzouasis	Ioannis A. Gouzouasis, Irene S. Karanasiou, and Nikolaos K. Uzunoglu **Exploring the enhancement of the imaging properties of a microwave radiometry system for possible functional imaging using a realistic human head model**	Ioannis Gouzouasis National Technical University of Athens, Iroon Polytechniou 9, Zografou Campus, Athens 15773, Greece igouzouasis@esd.ece.ntua.gr	**POSTER**
19	115_Camarda	Manuela Camarda, Nicola Belcari, Alberto Del Guerra, Luigi Spontoni, Sara Vecchio, Paolo Bennati, Maria Nerina Cinti, Roberto Pani, Renato Campanini, Emiro Iampieri, Nico Lanconelli **SPEMT imaging with a dedicated VAoR dual-head camera: preliminary results**	Manuela Camarda Department of Physics "E. Fermi", University of Pisa and INFN branch of Pisa, Italy manuela.camarda@pi.infn.it	**POSTER**

20	116_Boniatis	Boniatis I., Costaridou L., Panagiotopoulos E., and Panayiotakis G. **Grading and Quantification of Hip Osteoarthritis Severity by Analyzing the Spectral Energy Distribution of Radiographic Hip Joint Space**	Ioannis Boniatis University of Patras, School of Medicine, Department of Medical Physics, 265 00 Patras, Greece iboniat@yahoo.com	**ORAL** **S_V**
21	117_Shalchian	B. Shalchian, H. Rajabi, H. Soltanian-zadeh, F. Kalantari **Noise reduction in simulated PET images using wavelet and thresholding method**	Bahareh Shalchian Department of medical physics, medical sciences faculty, Tarbiat Modares University, Tehran, Iran baharehshalchian@gmail.com	**POSTER**
23	118_Kalantari	F.Kalantari, H.Rajabi, N.Yaghoobi **Compensation of cross-contamination in simultaneous ^{201}Tl/^{99m}Tc myocardial perfusion SPECT imaging**	Faraz Kalantari Department of Medical Physics, Tarbiat Modares University, Tehran, Iran faraz241060@yahoo.com	**ORAL** **S_V**
24	119_Kalantari	F.Kalantari, H.Rajabi, N.Yaghoobi, A.Bitarafan, K.E. Gorji, F.Rastgoo, H.Malek, S.H.Firoozabadi **Energy window setting for optimum Tl-201 heart imaging**	Faraz Kalantari Department of Medical Physics, Tarbiat Modares University, Tehran, Iran faraz241060@yahoo.com	**ORAL** **S_V**
25	120_Kalantari	F.Kalantari, H. Rajabi **Scatter Correction in SPECT Imaging of Heart Using Deconvolution Method: a simulation study**	Faraz Kalantari Department of Medical Physics, Tarbiat Modares University, Tehran, Iran faraz241060@yahoo.com	**ORAL** **S_I**

26	121_Taleshi_Ahangari	Hadi Taleshi Ahangari, Hossien Rajabi, Faraz Kalantari **A new method for attenuation correction in SPECT using dual energy acquisition**	Hossien Rajabi Department of Medical Physics, Tarbiat Modares University, Tehran, Iran hrajabi@modares.ac.ir	**ORAL** **S_I**
27	122_Ozdemir	Mahir Sinan Ozdemir, Yves De Deene, Eric Achten, Ignace Lemahieu **A systematic comparison of absolute quantification schemes for proton magnetic resonance spectroscopy in presence of standing waves**	Mahir Ozdemir Department of Electronics and Information Systems, Medical Image and Signal Processing (MEDISIP), Gent University, Sint-Pietersnieuwstraat 41, Gent, Belgium mahir.ozdemir@ugent.be	**POSTER**
29	123_Chen	Chien-chuan Chen, Yau-yau Wai, Ho-ling Liu **MR image quality testing of k-space- and image-based parallel imaging techniques using the ACR phantom**	Chien-chuan Chen Department of Diagnostic Radiology, Chang Gung Memorial Hospital, Taoyuan, Taiwan Department of Medical Imaging and Radiological Sciences, Chang Gung University, Taoyuan, Taiwan andersen.chen@gmail.com	**POSTER**
30	124_Ozdemir	Mahir Sinan Ozdemir, Yves De Deene, Eric Achten, Ignace Lemahieu **Quantitative proton magnetic resonance spectroscopy without water suppression**	Mahir Ozdemir Department of Electronics and Information Systems, Medical Image and Signal Processing (MEDISIP), Gent University, Sint-Pietersnieuwstraat 41, Gent, Belgium mahir.ozdemir@ugent.be	**ORAL** **S_II**

31	125_Karathanasis	K. T. Karathanasis, I. S. Karanasiou and N. K. Uzunoglu **A FEM Simulation study of the optimization of the imaging attributes of a Microwave radiometry system with possible functional imaging capabilities**	Konstantinos Karathanasis National Technical University of Athens, Iroon Polutexneiou 9, Zografou Campus, Athens 15773, Greece kkarathanasis@esd.ece.ntua.gr	**ORAL** **S_II**
33	126_Weber	M. Fulterer, B. Gundlich , P. Musmann, S. Schneider, S. Weber **Investigation on Activity from Outside the Field of View in the ClearPET™ Neuro using Monte Carlo Simulations**	Simone Weber (1) Zentralinstitut für Elektronik, Forschungszentrum Jülich GmbH, D-52425 Jülich, Germany (2) Department of Mathematics and Technology, RheinAhrCampus, 53424 Remagen, Germany (3) Institute of Material Physics, TU Graz, A-8010, Austria s.weber@fz-juelich.de	**POSTER**
34	127_Moutsatsos	A. Moutsatsos, L. Petrokokkinos, I. Kantemiris, O. Benekos, E. Efstathopoulos, P. Papagiannis, V. Spevacek, J. Semnicka, P. Dvorak and I. Seimenis **On the use of high field strength and parallel imaging techniques for MRI-based polymer gel dosimetry of radio-surgical beams**	Argyris Moutsatsos Medical Physics Department, Medical School, University of Athens allright@ath.forthnet.gr	**ORAL** **S_IX**

35	128_Arikidis	Nikolaos Arikidis, Spyros Skiadopoulos, Anna Karahaliou, Eleni Likaki, George Panayiotakis, Lena Costaridou **Integrating multiscale active contours and region growing for microcalcifications segmentation in mammography**	Arikidis Nikolaos Department of Medical Physics, School of Medicine, University of Patras, 265 00 Patras, Greece arikidis@yahoo.com	**ORAL** **S_V**
36	129_Giamalaki	M.I.Giamalaki, I.S.Karanasiou and N.K.Uzunoglu **FOCUSED MICROWAVE RADIOMETRY FROM A POSSIBLE FUNCTIONAL IMAGING PERSPECTIVE: THEORETICAL OPTIMIZATION OF THE PROPERTIES OF A MICROWAVE RADIOMETRY SYSTEM**	Melpomeni I. Giamalaki Microwave and Fiber Optics Laboratory, School of Electrical and Computer Engineering, National Technical University of Athens, Greece melina@esd.ece.ntua.gr	**ORAL** **S_II**
38	130_Delis	H Delis, V Vlachopoulou, G Spyrou, L Costaridou, G Tzanakos and G Panayiotakis **Investigating the dependence of breast calcifications Signal to Noise Ratio on mammographic spectra: Monte Carlo simulation studies**	Harry Delis University of Patras, Faculty of Medicine, Department of Medical Physics, **265 00 Patras, Greece** hdelis@med.upatras.gr	**POSTER**
39	131_Oikonomou	A. Oikonomou, I.S. Karanasiou and N.K. Uzunoglu **Potential brain imaging using near field radiometry**	Athina Oikonomou National Technical University of Athens, 9 Iroon Polytechneiou str, 15773, Zografou, Greece aoikon@esd.ece.ntua.gr	**ORAL** **S_II**

41	132_ Verhaeghe	Jeroen Verhaeghe, Xiaoyan Zhao, Stefaan Vandenberghe, Long Zhang, Steven Staelens, Yves D'Asseler and Ignace Lemahieu **Use of a stereo-vision system for head motion correction for PET acquisitions**	Jeroen Verhaeghe Department of Electronics and Information Systems, MEDISIP, Ghent University-IBBT-IBiTech, B-9000 Ghent Jeroen.Verhaeghe@ugent.be	**ORAL** **S_II**
42	133_Karaiskos	P. Karaiskos, J. Malamitsi, J. Andreou, V. Prassopoulos, B. Valotassiou, F. Laspas, C. Paraskevopoulou, P. Sandilos and M. Torrens **On the accuracy of a mutual information algorithm for PET-MR image registration**	Pantelis Karaiskos, Ph.D. University of Athens, Medical School, Medical Physics Department, Athens, Greece pkaraisk@med.uoa.gr	**POSTER**
43	134_Kantemiris	I. Kantemiris, P. Karaiskos, E. Georgiou, A. Angelopoulos, N. Giokaris **On the feasibility of real time imaging in radiotherapy using antiproton beams**[1]	Ioannis Kantemiris University of Athens, Physics Dpt., Division of Nuclear & El. Particle Physics, Greece ikantem@phys.uoa.gr	**ORAL** **S_II**
44	135_Lo_Meo	S. Lo Meo, N. Lanconelli, F.L. Navarria, R. Pani, A. Perrotta **A comparison between Geant4 and EGSnrc simulation codes for SPET applications**	Sergio Lo Meo Dipartimento di Fisica, Università di Bologna, and INFN Bologna – Italy lanconelli@bo.infn.it	**POSTER**
46	136_Lanconelli	S. Masetti, M. Fiaschetti, M. Mariselli, L. Roma, P.L. Rossi, N. Lanconelli, G. Baldazzi **Preliminary results of a Multi-Energy CT system for small animals**	Nico Lanconelli University of Bologna, Dept. of Physics, 40127 Bologna, Italy lanconelli@bo.infn.it	**POSTER**

48	137_Ching-Han_Hsu	Chih-Chieh Liu, Ching-Han Hsu, Ing-Tsung Hsiao, Kurt M Lin **Effect of Geometric Models of Convergence Rate of Iterative Image Reconstructions**	Ching-Han Hsu Department of Biomedical Engineering and Environmental Sciences, National Tsing Hua University, Taiwan cghsu@mx.nthu.edu.tw	**POSTER**
49	138_Ching-Han_Hsu	Po-Chia Huang, Ching-Han Hsu, Ing-Tsung Hsiao, Kurt M Lin **An Accurate and Efficient System Model of Iterative Image Reconstruction in High-Resolution Pinhole SPECT for Small Animal Research**	Ching-Han Hsu Department of Biomedical Engineering and Environmental Sciences, National Tsing Hua University, Taiwan cghsu@mx.nthu.edu.tw	**POSTER**
50	139_Ing-Tsung_Hsiao	Hsuan-Ming Huang, Ing-Tsung Hsiao **A Fast OS-Type Bayesian Reconstruction with an Edge-Preserving Median Prior**	Ing-Tsung Hsiao University of Missouri-Columbia, Missouri, USA Chang Gung University, Taoyuan, Taiwan ihsiao@mail.cgu.edu.tw	**POSTER**
51	140_Pantelis	Pantelis Evaggelos, Antypas Christos, Petrokokkinos Loukas, Verigos Kosmas, Doukaki Kleanthi, Nikolaos Salvaras and Tzouras Argyris **Image guidance quality assurance of a G4 CyberKnife® robotic stereotactic radiosurgery system**	Evaggelos Pantelis Medical Physics Department, CyberKnife Center, Iatropolis – Magnitiki Tomografia Clinic and Diagnostic center, Athens, Greece vpantelis@phys.uoa.gr	**POSTER**

52	141_Gorji	K. E. Gorji, H. Rajabi, H. Zaidi, E. Hajizadeh **Reducing of the respiratory motion artifacts in PET cardiology: A simulation study**	kourosh gorji Department of Medical Physics, Tarbiat Modares University, Tehran, Iran kourosh_gorji@yahoo.com	**ORAL** **S_VII**
53	142_Ing-Tsung_Hsiao	Hsuan-Ming Huang, Ing-Tsung Hsiao, Meei-Ling Jan **Fast Iterative Reconstructions: Simulation and Application for Animal CT**	Ing-Tsung Hsiao University of Missouri-Columbia, Missouri, USA Chang Gung University, Taoyuan, Taiwan ihsiao@mail.cgu.edu.tw	**ORAL** **S_III**
54	143_Tung-Hsin_Wu	Liang-Kung Chen, Chia-Lin Chen, Jason JS. Lee, Yung-Hui Huang, Kun-Mu Lu, Yeu-Sheng Tyan and Tung-Hsin Wu **Characterization of the univariate and multivariate techniques on the Analysis of Simulated and fMRI Datasets with Visual Task**	Tung-Hsin Wu Department of Medical Imaging and Radiological Sciences, Chung Shan Medical University, Taiwan woodchio@yahoo.com.tw leehomliang@gmail.com	**POSTER**
55	144_HLChen	Hsiu-Ling Chen, Yung-Hui Huang, Tung-Hsin Wu, Shih-Yuan Wang, Ching-Ching Yang, Jason J.S. Lee **Three-dimensional imaging for dose distribution and mapping in intraoral and panoramic radiographies**	Jason JS Lee Dept. of Biomedical Imaging & Radiological Sciences National Yang-Ming University Taipei, Taiwan 112 jslee@ym.edu.tw	**ORAL** **S_IX**

57	145_Tung-Hsin_Wu	Chia-Hao Liang, Jason JS. Lee, and Tung-Hsin Wu **Integration of PET-CT and cone-beam CT for image-guided radiotherapy for high image quality and registration accuracy**	Tung-Hsin Wu Department of Medical Imaging and Radiological Sciences, Chung Shan Medical University woodchio@yahoo.com.tw	**POSTER**
59	146_Kokkinou	Kokkinou E., Boniatis I., Costaridou L., Saridis A., Panagiotopoulos E., Panayiotakis G. **Monitoring of Bone Regeneration Process by means of Texture Analysis**	Evdoxia Kokkinou University of Patras, School of Medicine, Department of Medical Physics, GREECE ekokkin@upatras.gr	**ORAL** **S_V**
60	147_Petrokokkinos	Petrokokkinos Loukas, Kozicki Marek, Pantelis Evaggelos, Seimenis Ioannis, Pantelis Karaiskos, Antypas Christos, Fijuth Jacek, Sakelliou Loukas **Characterization of a new polymer gel for radiosurgery dosimetry using Magnetic Resonance Imaging**	Loukas Petrokokkinos 1. University of Athens, Physics Department, Nuclear and Particle Physics Section, 15771, Athens, Greece lpetrok@phys.uoa.gr	**ORAL** **S_IX**
61	148_Georgiev	V. Georgiev, L. Costaridou and G. Panayiotakis **Visually losless medical image compression threshold based on wavelet activity measures**	Verislav Georgiev Department of Medical Physics, School of Medicine, University of Patras, Patras 26500, Greece verislav@med.upatras.gr	**POSTER**

62	149_Polychronopoulou	A. Polychronopoulou, D. Thanasas, N. Giokaris, A. Karabarbounis, D. Maintas, C.N. Papanicolas and E. Stiliaris **Study of the optical properties of both continuous and pixelated scintillation crystals**	Athanasia Polychronopoulou Physics Department, University of Athens, GREECE n.polychronopoulou@iasa.gr	**POSTER**
63	150_Thanasas	D. Thanasas, A. Polychronopoulou, N. Giokaris, A. Karabarbounis, D. Maintas, C.N. Papanicolas and E. Stiliaris **A Correction Method of the Spatial Distortion in Planar Images from Gamma Camera Systems**	Dimitris Thanasas Physics Department, University of Athens, GREECE dthanas@phys.uoa.gr	**ORAL** **S_III**
64	151_Bouziotis	P. Bouziotis, E. Gourni, A. L. Harris, G. Loudos, N. Sakellios, S. Xanthopoulos, S. Archimandritis, A. D. Varvarigou **Labelling of bevacizumab with Technetium-99m: initial *in vitro* and *in vivo* studies**	Penelope Bouziotis N.C.S.R. "Demokritos", Aghia Paraskevi, Athens, GREECE pennybil@yahoo.gr	**ORAL** **S_IX**
65	152_Van_Holen	Roel Van Holen, Stefaan Vandenberghe, Steven Staelens, Erwann Rault, Jan De Beenhouwer and Ignace Lemahieu **Reducing High Energy Contamination in SPECT using a Rotating Slat Collimator**	Roel Van Holen Ghent University, Department of Electronics and Information Systems, MEDISIP, Ghent, Belgium Roel.VanHolen@UGent.be	**ORAL** **S_VII**
66	153_Pedash	V. Y. Pedash, A. Gektin, A. Dyomin **Synogram correction technique for non-parallel projection SPECT imaging**	Vyacheslav Yu. Pedash Institute for scintillation materials NAS of Ukraine, Kharkov, Ukraine pedash@isma.kharkov.ua	**ORAL** **S_VI**

67	154_Zhou_Rong	Zhou Rong, Ma Tianyu, Liu Yaqiang, Wu Zhaoxia, Wang Shi, Jin Yongjie **Calibration of Pinhole MicroSPECT Using a Single Point Source**	Zhou Rong Department of Engineer Physics, Tsinghua University, Beijing, 100084, China yichangren@gmail.com	**ORAL** **S_III**
69	155_Kerek	I. Valastyán, D. Bone, L-Å Brodin, H. Elmqvist, A. Kerek, J. Molnár, D. Novák, and T. Ribbe **Ectomography – tomographic technique for mobile imaging system**	Andras Kerek Royal Institute of Technology, Stockholm kerek@kth.se	**ORAL** **S_II**
70	156_Kerek	I. Valastyán, D. Bone, A. Kerek J. Molnár, D. Novák **Unified software platform for nuclear medical image representation, visualization and reconstruction**	Andras Kerek Royal Institute of Technology, Stockholm kerek@kth.se	**POSTER**
71	157_Spyropoulou	Spyropoulou V., Kalivas N., Gaitanis A., Michail C., Panayiotakis G., Kandarakis I. **Modeling imaging performance and low contrast detectability in digital mammography**	Ioannis Kandarakis Department of Medical Instruments Technology, Technological Educational Institution of Athens, GREECE kandarakis@teiath.gr	**POSTER**
72	158_Petropoulou	Petropoulou A., Kalivas N., Kandarakis I., Valais I. and Panayiotakis G. **A theoretical model for single-crystal scintillators in the diagnostic energy range**	Ioannis Kandarakis Department of Medical Instruments Technology, Technological Educational Institution of Athens, GREECE kandarakis@teiath.gr	**POSTER**

73	159_Konstantinidis	Konstantinidis A., Liaparinos P., Panayiotakis G., Kandarakis I. **Investigation of two heavy element scintillators by Monte-Carlo methods**	Ioannis Kandarakis Department of Medical Instruments Technology, Technological Educational Institution of Athens, GREECE kandarakis@teiath.gr	**POSTER**
74	160_Valais	Ioannis G. Valais, Christos Michail, Stratos David, Anastasios Konstantinidis, Dionysis Cavouras, Costas D. Nomicos, George S. Panayiotakis and Ioannis S. Kandarakis **Comparative evaluation of scintillators under x-ray imaging conditions**	Ioannis Kandarakis Department of Medical Instruments Technology, Technological Educational Institution of Athens, GREECE kandarakis@teiath.gr	**POSTER**
75	161_Kalivas	Kalivas N, Valais I., Costaridou L, Kandarakis I, Cavouras D, Panayiotakis G **Evaluating optical spectral matching of phosphor-photodetector combinations**	Ioannis Kandarakis Department of Medical Instruments Technology, Technological Educational Institution of Athens, GREECE kandarakis@teiath.gr	**POSTER**
76	162_Spyropoulou	Spyropoulou V., Michail C., Kandarakis I. , Valais I, Dimitropoulos N., Panayiotakis G. **The influence of software filtering in digital mammography image quality**	Ioannis Kandarakis Department of Medical Instruments Technology, Technological Educational Institution of Athens, GREECE kandarakis@teiath.gr	**POSTER**
77	163_Kun-Ju_Lin	Lin, Kun-Ju; Hsiao, Ing-Tsung, Hong, Ji Hong; Lin Chung-Fu, Wey, Shiaw-Pyng **Optimize ^{18}F-FDG Positive Tumor Volume Delineation in microPET – correlate with autoradiography and histopathology results.**	Kun-Ju Lin Department of Nuclear Medicine, Chang Gung Memorial Hospital Taiwan lin4857@adm.cgmh.org.tw	**POSTER**

79	164_Costaridou	KARAHALIOU A., VASSIOU K., SKIADOPOULOS S., KANAVOU D., YIAKOYMELOS A., COSTARIDOU L. **QUANTIFYING HETEROGENEITY OF LESION UPTAKE IN DYNAMIC CONTRAST ENHANCED MRI FOR BREAST CANCER DIAGNOSIS**	Lena Costaridou Department of Medical Physics, School of Medicine, University of Patras, 26500 Patras, Greece costarid@upatras.gr skiado@med.upatras.gr	**POSTER**
80	165_Meei-Ling_Jan	Meei-Ling Jan , Yu-Ching Ni, Chen-Yu Liu, Zhi-Kun Lin, Mei-Hsiu Liau, T. Yamashita, Norihisa Tsurumi, Sammy Chen, Lie-Hang Shen **Tumor-bearing mice imaging by using a high-throughput positron imager system with planar tomography reconstruction**	Meei-Ling Jan Institute of Nuclear Energy Research, Longtan 325, Taiwan, ROC mljan@iner.gov.tw	**POSTER**
82	166_Bang-Hung_Yang	Bang-Hung Yang, Yuan-Hwa Chou, Jyh-Cheng Chen,Tung-Ping Su, Shyh-Jen Wang **Changes of regional cerebral flow when playing a 3D platform video game using voxel-by-voxel analysis**	Bang-Hung Yang Department of Nuclear Medicine, Taipei Veterans General Hospital, Taiwan bhyang@vghtpe.gov.tw	**ORAL** **S_IX**
83	167_Liang	H. C. Liang, M. L. Jan, W. C. Lin, S. F. Yu, J. L. Su, L. H. Shen **Development of an LYSO Based Gamma Camera for Positron and Scinti-mammography**	Meei-Ling Jan Institute of Nuclear Energy Research, Longtan 325, Taiwan, ROC mljan@iner.gov.tw	**POSTER**
85	168_Fang	U.T. Fang, M.L. Jan, C.H. Yeh, H.C. Lu, H.T. Tsai, L.T. Huang, L.H. Shen **A Quantitative Method for Monitoring Pulmonary Fibrosis Rats by Micro-CT 3D Images**	Meei-Ling Jan Institute of Nuclear Energy Research, Longtan 325, Taiwan, ROC mljan@iner.gov.tw	**POSTER**

87	169_ErwannRault	Erwann Rault, Stefaan Vandenberghe, Steven Staelens, and Ignace Lemahieu **Improving the reconstruction of Yttrium-90 Bremsstrahlung images using Monte Carlo based reconstruction**	Erwann Rault ELIS department, MEDISIP, Ghent University, Belgium erwann.rault@ugent.be	**ORAL** **S_VI**
89	170_Tseng	Fan-Pin Tseng, Meei-Ling Jan, Yu-Ting Fang, Zhi-Kun Lin, Lie-Hang Shen **Improvement of quantitative micro-PET images of the rat brains using 3D deconvolution methods**	Meei-Ling Jan Institute of Nuclear Energy Research, Longtan 325, Taiwan, ROC mljan@iner.gov.tw	**POSTER**
91	171_Carney	Jonathan P. J. Carney and Brian J. Lopresti **POST-INJECTION TRANSMISSION IMAGING FOR ATTENUATION CORRECTION ON A MICROPET SCANNER**	Jonathan Carney P.E.T. Facility, Department of Radiology, University of Pittsburgh, Pittsburgh, Pennsylvania 15260, U.S.A carneyjp@upmc.edu	**ORAL** **S_I**
92	172_Munar	J.M. Benlloch, V. Carrilero, J.V. Catret, R. Colom, C. Correcher, M. Delgado, E. Gorospe, R. Gadea, A.J. González, V. Herrero, Ch. Lerche, C. Mora, F.J. Mora, C. Morera, A. Munar, A. Orero, N. Pavón, M.A. Pozo, A. Ros, F. Sánchez, A. Sebastià, A. Soriano, L. Urrutia, L.F. Vidal **Firsts Results of a New High Resolution PET System for Small Animals using large continuous Scintillating Crystals**	Antoni Munar UJI Universitat Jaume I Departament de Fisica Experimental 12071 Castello de la Plana (SPAIN) munar@uji.es	**ORAL** **S_III**

94	173_Houzard	Houzard Cl, Maintas C, Cachin F, Mognetti Th, Galy G, Slosman D , Maubland J, Itti R, Maintas D. **Influence of tumor mean atomic number and density on CT attenuation corrected PET: Phantom studies**	Cl. Houzard Centre de Médecine Nucléaire, Groupe Hosptitalier Lyon Est, 59 Boulevard Pinel 69500Bron France maintasd@yahoo.fr	**ORAL** **S_I**
95	174_Houzard	C. Houzard, C. Tychyj, I. Morelec, F. Ricard, P. Got, F. Cotton, F. Giammarile, D.Maintas **Feasibility of iodine contrast enhanced CT-scan during a 18F-fluorodeoxyglucose (18FDG) Positron Emission Tomography (PET-CT) study**	Cl. Houzard PAM d'imagerie Centre hospitalier Lyon-Sud, Lyon maintasd@yahoo.fr	**ORAL** **S_I**
96	175_Maintas	C. Maintas, Cl. Houzard, Th. Mognetti, G.Galy, D.Slosman, J.Maubland, R.Itti, D.Maintas **The metabolic activity of high density tissue in PET is influenced by CT attenuation correction? A phantom simulation study**	C. Maintas Institute of Isotopic Studies, Athens Medical Centre, Greece maintasd@yahoo.fr	**ORAL** **S_I**
97	176_Weitzel	T. Weitzel, T. Krause, M. Hofmann **Impact of Statistical Region Growing on the Recovery of Standard Uptake Values (SUV) for Small Lesions by using Fourier-Transform-Interpolation, Deconvolution and Statistical Region Growing ("FIDES") to determine SUV.**	T. Weitzel, M. Hofmann Clinic for Nuclear Medicine, Molecular Imaging and Therapy Group (MIT-Bern,CH), Inselspital, Freiburgstrasse 10, 3010 Bern. m.hofmann@klinikum-hildesheim.de	**ORAL** **S_I**
98	177_Weitzel	T. Weitzel, T. Krause, M. Hofmann **Contrast improvement of anatomical and metabolic features in PET imaging by using principal component analysis of dynamic PET Data to generate multimodal images.**	T. Weitzel, M. Hofmann Clinic for Nuclear Medicine, Molecular Imaging and Therapy Group (MIT-Bern,CH), Inselspital, Freiburgstrasse 10, 3010 Bern. m.hofmann@klinikum-hildesheim.de	**ORAL** **S_VI**

Progress in instrumentation and processing: from Nuclear Medicine to Molecular Imaging.

Andrew Todd-Pokropek

Department of Medical Physics and Bioengineering
University College London

ABSTRACT

While the Anger gamma camera was dominant for several decades for nuclear medicine imaging, there are a number of significant developments in progress. The large increase of the usage of PET scanners has been a result of new detector materials such as LSO, GSO, YAP etc, improved electronics and algorithms such as list mode reconstruction and in particular the combination with CT. Finally although investigated many years ago, reliable time of flight scanners have been introduced, with the corresponding reconstruction algorithms. μPET and μSPECT systems are also now widely available, where the use of multiple pinholes for μSPECT has resulting in resolutions of the order of 0.1mm to be in reached. Solid state pixelated detectors are also of considerable interest including CaZnTe, LnBr, and CCD arrays. Readout of such finely cut pixelated arrays is often via the dual usage of PMT and APDs (or now SiPMs). One use of such detector arrays in the Compton camera one example of which has been developed at UCL. There is also considerable interest in simultaneous radioisotope tracer + MRI imaging. Another development being pursued at UCL is that of combined mammographic X-ray, scintigraphic and optical imaging. An additional driver particular for the small animal system has been that of so-called molecular imaging and the exploration of cellular/ molecular chemistry and gene expression and therapy. On the processing side in addition to improved tomographic reconstruction, the goal is still that of improved quantitative accuracy and functional modelling. Partial volume correction has been addressed by a number of groups (e.g. PVELab) with some success. Finally motion and breathing correction has been addressed using MRI based models and intelligent gating or list mode image formation. These advances in instrumentation and data handling together with the inherent power of tracer technology has resulted in the increasing use of nuclear medicine/ molecular imaging methods in modern medicine.

ANALYTICAL FUSION OF DIFFERENT MODALITY IMAGES BASED ON PRIOR KNOWLEDGE

Michael L. Goris[1], J.Hongyun Zhu[1] and Daniel Y Sze[2]. [1]Division of Nuclear Medicine. [2]Division of Interventional Radiology. Stanford University School of Medicine. Stanford, California

Background: Fusion is the simultaneous and combined analysis of two images mapping identically in the same object space, but recording a different attribute of the object. Most fusion has been performed as visual representation in which the attributes are represented independently into overlapping but independent color scales. In this work we explore fusion, in which the attributes are combined in a mathematical or logical manner, to address a specific goal.

Methods: The first approach is mathematical, and concerns a particular combination of brain imaging: In patients treated for brain tumors, the usually clear delineation of pathology by MRI is compromised because the treatment itself may produce an ambiguous signal. Specifically, a FLAIR sequence will show post-treatment edema and recurrent tumor as a high signal intensity region. FDG PET on the other hand will show little or no density in the former, and (near normal) in the latter. A viable tumor would also show increased density in PET and post contrast T1 sequence, but not all post T1 high densities represent regions with high metabolic activity. The combination of these a-priori judgments (or prior knowledge) can be done in different manners: After normalization, the product MxP would favor viable tumor and the artangent of (P/M) would likely represent non-viable or non-malignant lesions (Figure 1).

In the second approach, in preparation for a treatment of liver metastases with radioactive ^{90}Y-labeled microspheres, the liver is infused intra-arterially with 99mTc macroaggregates, imaged, and reinjected with 99mTc colloid and imaged. The result is two in-line registered image volumes, defining MAA perfused tumor and liver, and functional liver (colloid) (Figure 2). The analysis of the fusion allows the computation of relative and absolute volumes, and relative doses to liver and tumor. We found that the relative dose to normal liver perfused by MAA is the best predictor of post therapy toxicity (as measured by the liver enzyme elevation). In cases of toxicity, the average relative volume was 66%, in the absence of toxicity, the relaive volume was 33% ($p<0.01$), with only one case overlapping.

Figure 1 **Figure 2**

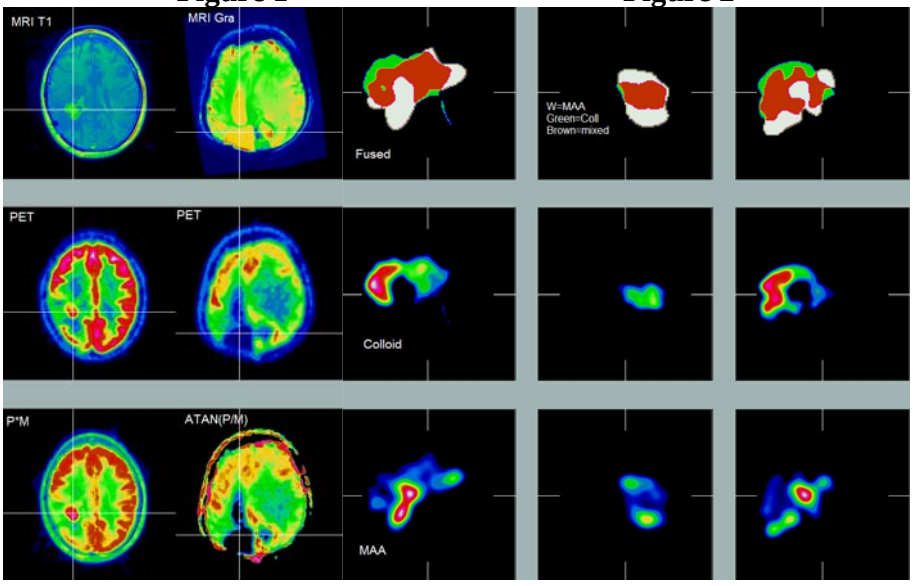

Conclusion: Fusion is more than a combined visual display, but is a potentially powerful analytical tool, combining the data from more than one image or object attribute..

The MIRaS (Medical Image Radiotherapy and Simulation) project.

J.I. Lagares, P. Arce, J.D. Soler, G. Pereira, M. Embid.

CIEMAT, Medical Physics Unit, Technology Department, Madrid, Spain.

Introduction:

The Medical Imaging has been increased, its importance on the medical diagnostic for many pathologies and, some times the simultaneous use of images from different techniques has the better way to give better analysis and results. In fact, for Cancer disease, the image has a special importance and its use is mandatory for radiotherapy treatments. In addition, the Monte Carlo (MC) technique in simulation has demonstrated to be a powerful tool to solve the particle transport though matter. The use of this technique in radiotherapy treatment is specially appreciated in hospital environments for a detailed verification of radiotherapy treatments, but it needs expertise on computational fields and high performance computing.

MIRaS is a computational project on Medical Imaging, Radiotherapy and MC Simulation to ease the Medical Image analysis and the use of MC simulation in Radiotherapy treatment.

The main goals of MIRaS are to provide a single interface to use, manipulate and to analyse multiple type of images from the some or different image techniques simultaneously. Also, let to verify to do planification of radiotherapy treatments using free available MC codes.

Material and Methods:

The MIRaS project has been developed under C++ language. It is based on open source packages like DCMtk for DICOM format files, GTK+ and OpenGL. Actually, the code is divided on two independent modules: The MIRaS image interface and MIRaS MC calculation module, both codes can be run independently. The image module is just on prelimiray steps, but the image manager to read, sort and access to the images information is next to be completed. The calculation module is ready to work with the MC codes as BEAMnrc-DOSXYZnrc under EGSnrc and GEANT4 under GAMOS (Geant4-based Architecture for Medicine-Oriented Simulations) environment. GAMOS is a powerful plug-in based tool to ease the use of GEANT4 of non-computer experts and, at the same time, it provides easily all the functionality of GEANT4 to more advanced users. The MIRaS calculation module includes some new plug-ins over GAMOS to run the radiotherapy simulations. The program structure is ready to implement other simulation packages like MCNPX. The input of MIRaS calculation module is a set of text files with an easy meta-language to submit a full treatment simulation reading the DICOM-RT treatment plan, the patient information and other simulation data. It provides the functionality to do the simulations on a local machine or a remote PC cluster, and the integration with GRID technologies will be provided.

A comparison between BEAMnrc and GEANT4 has been performed to validate the use of MIRaS. Actually MIRaS is available to be used on the hadrontherapy field.

Conclusions:

MIRaS is an ambitious project, which can be applying immediately on radiotherapy or can be used just for compare BEAMnrc and GEAM4 results on the same geometry. Its open source character permits the possibilities to establish international collaboration to follow developing. On November course on GAMOS and MIRAS code are planned. More information in http://www.ciemat.es/recursos/doc/Formacion/Cursos_abiertos/1121821923_2832007114721.pdf.

MIRaS will be a powerful tool to be used on Hospitals and universities environments.

Simulation of PIXSCAN, a photon counting micro-CT for small animal imaging

F. Cassol Brunner, R. Khoury, D. Benoit, C. Meessen, A.Bonissent, C. Morel

Centre de Physique des Particules de Marseille (CPPM), IN2P3/CNRS and Université de la Méditerranée Aix-Marseille II, France

Abstract

A main challenge in the development of new detectors is the achievement of a satisfactory comprehension of the instrument behaviour. We present the simulation work developed to understand and characterize an innovative micro-CT scanner. The PIXSCAN scanner is a photon counting device based on hybrid pixel detectors. Its working principle is expected to improve the contrast for soft tissues and to reduce both the scan duration and the dose absorbed by the animal. A prototype of the scanner, PIXSCAN-XPAD2, has been assembled and studied in order to achieve a proof of principle of the system. The image quality of the demonstrator is affected by a number of limiting factors. The estimation of the intrinsic properties of the imaging system can be achieved by an unfolding of the different degrading elements. For this, both an analytical and a Monte Carlo simulation of the prototype and of the evaluation phantoms have been developed to ensure a satisfactory comprehension of the data. The Monte Carlo simulation was based on the GATE package. It included the complete simulation of photon propagation in matter, together with the modelling of the source spectrum, the scanner geometry and the sensor response. The analytical simulation was much more approximate, its merit was the rapidity which permitted fast preliminary results. Several figures of merit were studied and showed good agreement with real data (see figure 1 and figure 2 as example). Hence, the developed simulations can be used as a valid tool for the estimation of the ultimate PIXSCAN performances, in terms of spatial resolution, contrast measurement and dose reduction.

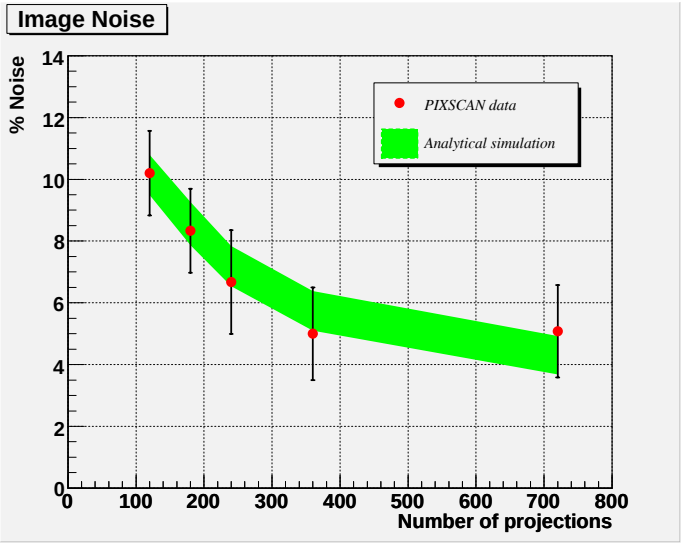

Figure 1

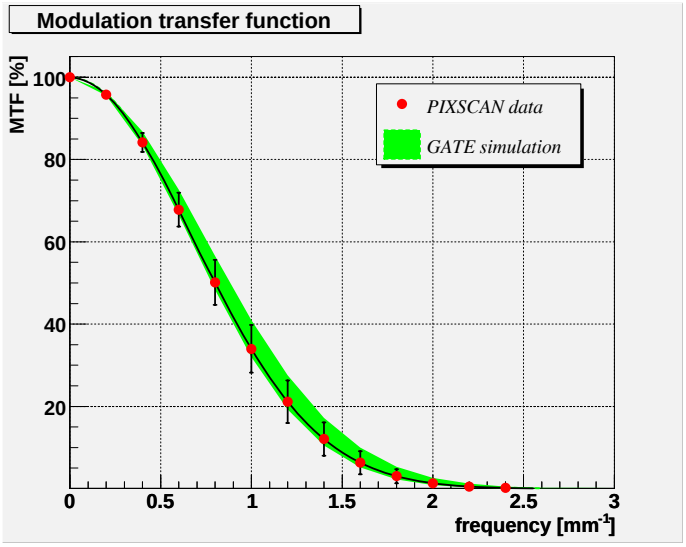

Figure 2

Photon and primary electron arithmetics in photoconductors for digital mammography: Monte Carlo simulation studies

T Sakellaris[1] , G Spyrou[1,2] , G Tzanakos[3] and G Panayiotakis[1]

[1]University of Patras, School of Medicine, Department of Medical Physics,
265 00 Patras, Greece
[2]Biomedical Research Foundation, Academy Of Athens,
115 27, Athens, Greece
[3]University of Athens, Department of Physics, Div. Nucl. & Particle Physics,
157 71 Athens, Greece

Among the most important components of a direct detector for digital mammography is the detecting material. Materials like a-As_2Se_3, GaSe, GaAs, Ge CdTe, CdZnTe, $Cd_{0.8}Zn_{0.2}Te$, ZnTe, PbO, TlBr, PbI_2 and HgI_2 are potential candidates and are currently investigated. The x-ray generated primary electrons inside the photoconductor's bulk consist the primary signal which propagates in the material and forms the final signal (image). An already developed model for a-Se (Sakellaris *et al* 2005), based on Monte Carlo methods, has been properly extended to simulate the primary electron production in the photoconductors mentioned. The model simulates the primary photon interactions (photoelectric absorption, coherent and incoherent scattering), as well as the atomic deexcitations (fluorescent photon production, Auger and Coster-Kronig electron emission). A characteristic result is shown in figure 1 that presents the energy distribution of primary electrons inside PbI_2 when it is irradiated with an x-ray spectrum resulting from W, with 30 kV_p, half value layer: 0.81 mm Al and 1.02 mm Al filter.

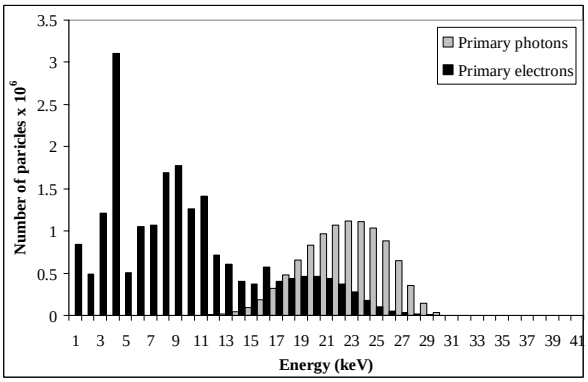

Figure 1. The energy distribution of primary electrons inside PbI_2 after the irradiation with an x-ray spectrum resulting from W, with 30 kV_p, half value layer: 0.81 mm Al and 1.02 mm Al filter.

In this study, the arithmetics of: (i) fluorescent photons produced, (ii) forwards and backwards escaping primary and fluorescent photons and (iii) emitted primary electrons, are being investigated for 39 monoenergetic spectra with energies between 2 and 40 keV. The results for the various materials (with a-Se included) are analyzed and compared at

typical mammographic energies (15, 20, 25 and 30 keV). According to their atomic compositions the materials are grouped in four categories as shown in table 1.

Table 1. The four categories of materials into consideration

Category	Materials
A	a-Se, a-As_2Se_3, GaSe, GaAs, Ge
B	CdTe, CdZnTe, $Cd_{0.8}Zn_{0.2}Te$, ZnTe
C	PbO, TlBr
D	PbI_2, HgI_2

At energies E<30 keV the fluorescent photon production is constant between the K and L-edges. At higher energies though, it decreases in materials of category A and increases in materials of categories B and D.

The fluorescent photons escape *backwards*. Similarly, except for materials in category A at E>30 keV, the primary photons escape *backwards* although their number is very small. At E>30 keV in materials of category A, the number of primary photons that escape *forwards* significantly increases and becomes higher than the number of escaping fluorescent photons.

The production of fluorescent photons and the escaping of photons are the competing factors that affect the primary electron production and subsequently the detector's total electron yield. Consequently the number of primary electrons: (a) is generally constant between the K and L-edges, (b) increases at energies where there is an increasing absorption of high energy fluorescent photons and (c) decreases at E>30 keV, in materials of category A, where the escaping primary photons increase.

Table 2 presents the materials with the minimum and maximum fluorescent photon production, escaping of photons (primary and fluorescent), and primary electron production, at 15, 20, 25 and 30 keV.

Table 2. The materials with the minimum and maximum fluorescent photon production, escaping of photons (primary and fluorescent), and primary electron production, at 15, 20, 25 and 30 keV.

Energy (keV)	Fluorescent photon production		Escaping of photons		Primary electron production	
	min	*max*	*min*	*max*	*min*	*max*
15	CdTe	GaSe	CdTe	a-Se	PbO	ZnTe
20	CdTe	GaSe	CdTe	a-Se	PbO	TlBr
25	CdTe	GaSe	CdTe	a-Se	PbO	TlBr
30	HgI_2	$Cd_{0.8}Zn_{0.2}Te$	ZnTe	CdTe	PbO	CdTe

The results provide insights concerning the physics of primary electron production from x-ray absorption in the various photoconductors investigated. Additionally the calculations of the number of fluorescent photons, escaping photons and primary electrons for certain energy and number of incident photons, can contribute in the prediction of initial gain, amplification or loss of information in the detectors.

Monte Carlo simulation studies of spatial resolution in magnification mammography using the edge method

M. Koutalonis[1], H. Delis[1], G. Spyrou[1,2], L. Costaridou[1], G. Tzanakos[3] and G. Panayiotakis[1]

[1)] *University of Patras, Department of Medical Physics, 265 00 Patras, Greece.*
[2)] *Biomedical Research Foundation, Academy of Athens, 115 27 Athens, Greece.*
[3)] *University of Athens, Department of Physics, 157 71 Athens, Greece.*

The image quality requirements for the accurate and early detection of microcalcifications and breast lesions have placed strict constraints upon the techniques and equipment utilized in mammography. Magnification is a special technique applied in cases where breast complaints have already been noticed by a woman or her physician, in order to examine a specific area of the breast. Small sized focal spots are essential in such techniques in order to reduce as much as possible the resultant geometrical unsharpness [1, 2]. Both magnification and focal spot size have a critical effect on spatial resolution. European regulations designate that spatial resolution in mammography should not be less than 14 lp/mm. Several authors have studied experimentally the effect of focal spot size on spatial resolution in contact mammography or under magnification using phantoms containing bar patterns but, due to constructive reasons, only a small range of focal spot sizes has been studied.

In this study, a validated Monte Carlo simulation model [3] is utilized in order to study the effect of a wide range of focal spots (from 0.04 mm to 0.30 mm) on spatial resolution under magnification conditions as well as the effect of the degree of magnification on spatial resolution. Conclusions about focal spot sizes that can be used at each degree of magnification according to the existing regulations are also extracted. A 4 cm thick sharp edge consisted of lead, non-transparent to x-rays, was imaged under various conditions in order to produce an edge spread function (ESF). The focus to breast holder distance varied from 60 cm to about 24 cm in order to achieve different degrees of magnification between 1.0 and 2.0, while the spectrum utilized for the calculations was the Mo/0.030mmMo at 28 kVp. To produce the corresponding ESF from each image, a region of interest (ROI) was selected including 2 mm at each side of the edge transition. The greylevel values along these distances correspond to the ESF. These ESFs were numerically differentiated to obtain the line spread function (LSF), from which the modulation transfer function (MTF) was calculated by a Fourier transform. This method of measuring the MTF has gained popularity recently due to its simplicity and the appropriateness especially for digital imaging. The corresponding MTFs were fitted with Gaussian curves. The spatial resolution in lp/mm can be extracted from the MTF and corresponds to spatial frequencies where MTF is below a specific threshold. This threshold varies among the different authors between 2% and 5%, most of whom stretch it as far as possible. For the purpose of this study it was considered 5%.

Increasing the degree of magnification from 1.0 to 2.0 induces a degradation of spatial resolution which varies from 49% for the 0.04 mm focal spot to 53.2% for the 0.14 mm one, mainly due to the geometrical unsharpness. For focus sizes larger than 0.14 mm and up to 0.30 mm the degradation is high, even for low degrees of magnification. As far as the focal spot size is concerned, the increase from 0.04 mm to 0.30 mm reduces the spatial resolution by 15.2%. This percentage is higher under magnification and increases almost linearly. Focal spots larger than 0.12 mm should not be used when magnification is performed as they result in spatial resolution lower than the limit of 14 lp/mm. For low degrees of magnification up to 1.4, focal spot sizes between 0.04 mm and 0.12 mm are considered appropriate. However, for higher degrees of magnification the focal spot dimension should be even smaller. The construction of a microfocus of 0.04 mm would result in acceptable values of spatial resolution even in high degrees of magnification.

References

[1] M Koutalonis, H Delis, G Spyrou, L Costaridou, G Tzanakos and G Panayiotakis, Contrast-to-noise ratio in magnification mammography: a Monte Carlo study, *Phys. Med. Biol.* 52, 2007, 3185-99.

[2] M Koutalonis, H Delis, G Spyrou, L Costaridou, G Tzanakos and G Panayiotakis, Monte Carlo generated conversion factors for the estimation of average glandular dose in contact and magnification mammography, *Phys. Med. Biol.* 51, 2006, 5539-5548.

[3] Spyrou G, Panayiotakis G and Tzanakos G 2000 MASTOS: MAmmography Simulation Tool for design Optimization Studies *Med. Inform. Internet Med.* **25** 275-293

Automated detection of arterial input function in DSC perfusion MRI in a stroke rat model

Mai-Yu Yeh[1, 2], Tsong-Hai Lee[3], Tzuu-Kang Chyi[4], Ho-Ling Liu[1, 2]

[1]Graduate Institute of Medical Physics and Imaging Science, Chang Gung University, Taoyuan, Taiwan; [2]MRI Center, Chang Gung Memorial Hospital, Taoyuan, Taiwan; [3]Stroke Section, Department of Neurology, Chang Gung Memorial Hospital and Chang Gung University, Taoyuan, Taiwan; [4]Molecular Imaging Center Chang Gung Memorial Hospital, Taoyuan, Taiwan.

Introduction: Dynamic susceptibility contrast (DSC) perfusion MRI has been widely applied to assess ischemia in small animal stroke models. Quantitative CBF estimation requires deconvolution of the tissue concentration time curves with an arterial input function (AIF). However, image-based determination of AIF in rodent is challenging due to limited spatial resolution. We evaluated the feasibility of automated AIF detection and compared the results with those obtained from commonly applied semi-quantitative analysis. **Methods:** Permanent occlusion of bilateral common carotid artery was used to induce ischemia in a spontaneous hypertensive rat (240gm, 12-week). DSC imaging was performed on a 3-T MR scanner, using a wrist coil, with a SE-EPI sequence (TR/TE = 700/80 ms, FOV = 41 mm, matrix = 64, 3 slices, SW = 2 mm), starting from 7 s prior to contrast injection (1.2ml/kg, Schering AG). The experiment was performed at pre-operation, 1-day, 1-week and 4-week post-operation. For quantitative analysis, AIF was obtained from 10 voxels with greatest contrast enhancement and used for deconvolution. For the semi-quantitative analysis, relative CBF was estimated by the integral divided by the first moment of the relaxivity time curves. **Results:** No significant differences were observed between the AIF obtained in three different ROIs, whole brain, hemisphere without lesion and hemisphere with lesion. Comparing the CBF ratios (lesion/normal) between quantitative and semi-quantitative analyses, a similar trend at different operative time points was found. **Conclusion:** The automated method was able to detect AIF with similar shapes as could be found in literatures. In this study, arterial inputs to hemispheres with and without lesion were found to be similar, thus the quantitative analysis led to comparable CBF ratios than the semi-quantitative analysis. However, when the regional blood supply is altered, being capable of determining local AIF will be crucial for the accurate assessment of ischemia status.

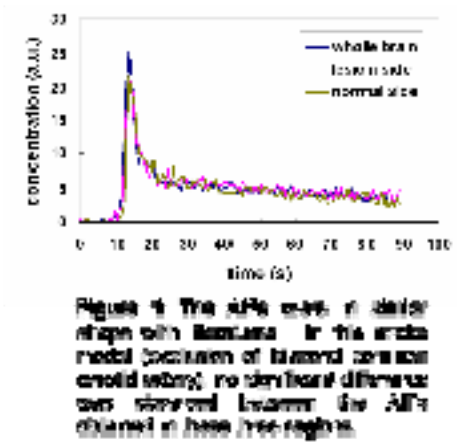

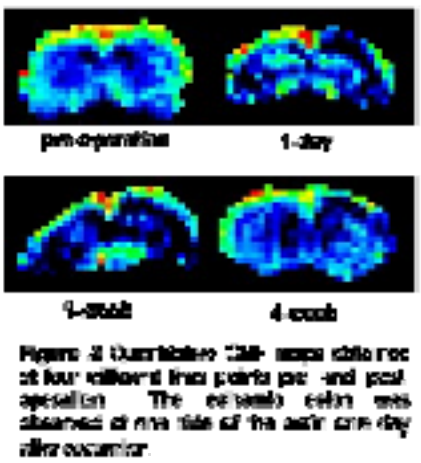

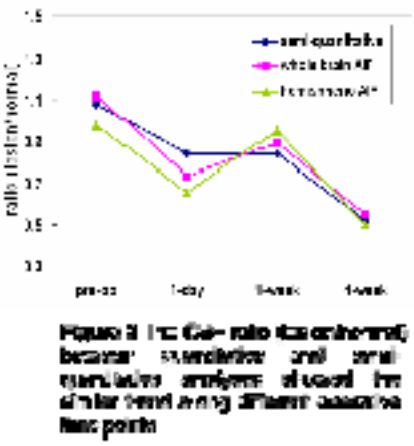

An automated methodology for the segmentation of in vivo acquired DSA images: application in the New Zealand hindlimb ischemia model

George C. Kagadis[a], Panagiota Spyridonos[a], Dimitris Karnabatidis[b], Athanassios Diamantopoulos[b], Konstantinos Katsanos[b], Antonis Daskalakis[a], Nikolaos Samaras[b], John Maroulis[c], Efrosini Sourgiadaki[d], Dionisios Cavouras[e], Dimitris Siablis[b], George C. Nikiforidis[a]

[a]*Department of [a]Medical Physics, [b]Radiology, [c]Surgery and [d]Anesthesiology, School of Medicine, University of Patras, GR 26500 Rion, Greece*

[e]*Department of Medical Instrumentation Technology, Technological Education Institution of Athens, Agiou Spyridonos Street,GR 12210 Aigaleo, Athens, Greece*

Abstract

Purpose:

In-vivo dynamic visualization and quantification of vascular networks represent an interesting methodological necessity of both therapeutic angiogenesis and tumor anti-angiogenesis studies. Our purpose was to develop a user free computerized tool for the automated segmentation and quantitative assessment of in-vivo acquired DSA images by using Matlab.

Materials and Methods:

The concept of image structural tensor was used in order to accomplish vessel segmentation. Vessel delineation was based on the estimation of the largest eigenvalue of the structural tensor. The resulted eigenvalue matrix was treated as gray-matrix from which the vessels were gradually segmented and then categorized in three sub-groups. The histogram percentiles, corresponding to 85%, 65% and 47% of prime eigenvalue gray-matrix were optimally found to give the thresholds T1, T2 and T3 respectively, for extracting vessels of different size. We tested the software on a series of DSA images in both normal rabbits (group A) and in rabbits with experimental induced chronic hindlimb ischemia (group B).

Results:

The result was an automated computerized tool developed in Matlab environment that can be used to process images as a batch process without any user intervention. Higher total vascular area and length were calculated in group B compared to group A (p=0.0242 and p=0.0322 respectively). In conclusion, a promising new tool for the

analysis of macro- and micro-vascular networks in DSA images was developed. It can be easily used in either experimental or clinical studies. Its main advantage is the fast and automatic execution of image processing that could be easily adapted to a user friendly interface.

A Calibration method for the PIXSCAN: Small Animal X-ray CT Scanner

R. Khoury, A. Bonissent, JC. Clemens, C. Messeen, E. Vigeolas, M. Billault, C. Morel

Centre de Physique des Particules de Marseille (CPPM), IN2P3/CNRS and Université de la Méditerranée Aix-Marseille II, France

ABSTRACT

Reconstruction in Cone Beam Tomography from scanner data requires a complete and precise description of the source-detector system. Small misalignment of the imaging system may cause severe distortion of the reconstructed image; it takes special care to ensure that the geometry of the system is well known. We present a high precision method for the geometric calibration in Cone-Beam CT for the PIXSCAN, a small animal X-ray-CT scanner based on hybrid pixel detectors (XPAD2). The specificities of the XPAD2 detectors (dead pixels, tilts and gaps between modules…) made the calibration of the PIXSCAN a hard stuff. The method uses a calibration object consisting of a hollow cylinder of polycarbonate on which we positioned four metallic balls (see Figure 1). It requires 360 X-ray images (1° increments). An analytic expression of the 3 image ellipses has been derived. It is used for a least squares regression of the 13 alignment parameters, after a correction of the internal XPAD2 geometry. Our method is rapid and completely automated; its precision is about 30µm (see Figure 3), a mouse reconstruction is shown in Figure 4.

Fig1. Calibration phantom.

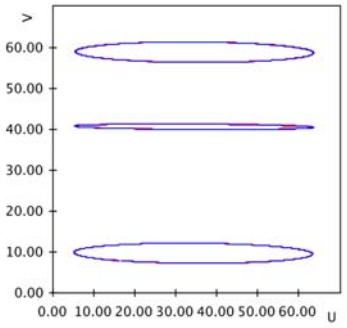

Fig2. Trajectories fitted (blue) and calculated (red) of the ellipses.

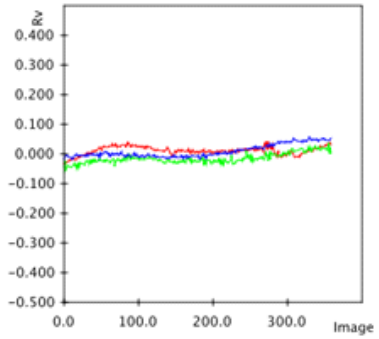

Fig3. Ellipses centres residuals in the y direction.

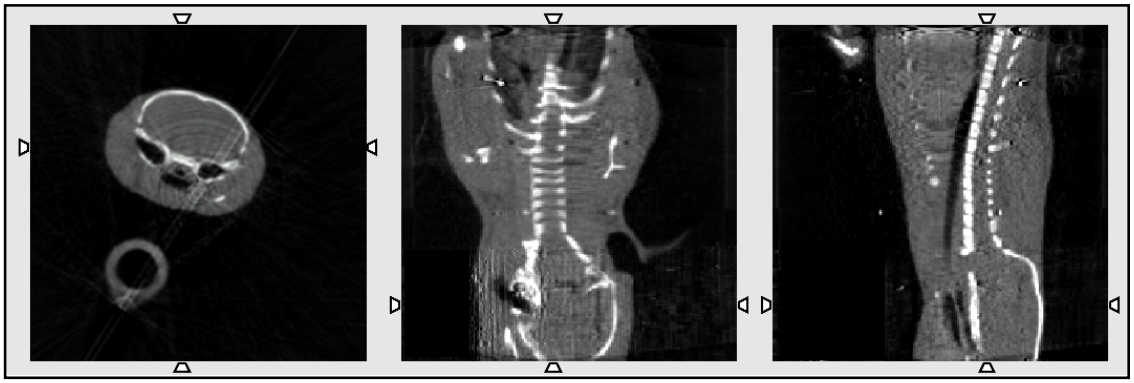

Fig4. Image reconstruction of a mouse

Exploiting Unsupervised and Supervised Classification for Segmentation of the Pathological Lung in CT

P. Korfiatis[1], C. Kalogeropoulou[2], D. Daoussis[3],T. Petsas[2], A. Antonopoulos[3], and Lena Costaridou[1]

[1] Department of Medical Physics, School of Medicine, University of Patras, 265 00 Patras, Greece
[2]Department of Radiology, University Hospital of Patras, 265 00 Patras, Greece
[3]Depertment of Rheumatology, University Hospital of Patras, 265 00 Patras, Greece
costarid@upatras.gr

Recently, the challenge of segmenting lung fields in presence of pathologies attached to borders from CT data is highlighted. [1-3]. Among lung pathologies, a special category is interstitial pneumonias (IP) whose quantification and characterization is a difficult task for radiologists, due to complexity and variability of its morphologic patterns. High resolution computed tomography (HRCT) is the method of choice to image diffuse parenchymal lung disease (DPLD) such as IP. Several HRCT based computer aided diagnostic schemes for DLPDs have been proposed [4, 5]. These systems focus on the final stages of lung analysis, utilizing suboptimal segmentation techniques for lung field delineation. This is expected to have serious consequences in the analysis steps that follow, especially in case of DLPDs.

In this work, a segmentation algorithm is proposed for delineating abnormal lung border. The system exploits the combination of two increasingly complex segmentation methods. First the Markov random field technique was chosen for unsupervised segmentation as it was used to model the joint probability distribution of the image pixels in terms of local spatial interactions. The initial segmentation result was further processed for refinement, exploiting textural differentiation between lung tissue (normal and abnormal) and lung surrounding tissue (pleura and thoracic wall). Several categories of textural features were extracted from original gray level and wavelet coefficient domains. A support vector machine classifier is used to distinguish the lung tissue from the surrounding tissue resulting in further delineation of lung border. The proposed system was applied on a database of HRCT cases. Clinical cases corresponding to patients diagnosed with IP, secondary to connective tissue diseases mainly scleroderma and mixed connective tissue disease. All HRCT images were obtained with a Multislice (16x) CT (LightSpeed, GE), at the University Hospital of Patras. A total of 578 HRCT images selected from 17 patients were analyzed. Images were selected by an expert radiologist and care was taken to choose cases with pathology affecting the lung border.

The performance of the proposed method was assessed using quantitative metrics, by comparing automatically derived lung borders to the manually traced borders by an experienced radiologist. Segmentation performance in terms of overlap was 0.924±0.021, and for shape differentiation mean, rms and maximum distance were 1.663±0.816, 2.334±1.574 and 8.0515±6.549 mm, respectively.

An accurate automated method is proposed for segmenting the pathological lung. Besides its generic character, the method is envisioned as an initial step of a computer aided quantification and classification scheme of DPLD.

Acknowledgment. This work is supported by the Caratheodory Programme (C.180) of the University of Patras.

References

[1] Armato, S.G., Sensakovic III, W.F.: Automated lung segmentation for thoracic CT: Impact on computer-aided diagnosis. Acad Radiol 11, 1011–1021 (2004)
[2] Sluimer I., Prokop M., Van GInneken B.: Toward automated segmentation of the pathological lung in CT. IEEE Trans. Med. Imaging 24, 1025-1031 (2005)
[3] Korfiatis P., Skiadopoulos S., Sakellaropoulos P., Kalogeropoulou C., Costaridou L.: Automated 3D segmentation of lung fields in thin slice CT exploiting wavelet preprocessing. IN Kropatsch W.G., Kampel M., and Hanbury A. (Eds.): CAIP 2007, LNCS vol. S 4673, pp. 237-244. Springer, Heidelberg (2007)
[4] Sluimer I., Prokop M., Hartmann I., Van GInneken B.: Automated classification of hyperlucency, fibrosis, ground glass, solid, and focal lesions in high-resolution CT of the lung. Med. Phys. 33, 2610-2620 (2006)
[5] Uchiyama Y., Katsuragawa S., Abe H., Shiraishi J., Li F., Li Q., et al.: Quantitative computerized analysis of diffuse lung disease in high-resolution computed tomography. Med. Phys. 30, 2440-2454 (2003)

Imaging atherosclerotic plaque biology using radionuclides

Yared Tekabe,[1] Qing Li,[1] Marija Sedlar,[1] Stan Majewski,[2] Ann Marie Schmidt,[1] Lynne L Johnson[1]

[1]Columbia University, New York, NY; [2] Thomas Jefferson National Accelerator Facility, Newport News, VA

The radionuclide signal in small animal imaging is limited by dose and by limited tracer binding sites and therefore it is important to either amplify the signal by chemical modification or develop probes against abundant signals in the plaque. The hallmark lesion in atherosclerosis is the thin cap fibroatheroma with components of apoptosis of macrophages and smooth muscle cells (SMCs), inflammation (macrophages), and matrix metalloproteinase (MMP) upregulation and expression (plaque remodeling). In diabetes atherosclerosis takes an accelerated course. Advanced glycated endproducts are nonenzymatically glycosolated proteins that bind receptors and have been implicated in accelerating atherosclerosis in diabetes. These receptors for advanced glycated endproducts (RAGE) also bind other inflammatory cytokines implicated in non-diabetic atherogenesis. We are interested in developing a number of radionuclides that target specific biological signals in atherogenesis and plaque instability. The targeted agents we are using in relevant murine models include: ^{99m}Tc-Annexin V, ^{99m}Tc-MMI (broad based MMP inhibitor), Z2D3, a murine monoclonal antibody directed against proliferating smooth muscle cells, and a novel antibody against a peptide sequence on the v domain of RAGE. We have shown focal uptake of each of these tracers in aortic atherosclerotic plaque of apoE null mice fed high fat diet by high-resolution planar and SPECT imaging. The uptake correlated with immunohistopathological markers for apoptosis (caspase) in macrophages and SMC's, MMP's 3 and 9 expressed on macrophages, proliferating smooth muscle cells (a-actin, BrdU), and RAGE expressed on macrophages and SMCs. Results of these experiments showed that tracers can be used separately or together to target different stages/components of the plaque. This work has potential uses as an in-vivo and non-destructive approach to phenotyping novel genetically modified mouse models of atherosclerosis and for drug discovery.

Combined live wire and active surface approach for volume-of-interest segmentation

Gudrun Wagenknecht and Markus Losacker
Central Institute for Electronics, Research Center Juelich, D-52425 Juelich, Germany

Aim: Volume-of-interest (VOI) segmentation is an important prerequisite for quantitative analysis of structural and functional changes in multimodal tomographic images (e.g., CT, MRI, PET, SPECT). A suitable VOI segmentation method should allow user interaction to position the VOI and be automated to support the user as much as possible. A new combined 2D/3D approach for semi-automatic VOI segmentation was developed and evaluated.
Methods: The new method combines a 2D live wire (LW) [1] with a 3D active surface approach (ASM) [2] integrated into MITK [3] to provide the GUI for user interaction and visualization. **2D LW:** The 2D LW approach allows the user to initialize the VOI close to the desired position by segmenting regions of interest (ROIs) in a few sample slices. In order to extract a ROI boundary contour, the user need place only a few points on it. The contour pieces in between are determined automatically as cost-optimal paths in the image-based cost-weighted graph using the Dijkstra algorithm [4]. Local costs are calculated from gradient-based image features, adjustable to image quality and the VOI to be extracted. **Interface LW-ASM:** The start mesh of the ASM is generated from the 2D LW-segmented sample ROIs. For this, each ROI is filled by region growing and ROIs are then interpolated to build a binary start volume. Interpolation can be based on slice replication to generate a steplike volume or on Thirion's demons-based registration [5] to build a smooth volume. Finally, the marching cubes algorithm [6] transforms the binary start volume into a triangular start mesh. **3D ASM:** The 3D ASM approach finds the final VOI segmentation based on the start mesh which is deformed until internal and external "forces" are in balance. The external generalized gradient vector flow (GGVF) field [7] attracts the mesh to the edges and the Taubin filter approach [8] steers the internal smoothness of the mesh, avoiding volume loss. In addition, ballon forces can be applied to shrink or expand the mesh. Parametrization of the ASM is adjustable. The result can be saved as surface mesh and after voxelization [9] as binary and gray value VOI.
Results: In order to show the advantage of the new approach, software phantoms of different size and image quality (noise level) were used to evaluate the segmentation performance quantitatively compared to a simple polygon initialization. Phantoms have a spherical shape with a cylindrical element in the middle. Both parts can be varied in size. Gray values are 170 (phantom) and 85 (background). Additive Gaussian noise with $\sigma_1 = 21.25$ and $\sigma_2 = 42.50$ is applied. In the same sample slices (each 5th and "step" slices), the ROIs are segmented with LW (4 points) and polygons (4 and 8 points) to build the start mesh. The results show that for each phantom, LW-based initialization yields similar or better results with less than half the user interaction as polygon-based initialization. Sample segmentations of real data sets show the performance of the method for segmenting different kinds of VOIs.
Conclusions: The combined 2D/3D approach is a good choice for semi-automatic VOI segmentation regarding user interaction and segmentation quality. Positioning the VOI near the exact boundaries based on the 2D LW approach reduces user interaction and improves 3D ASM-based segmentation accuracy at different image qualities.
Acknowledgements: This study is part of the EU-funded EMIL program (LSHC-2004-503569).

References: 1. Wagenknecht G et al.; NIMA 569 (2); 481-487 (2006). 2. Belitz H et al.; Proc. IEEE Int. Symposium on Biomedical Imaging: From Nano to Macro; 402-405 (2006). 3. http://www.mitk.org. 4. Dijkstra EW; In: Numerische Mathematik 1; 269-271 (1959). 5. Thirion JP; Medical Image Analysis 2(3); 243-260 (1998). 6. Lorensen WE et al.; Proc. SIGGRAPH '87; 163-169 (1987). 7. Xu et al; Signal Processing – An International Journal 71 (2); 131-139 (1998). 8. Taubin G; Proc. SIGGRAPH ´95; 351-358 (1995). 9. Sramek et al.; Volume Graphics; 119-134 (2000).

Evaluation of brain perfusion in specific Brodmann areas in Frontotemporal dementia and Alzheimer disease using automated 3-d voxel based analysis

V. Valotassiou[1], J. Papatriantafyllou[2], N. Sifakis[3], P. Georgoulias[1], C. Karageorgiou[3], C. Zerva[2].

[1] Nuclear Medicine Dpt, University Hospital of Larissa, Larissa, Greece
[2] Neurology Dpt, General Hospital "G. Gennimatas", Athens, Greece
[3] Nuclear Medicine Dpt, "Alexandra" University Hospital, Athens, Greece

Introduction

Brain perfusion studies with single-photon emission computed tomography (SPECT) have been applied in dementing patients in order to provide better discrimination between frontotemporal dementia (FTD) and Alzheimer's disease (AD). Such studies have been evaluated either by visual interpretation and/or region of interest (ROI) analysis. However, in some cases, FTD and AD may share common brain perfusion abnormalities and the visual analysis and/or ROI approach may not accurately detect specific focal changes for each pathology. Recently, several processing protocols for 3D voxel-by-voxel analysis of brain perfusion SPECT, have been applied.

Aim

To assess the perfusion of specific Brodmann (Br) areas of the brain cortex in FTD and AD patients, using NeuroGam processing program to provide 3D voxel-by-voxel cerebral SPECT analysis.

Material and methods

We studied 34 consecutive patients from an outpatient Memory Clinic. We used the established DSM-IV criteria for the diagnosis of dementia and the specific established criteria for the diagnosis of FTD and AD. All the patients had a neuropsychological evaluation with a battery of tests including the mini-mental state examination (MMSE).Twenty-six patients (16 males, 10 females, mean age 68.76±6.51 years, education 11.81±4.25 years, MMSE 16.69±9.89) received the diagnosis of FTD and 8 patients (all females, mean age 71.25±10.48 years, education 10±4.6 years, MMSE 12.5±3.89) the diagnosis of AD. All the patients had either a computed tomography (CT) or a magnetic resonance imaging (MRI) of the brain to exclude the presence of anatomical brain lesions. All the patients underwent a brain SPECT 20 min after the intravenous administration of 740MBq of 99mTc-HMPAO, using a single-headed camera (ultra high resolution parallel-hole collimator, 30 sec/projection, 128 projections on a 128x128 matrix). We applied the NeuroGam Software on the reconstructed data, for the evaluation of brain perfusion in specific Br areas in the left (L) and right (R) hemispheres.

Results

Statistically significantly hypoperfusion in FTD compared to AD patients, was found in the following Br areas: 11L ($p<0.0001$), 11R, 20L, 20R, 32L, 38L, 38R, 44L ($p<0.001$), 32R, 36L, 36R, 45L, 45R, 47R ($p<0.01$), 9L, 21L, 39R, 44R, 46R, 47L ($p<0.05$). On the contrary, AD patients presented significant ($p<0.05$) hypoperfusion in Br 7R area.

Conclusion

NeuroGam processing program for 3D voxel-by-voxel analysis of brain perfusion SPECT could result in enhanced accuracy for the differential diagnosis between AD and FTD patients. Moreover, the results confirm the preferential impairment of networks in different regions in FTD patients compared with AD patients.

COMPUTER ASSISTED CHARACTERIZATION OF CERVICAL INTERVERTEBRAL DISC DEGENERATION IN MRI

S. Michopoulou[1], I. Boniatis[1], L. Costaridou[1], D. Cavouras[2], E. Panagiotopoulos[3], G. Panayiotakis[1]

[1] University of Patras, School of Medicine, Department of Medical Physics, 265 00 Patras, Greece
[2] Technological Educational Institute of Athens, Department of Medical Instrumentation Technology, 122 10 Athens, Greece
[3] University of Patras, School of Medicine, Department of Orthopaedics, 265 00 Patras, Greece

Intervertebral disc degeneration is an age associated condition resulting among others, in the narrowing of intervertebral disc space. Disc space narrowing causes the reduction of the foraminal area, which can result in pain, due to nerve root compression[1]. One of the ways to investigate intervertebral disc degeneration in clinical practice is the assessment of disc space narrowing[2] or the analysis of disc morphology[3]. In the present study, a texture based image analysis approach is proposed for the automatic assessment of cervical intervertebral disc degeneration, motivated by previous research concerning joint degenerative alterations[4].

In this study, T2-weighted midsaggital magnetic resonance images of the cervical spine were exploited expecting to capture texture differentiation[5] due to biochemical composition alterations of intervertebral discs. Images were acquired using a 1.5T magnetic resonance scanner (GE Signa HD) and a neurovascular coil. All images were evaluated by an experienced physician, who characterized the intervertebral discs as normal or degenerated (narrowed) employing the Matsumoto's scale[2]. A case sample of 50 manually segmented Regions Of Interest (ROIs), corresponding to cervical intervertebral discs (25 normal and 25 degenerated as assessed by disc space narrowing), was analyzed. First and second order statistical textural features were extracted from each ROI. Student's paired t-test ($p<0.05$) was used to investigate the existence of features capable of demonstrating statistically significant differences between normal and degenerated discs. This statistical analysis revealed statistically significant differences for all features tested and this finding may be considered as indicative of differentiations of intervertebral disc image texture due to disc degeneration.

Following, using these features a pattern recognition system[5] based on the Least Squares Minimum Distance (LSMD) classifier was designed. The LSMD classifier discriminated successfully 47 out of 50 discs, accomplishing an overall classification accuracy of 94%. In addition the system's sensitivity in detecting a degenerated disc was 96% and its specificity was 92%. The proposed system may be of value to the physicians (orthopedic surgeons, radiologists, neurosurgeons) as a decision support tool for the assessment of the intervertebral disc space narrowing in the cervical spine.

References

1. Friedenberg Z, Miller W, (1963), "Degenerative disc disease of the cervical spine", The Journal of Bone And Joint Surgery America, Volume 45, pp 1171-1178.
2. Matsumoto M, Fujimura Y, Suzuki N, Nishi Y, Nakamura N, Yabe Y, Shiga H, (1998), "MRI of cervical intervertebral discs in asymptomatic subjects", The Journal of Bone And Joint Surgery, Volume 80-B, Number 1, pp 19–24.
3. Roberts N, Gratin C, Whitehouse G, (2005), "MRI analysis of lumbar intervertebral disc height in young and older populations", Journal of Magnetic Resonance Imaging, Volume 7, Number 5, pp 880-886.
4. Boniatis I, Costaridou L, Cavouras D, Panagiotopoulos E, Panayiotakis G, (2006), "Quantitative assessment of hip osteoarthritis based on image texture analysis", The British Journal of Radiology, Volume 79, pp 232–238.
5. Costaridou L. ed, *(2005),* "Medical Image Analysis Methods", CRC Press, Taylor and Francis Group, Boca Raton, Florida, USA.

Exploring the enhancement of the imaging properties of a microwave radiometry system for possible functional imaging using a realistic human head model

Ioannis A. Gouzouasis, Irene S. Karanasiou, and Nikolaos K. Uzunoglu

National Technical University of Athens, Iroon Polytechniou 9, Zografou Campus, Athens 15773, Greece

Abstract

A novel Microwave Radiometry Imaging System (MiRaIS) has been developed and experimentally tested for feasible brain activation imaging via contactless measurements [1]-[3]. The technique implemented, is focused microwave radiometry with the use of an ellipsoidal conductive wall cavity for focusing and a sensitive radiometric receiver for the detection of the brain conductivity and temperature variation. Through analytical theoretical and experimental analysis, the system seems able to detect any change of the product of temperature (T) and conductivity (σ), that is change of T*σ [1], [2].

Phantom experimentation as well as human tests using single and multi-frequency receivers [1] has shown in the past promising outcome concerning the potential clinical value of the proposed system, which seems to be able to pick-up brain activation, possibly caused by cortex conductivity changes. The experiments demonstrated that the voltage output from the system is linearly correlated with the actual temperature of the subjects under measurement, when the conductivity of the media under testing remains unchanged. On the other hand, experimental data from cylindrical shaped de-ionized water tank phantoms in which saline solutions of different concentrations were infused, provide promising results concerning the system's ability of detecting conductivity variations [2].

However, in order to be able to study any specific brain area of interest, at various detection depths with the desired spatial resolution, the focusing properties of the system have to be improved [3]. Towards this direction, the present work investigates the use of dielectric materials as filling inside the whole ellipsoid geometry or as matching layers around the head model. Aim of both ideas is to improve the matching conditions on the skin-air interface, creating a stepped refraction index at that point. Results from the simulations performed in the present framework show the validity of this approach and also that focusing points appear to be sensitive to the spatial movement of the head. The simulations are carried out using a commercial FDTD tool along with an anatomically correct human head model, developed from MRI scans. SAR distributions are also calculated inside the head revealing the potential implementation of hyperthermia with the proposed system. In that case, microwave radiometry can be used for temperature monitoring.

Future research, including water tank phantoms filled with de-ionized and/or saline solutions in different temperatures and also human psychophysiological experiments, implementing the new proposed geometries of the system, will reveal, on one hand, the accordance with the theoretical and computational analysis and on the other, the possibility of the system to operate as a functional imaging tool and/or as a therapeutic hyperthermia device.

References

[1] I. S. Karanasiou, N. K. Uzunoglu and C. C. Papageorgiou, "Towards Functional Non-invasive Imaging of Excitable Tissues Inside the Human Body Using Focused Microwave Radiometry", IEEE Transactions on Microwave Theory and Techniques, Vol. 52, No. 8, August 2004.

[2] I. S. Karanasiou, N. K. Uzunoglu, "Single-frequency and Multiband Microwave Radiometry for feasible Brain-Conductivity Variation Imaging during Reactions to

External Stimuli", Nuclear Instruments and Methods in Physics Research A 569 (2006) 581–586.

[3] I. A. Gouzouasis, I. S. Karanasiou and N. K. Uzunoglu, "FDTD Study of the Focusing Properties of a Hybrid Hyperthermia and Radiometry Imaging System using a Realistic Human Head Model", (under publication).

[4] I. S. Karanasiou, Nikolaos K. Uzunoglu, S. Stergiopoulos and Winnie Wong, "A Passive 3D Imaging Thermograph Using Microwave Radiometry", *Innovation and Technology in Biology and Medicine*, vol. 25 (4), pp. 227-239, 2004.

[5] I. S. Karanasiou, C. Papageorgiou and N. K. Uzunoglu, "Is it possible to measure non-invasively brain conductivity fluctuations during reactions to external stimuli with the use of microwaves?", *International Journal of Bioelectromagnetism* IJBEM vol. 7, No. 1, pp.356-359, 2005

SPEMT imaging with a dedicated VAoR dual-head camera: preliminary results

Manuela Camarda[1], Nicola Belcari[1], Alberto Del Guerra[1], Luigi Spontoni[1], Sara Vecchio[1], Paolo Bennati[2], Maria Nerina Cinti[2], Roberto Pani[2], Renato Campanini[3], Emiro Iampieri[3], Nico Lanconelli[3]

[1] Department of Physics "E. Fermi", University of Pisa and INFN branch of Pisa, Italy
[2] Department of Experimental Medicine and Pathology, University of Rome "La Sapienza", Italy
[3] Department of Physics, University of Bologna, Italy

Single Photon Emission Computed Tomography (SPECT) performed with conventional scanners is an established technique in breast cancer investigation, despite the poor spatial resolution. Dedicated cameras can overcome the present clinical sensitivity limit (about 1 cm diameter) for the detection of small size tumours. We have developed a dedicated SPEMT (Single Photon Emission MammoTomography) scanner having two heads which revolve around one pendulum breast of the prone patient. Vertical Axes of Rotation (VAoR) geometry improves sensitivity and resolution by minimizing the radius of rotation. Monte Carlo simulation has been made for the system optimization and for the evaluation of the detector performances. Simulation results indicate that tumours of 8 mm diameter are detectable with a tumour/background uptake ratio of 5:1.

The proposed SPEMT scanner has two opposing detector heads of approximately 5×15 cm^2 each, with a system field-of-view of 147 mm ∅ and 41.6 mm height. The radius of rotation is 7.0 cm thus enabling to scan breasts up to 14 cm in diameter. Each head is composed by a pixelated NaI(Tl) crystal matrix (2.2 mm pitch, 6 mm thickness) with a 3 mm thick glass window coupled to three Hamamatsu H8500 64-anodes PMT's. A parallel holes lead collimator (22 mm thick, with 1.5 mm holes and 0.2 mm septa) is placed in front of the matrix. Dedicated electronic boards have been developed for digitization and acquisition. Data from each event are stored in list mode.

A dedicated software have been developed to recover events falling in the dead zones between adjacent PMT's. This is possible because light from those events firing the crystals in front of these areas, is spread out by the glass windows (3 mm thick matrix window + 1.5 mm thick PMT window) producing detectable signals in the two neighbouring PMT's. One single head has been fully characterized in stationary configuration in both active and dead area, using a ^{57}Co point like sealed source (122 keV). Spatial resolution on planar images, measured at increasing Source-to-Detector- Distances (SDD), ranges from 2.5 mm at SDD = 0.5 cm to 5.8 mm at SDD = 6 cm in the active area and from 2.6 mm to 6.8 mm in the recovered region. In order to estimate the intrinsic detector resolution the point ^{57}Co source was moved parallel to the collimator, at SDD=6 cm, with a step size of 2.0 mm. The measured average FWHM of the count distribution for the pixels is 6.7 mm. The sensitivity measured with the ^{57}Co source of 1.5 MBq for a SDD of 6 mm resulted in 140 cps/MBq in both regions.

The dedicated software also permit to implement Look up Table (LUT) corrections such as single pixel spectra alignment, dead time correction, activity correction, sensitivity normalization. To perform sensitivity correction, a home made planar phantom, uniformly filled with 111MBq of ^{99m}Tc, was used. The stationary head was flood field irradiated with ^{99m}Tc; LUT profile showed a Peak-to-Valley ratio of 5.2 and a spatial resolution of 1.1mm FWHM. Energy resolution was 13% at 140keV.

The very first image acquired (all corrections applied) with the SPEMT tomograph was a planogram of a home made breast phantom. It was a 14cm diameter beaker with two 8mm diameter small cylinders (0.5cc each) in the centre, representing two hot spots. Activity concentration of ^{99m}Tc in tumours was quite high in order to reduce acquisition time (370kBq/cc) and tumour-to-background ratio was 5:1. The two hot spots are clearly distinguishable.

The degradation of the energy and spatial resolution for scintillator pixels facing the dead area between two PMT's does not affect the imaging performance significantly. The first tomographic images of the breast phantom will be also presented.

Grading and Quantification of Hip Osteoarthritis Severity by Analyzing the Spectral Energy Distribution of Radiographic Hip Joint Space

Boniatis I.[†], Costaridou L.[†], Panagiotopoulos E.[‡], and Panayiotakis G.[†]

[†]University of Patras, School of Medicine, Department of Medical Physics, 265 00 Patras, Greece
[‡] University of Patras, School of Medicine, Department of Orthopaedics, 265 00 Patras, Greece

Osteoarthritis (OA) is a major cause of morbidity worldwide, representing the most common form of joint disorder [1]. The evaluation of hip OA severity concerns, on great extent, the utilization of qualitative grading scales [2]. In previous studies performed by our group, the texture as well as the shape of radiographic Hip Joint Space (HJS) have been utilized for the computer-based assessment of hip OA-severity [3, 4]. The present work is concerned with the development of a computer-based image analysis system for: (i) the automatic grading of hip OA severity, and (ii) the quantitative estimation of the severity of the disease by analyzing the spectral energy distribution of radiographic HJS. To the best of our knowledge, a similar approach has not been previously reported.

The sample of the study comprised 64 hips (18 normal, 46 osteoarthritic) corresponding to 32 unilateral and bilateral hip-OA patients. Orthopaedists assessed the severity of hip OA from pelvic radiographs by means of the Kellgren and Lawrence (KL) grading scale [1]. Accordingly, three major KL-based OA-severity categories were formed, labeled as: (i) "Normal / Doubtful", (ii) "Mild / Moderate", and "Severe", comprising 18, 16, and 30 hips, respectively. After radiographs digitization (i) the radiographic contrast was enhanced, and (ii) two Regions Of Interest (ROIs), corresponding to patient's HJSs, were determined, employing custom developed software. The Fourier spectrum of each HJS-ROI image was computed and was expressed in polar coordinates [5]. Accordingly, two one-dimensional spectral signatures, quantifying the radial and angular distribution of spectral-energy of HJS-ROI were formed, while a number of quantitative descriptors of the aforementioned signatures were calculated, employing custom developed algorithms. These descriptors were utilized in the design of a two-level hierarchical decision tree structure, employed for the discrimination among the three OA-severity categories. In particular, at the first level of the tree structure an ensemble of three classifiers (Bayes, k-Nearest Neighbor, and Probabilistic Neural Network), combined according to the Majority Vote rule [6], was used for the discrimination between normal and osteoarthritic hips. At the second level of the decision tree, the hips that had been successfully characterized as osteoarthritic at the first level, were further discriminated as of "Mild / Moderate" OA or "Severe" OA by the Bayes classifier. In addition, a spectral descriptors based regression model was designed for the quantification of the severity of the disease.

The overall classification accuracy accomplished at the first level was 98.4%, since the ensemble of classifiers assigned to the proper categories all the hips of the sample but one. At the second level of the decision tree structure, the highest possible (100%) classification accuracy was achieved, since the Bayes classifier characterized correctly all the hips of "Mild / Moderate" and of "Severe" OA. OA-severity values, as expressed by HJS-narrowing, correlated highly ($r = 0.9$, $p<0.001$) with the values predicted by the regression model.

The spectral energy of radiographic HJS may provide diagnostic information relevant to osteoarthritic alterations of the hip joint. The proposed system could contribute to OA-patient management.

[1] Arden, N. and Nevitt, M.C.: Osteoarthritis: Epidemiology. Best Pract. Res. Clin. Rheumatol. 20 (2006) 3–25
[2] Günther, K.P. and Sun, Y.: Reliability of Radiographic Assessment in Hip and Knee Osteoarthritis. Osteoarthritis Cartilage 7 (1999) 239–246
[3] Boniatis, I., Costaridou, L., Cavouras, D., Panagiotopoulos, E., Panayiotakis, G.: A Computer-Based Image Analysis Method for Assessing the Severity of Hip Joint Osteoarthritis. Nucl. Instr. Methods Phys. Res., Sect. A. 569 (2006) 610–613
[4] Boniatis I., Cavouras D., Costaridou L., Kalatzis I., Panagiotopoulos E., Panayiotakis G.: Computer-Aided Grading and Quantification of Hip Osteoarthritis Severity Employing Shape Descriptors of Radiographic Hip Joint Space", Comput. Biol. Med. 2007, to appear.
[5] Gonzalez, R.C. and Woods, R.E.: Digital Image Processing. 2nd ed. Prentice Hall, Inc., New Jersey (2002)
[6] Theodoridis, S. and Koutroumbas, K.: Pattern Recognition. 2nd ed. Elsevier Academic Press, Amsterdam (2003)

Noise reduction in simulated PET images using wavelet and thresholding method

B. Shalchian [1], H. Rajabi [2], H. Soltanian-zadeh [3], F. Kalantari [1]

1- PhD student, department of medical physics, medical sciences faculty, Tarbiat Modares University, Tehran, Iran
2- Assistant professor, department of medical physics, medical sciences faculty, Tarbiat Modares University, Tehran, Iran
3- Professor, department of electrical engineering, electrical and computer faculty, Tehran University, Tehran, Iran

Introduction

Medical imaging using positron emission is the second method after SPECT for tomography imaging in nuclear medicine. Although PET imaging is very useful in oncology, high noise level in these images reduces the diagnostic accuracy. Wavelet transform is one of the mathematical methods for noise reduction. It seems that using of wavelet transform may improves signal to noise ratio in PET images.

Materials & methods

In this research, we used SimSET software for simulation of PET images and we prepared images using NCAT phantom. The images were acquired using 250 million counts and in 128×128 matrices size. For reference image we acquired an image with high counts (2 milliards). Then, we reconstructed these images using programs that we wrote in MATLAB. After image reconstruction, 250 million counts image (noisy or initial image) and 2 milliard counts image (reference image) were normalized and then we used root mean square error to compare these images. Root mean square error (RMS) can show the difference between images. Then, we wrote some programs in MATLAB for de-noising. These programs were based on using of 54 different wavelets and two methods for thresholding (Global thresholding and Level dependent thresholding). Then, de-noised images were compared with reference image using root mean square error.

Results

After de-noising, RMS value between noisy and reference image in Global thresholding in the best state (for sym7 wavelet) is reduced about 91%. But in Level dependent thresholding, RMS value is dependent to other factors. In this method, by reducing ‘m’ factor (the number of the coarsest approximation coefficients), RMS reduces in both state of hard and soft thresholding and the quality of image is improved. Soft thresholding method gives better images in comparison to hard thresholding method in all of state. It seems Global thresholding has better result in noise reduction in comparison to Level dependent thresholding and the diagnostic quality of images in Global method is better.

Conclusion

Wavelet transform is useful method for de-noising in simulated PET images and it seems Global thresholding in this way is more efficient in comparison to Level dependent thresholding.

Keywords: PET imaging, SimSET, NCAT, de-noising, thresholding, root mean square error.

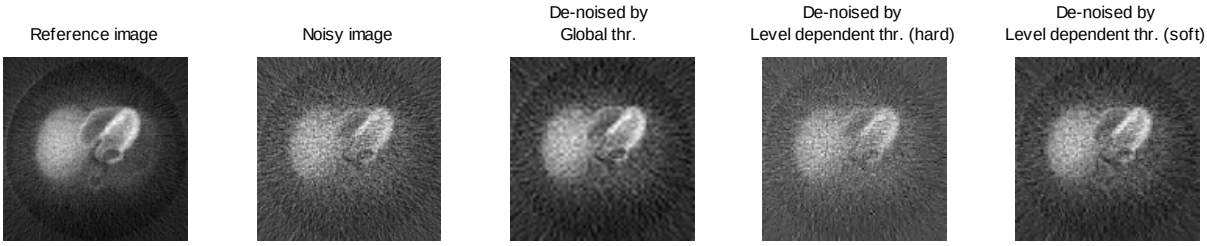

E-mail address: baharehshalchian@yahoo.com & hrajabi@modares.ac.ir **Figure 1** Comparison between reference and initial images and de-noised image that it de-noised using two methods: Global thresholding and Level dependent thresholding (hard and soft) for m = 6

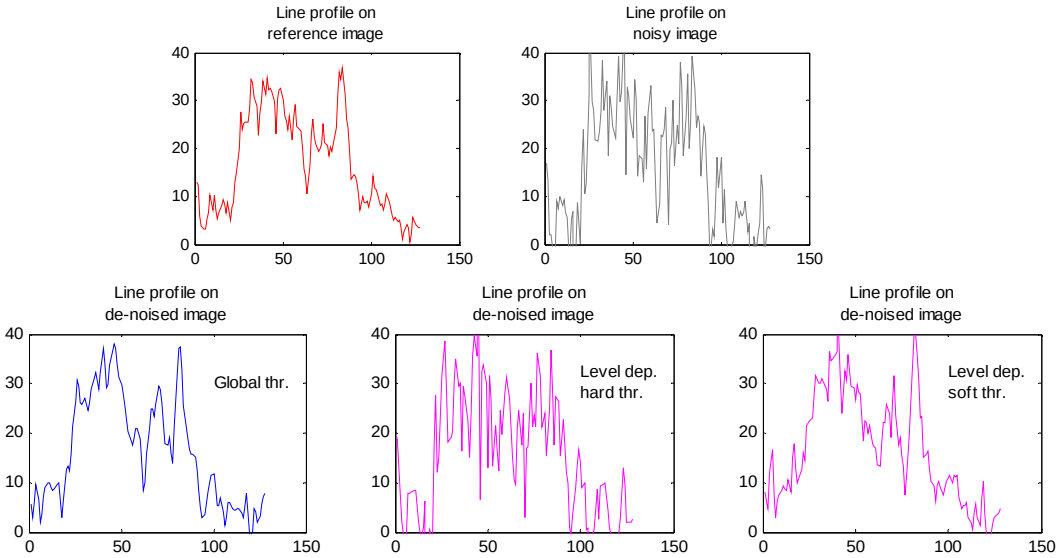

Figure 2 Comparison of pixel values in a special row (or line profile) between reference and initial images and de-noised image that it de-noised using two methods: Global thresholding and Level dependent thresholding (hard and soft) for m = 6

Compensation of cross-contamination in simultaneous $^{201}Tl/^{99m}Tc$ myocardial perfusion SPECT imaging

F.Kalantari [1], H.Rajabi [2,] N.Yaghoobi [3]

1- PhD Student, Department of Medical Physics, Tarbiat Modares University
2- Assistant Prof., Department of Medical Physics, Tarbiat Modares University
3- Department of Nuclear Medicine, Rajaei Heart Center, Tehran, Iran

Introduction: Several protocols are available for heart imaging using one radionuclide, based on redistribution or re-injection, or using two different radionuclides. All these methods require two separate acquisition and processing iterations.
A common protocol is the so called "dual isotope" protocol, in which thallium imaging is first performed patients at rest. Then a technetium-99m perfusion based agent is injected during patient's hyperactivity (stress) and imaging is performed. This approach provides an excellent method for the combined assessment of stress myocardial perfusion and myocardial viability. Theoretically, this imaging protocol can be performed simultaneously by defining different energy window for each radionuclide. However, a potential limitation of simultaneous dual isotope SPECT imaging is contribution of scattered photons from technetium-99m and lead X-rays produced in the collimator into the thallium-201 energy window, referred here as cross-contamination.
The aim of this study is introducing a modified middle energy window method to compensate for this cross-contamination.
Material and Methods: This investigation was performed in three steps: Monte Carlo simulation, phantom experiment and clinical study. In simulation step, the most suitable scatter correction functions characterized by their ability to model cross-contamination were determined. To achieve this goal, Root Mean Square errors between our estimated and real cross-contamination for each view were used. In next step our designed phantom was used for SPECT imaging in different energy windows and the results of simulation was reevaluated. In the last stage the SPECT images of eleven patients who had angiographic data were acquired in different energy windows.
In all the three stages, for each projection angle, the contaminant image to be subtracted from the image in the Tl-201 window was estimated as a linear combination of a scatter-window (90-110 keV) image, convolved by a 2D modified exponential function and the Tc-99m photopeak image, convolved by a Gaussian function.
Results: Significant improvements in contrasts of simultaneous dual Tl-201 images were observed in each step $(P < 0.001)$. In comparison to the previously described methods, the present method yield better results in terms of contrast.
Discussion and Conclusion: Simultaneous dual-radionuclide 99mTc/201Tl myocardial scintigraphy is feasible with 99mTc cross-contamination correction specific to each acquisition. There are many advantages by simultaneous dual isotope imaging. It halves the imaging time therefore double patients' throughput, improves scheduling flexibility, and guaranties the patients' comfort. In this study we introduced a new method by combining simulated and real images to find transfer functions between images in different energy windows.

E-mail: faraz241060@yahoo.com and hrajabi@modares.ac.ir

Energy window setting for optimum Tl-201 heart imaging

F.Kalantari [1], H.Rajabi [2], N.Yaghoobi [3], A.Bitarafan [1], K.E. Gorji [1], F.Rastgoo [3], H.Malek [3], S.H.Firoozabadi [3]

1- PhD Student, Department of Medical Physics, Tarbiat Modares University
2- Assistant Prof., Department of Medical Physics, Tarbiat Modares University
3- Department of Nuclear Medicine, Rajaei Heart Center, Tehran, Iran

Objectives: Poor sensitivity and poor signal to noise ratio because of low injected thallium dose and presence of scattered photons are the main problems in using thallium in scintigraphic imaging of the heart. Scattered photons are the main cause of degrading the contrast and resolution in SPECT imaging that result in error in quantification. Thallium decay is very complicated and photons are emitted in a wide range of energies of 68–82 keV. It seems possible to achieve more primary to scatter ratio and better image sensitivity simultaneously if the energy window setting is considered carefully.
Methods: This investigation was performed in three steps: Monte Carlo simulation, phantom experiment and clinical study. In simulation step, the new 4D digital NCAT phantom was used to simulate the distribution of activity (^{201}Tl) in patient torso organs. The same phantom was used to simulate the attenuation coefficient of different organs of the typical patient's body. Two small defects on different parts of left ventricle also were generated for further quantitative and qualitative analysis. The simulations were performed using the SimSET simulator to generate images of such patient. The emissions arising from Tl-201 decay were simulated in four steps using the energies and relative abundances. Energy spectra for primary and scatter photons were calculated. Changing the center and width of energy windows, optimum energy window characteristics were determined. In next step jaszczak phantom was prepared and used for SPECT imaging in different energy windows. In last step SPECT images of patients who had angiographic data were acquired in different energy windows. All of these images were compared qualitatively by four medical physicians independently. Finally a comparison was performed between our suggested window and conventional symmetric window.
Results: The optimum energy window was determined as a wider asymmetric window that its center is not placed on photo-peak of energy spectrum (77keV± 15%). This window increased the primary counts rate and PTSR considerably as compared with the conventional symmetric energy window (67keV± 10%). When this wider asymmetric window acquisition was compared with the conventional symmetric window one on a gamma camera, SPECT images using this asymmetric window clearly showed superior results qualitatively and quantitatively.
Conclusions: our study showed that conventional symmetric energy window (67keV± 10%) is not suitable for Tl-201 imaging and the optimum energy window was determined as 77keV± 15%.

E-mail: faraz241060@yahoo.com and hrajabi@modares.ac.ir

Scatter Correction in SPECT Imaging of Heart Using Deconvolution Method: a simulation study

F.Kalantari [1], H. Rajabi [2]

1- PhD Student, Department of Medical Physics, Tarbiat Modares University
2- Assistant Prof., Department of Medical Physics, Tarbiat Modares University

ABSTRACT

Objectives: Scattered photons are one of the main causes of degrading the contrast of lesions and resolution in SPECT imaging of the heart that result in error in quantification. Usual technique for rejection of scattered photons is through energy windowing; however because of limited energy resolution of current scintillation cameras it is impossible to avoid scatter photons from detection. Modeling of Compton scattering through finding suitable functions was proposed in this study. These functions were used for scatter correction through deconvolution in next step.

Methods: Monte Carlo simulation was used for creating projections of three different activity sources. These activity sources were a line source passed through left ventricle, a point source placed in left ventricle and finally real activity distribution of Tc-99m in torso organs. All of these sources were placed in a digital attenuation phantom which modeled a real patient body. Images of primary and scattered photons were acquired separately. Convolution and 2D deconvolution in Fourier domain was applied for estimating primary projections through total ones.

Results: In first step, scatter and total images were modeled as convolution of a modified exponential function with primary image. The best exponent value was determined for each of 64 views (0.115 to 0.150 according to heart to detector distance). In the next step, these functions were used for scatter correction through deconvolution. Sum of square differences between primary and scatter corrected images were decreased considerably, myocardium to cavity contrast increased for all of 64 views (34% ± 10%). Good agreement between real primary and scatter corrected images also were found ($P \geq 0.46$)

Conclusion: These results indicate that deconvolution technique for scatter compensation can significantly reduce the degrading roles of scattering in quantitative SPECT imaging.

Key words: Scatter, Convolution, Deconvolution, Monte Carlo, SimSET, NCAT, FFT

E-mail: faraz241060@yahoo.com and hrajabi@modares.ac.ir

A new method for attenuation correction in SPECT using dual energy acquisition

Hadi Taleshi Ahangari, Hossien Rajabi, Faraz Kalantari

Department of Medical Physics, Tarbiat Modares University, Tehran, Iran
Correspondence to: **hrajabi@modares.ac.ir**

Abstract:

Introduction: Gamma camera is widely used to detect photons emitted from the patient. Some of these emitted photons suffer from scattering and absorption because of the attenuation occurred through their path in patient's body. Therefore the attenuation is the most important problem in SPECT imaging. Some of the radioisotopes emit gamma rays in different energy levels. And consequently they have different counts and attenuation coefficients. In this study we have tried to correct the attenuation using two images simultaneously acquired from a single object in two energy windows.

Material and Methods:. NCAT phantom with an adequate attenuation coefficient and activity distribution is used in this study. Simulations were done using SimSET in 70±20 KeV and 167±20 KeV. A total of 128 projections were acquired over $360^{0.}$ The simulation repeated using NCAT phantom by SimSET. In the first group, no attenuation correction was used but the Zubal coefficients were used for attenuation correction in the second image group. The corrected and reference images compared UIQI.

Results: After the image reconstruction, a comparison between image groups was done using optimized UIQI to determine the quality of reconstructed images Similarities of images were investigated by considering the average sinograms for every Block-Size. Results showed that the proposed method improved the image quality.

Conclusion and Discussion: The proposed reconstruction method improved image resolution and contrast. Regional and general similarities of images could be determined respectively from acquired UIQI of small and large Block-Sizes. Resulted curves from both small and large Block-Sizes showed a good similarity between reconstructed and ideal images.

Keyword: SPECT, UIQI, Image processing, Attenuation correction, Thallium, NCAT, SimSET

A systematic comparison of absolute quantification schemes for proton magnetic resonance spectroscopy in presence of standing waves

Mahir Sinan Ozdemir [1], Yves De Deene[2], Eric Achten[3], Ignace Lemahieu[1]

[1]Department of Electronics and Information Systems, Medical Image and Signal Processing (MEDISIP), Gent University, Sint-Pietersnieuwstraat 41, Gent, Belgium
[2]Department of Radiotherapy, Gent University Hospital, De Pintelaan185, Gent, Belgium
[3]Department of Radiology, Gent University Hospital, De Pintelaan 185, Gent, Belgium

Introduction: In vivo proton magnetic resonance spectroscopy (^{1}H MRS) offers unique possibilities for non-invasive studies of the neurochemistry of the human brain. In addition, absolute quantification can provide further insight into the evaluation of metabolic changes. With the advantages in SNR and spectral resolution at higher field strengths, there is a growing interest in the application of MRS at 3 Tesla scanners with respect to its 1.5 Tesla counterpart. However, at higher field strength, comparable dimensions of the radiofrequency (RF) wavelength and human head may lead to generation of the standing waves (dielectric effects) which impairs the homogeneity of RF field. In this study, we systematically compared two quantification schemes, namely internal and external reference methods, in presence of standing wave-induced RF inhomogeneity at 3T and 1.5 T field strengths.
Methods: Measurements were performed on a 3 Tesla and a 1.5 Tesla whole-body MR scanner (Siemens), equipped with a knee coil and a head coil, respectively. All the spectra were acquired using a single voxel point-resolved spectroscopy (PRESS) localization with the following parameters: TR/TE = 1500/30 ms, voxel size = 20 mm^3, NEX=128, 1024 data points, spectral width of 1200 Hz. Spherical phantoms (500 ml) were prepared containing aqueous solutions of major brain metabolites (creatine, choline and N-acetylaspartate). 0.5% NaN3 was added as fungicide. NaCl was added in different amounts (0-1.5 % by weight) to change the conductivity and thus the RF penetration into the sample. For the external reference method, metabolite signals were calibrated against the signal obtained from a 20 mM creatine phantom scanned in an additional experiment. Unsuppressed water signal was used as internal reference for the absolute quantification in the second scheme. Signals were corrected for T1 and T2 relaxation effects and coil loading differences (external ref. method.) [1]. The (radiofrequency field) B_1 map was obtained by double-angle method [2]. Curve fitting was performed in the time domain by Linear Prediction Singular Value Decomposition (LPSVD) [3].
Results: The largest variation in B1 map was seen in the non-doped (distilled) water phantom with a dome-shaped flip angle profile (Fig 1a) as a result of standing waves generated as opposed to the 1.5 % NaCl doped phantom (Fig 1b) with a flat B1 profile. The attenuation of the RF penetration as a result of conducting medium leads to a flat flip angle profile. At 1.5 T, due to the increased RF wavelength, B1 profiles were flat for both non-doped and doped phantoms (Fig 2). At 3T, in presence of significant B1 inhomogeneity caused by standing waves, internal reference scheme was found to be more accurate (< 10 % error) than external reference method (15 % error). This can be attributed to the fact that both the reference signal (water) and the metabolite signals originate from the same voxel in the internal reference scheme. Therefore, the impact of B1 inhomogeneity on these signals is the same. This is confirmed by the results obtained in the absence of standing waves that both methods showed similar performance (< 10.5 % error).
Conclusion: Results suggest that in presence of standing waves internal reference is more accurate owing to the fact that reference water signal originates from the same voxel as metabolites of interests. Therefore, any inhomogeneity in any particular voxel effects the signals in a similar manner. However, in the absence of standing waves both methods performed almost identically. It should be noted that our results indicate also the pitfall of using non-doped water phantoms in MR imaging , thereby supporting the previous work [4] .

References: [1] Buchli R et al. NMR in Biomedicine, 7, 225-30 1994 [2] E.K Insko and L. Bolinger JMR, 103, 82-85, 1993 [3] R. Kumerasan and D. W.Tufts IEEE Trans., ASSP, 30, 833, 1982 [4] Tofts P S JMR B, 104, 143-47, 1994.

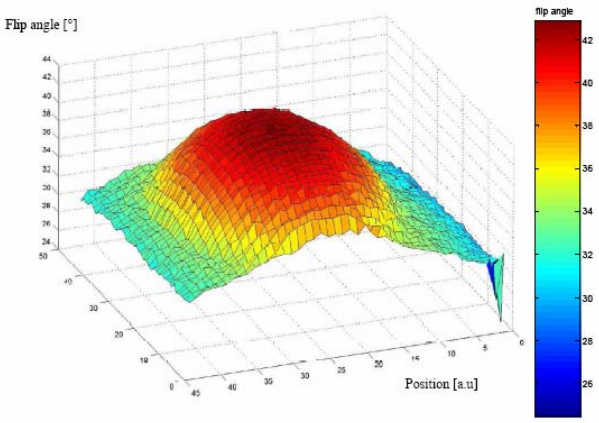

1a) Flip angle profile of a non-doped phantom at 3 T

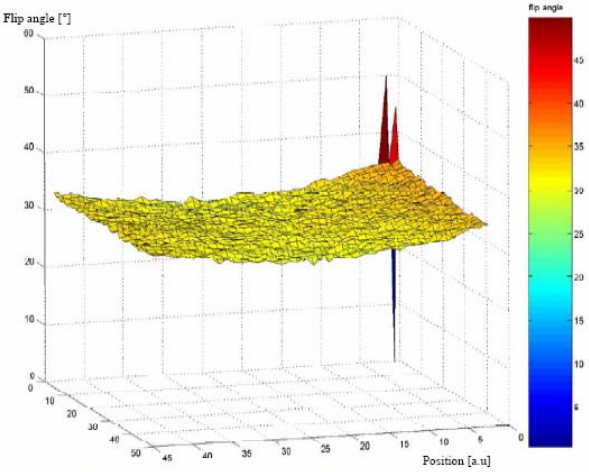

1b) Flip angle profile of a 1.5 % NaCl doped phantom at 3 T

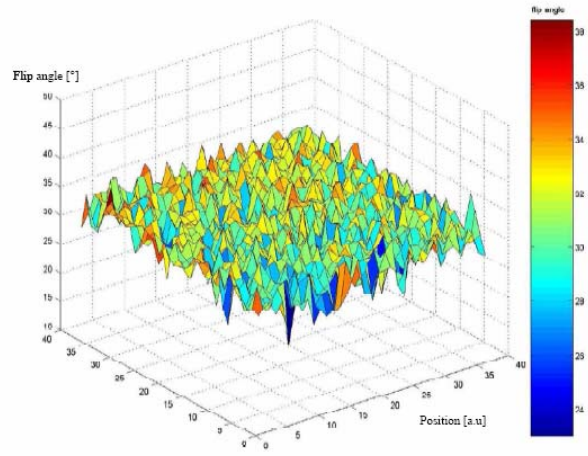

2a) Flip angle profile of a non-doped phantom at 1.5 T

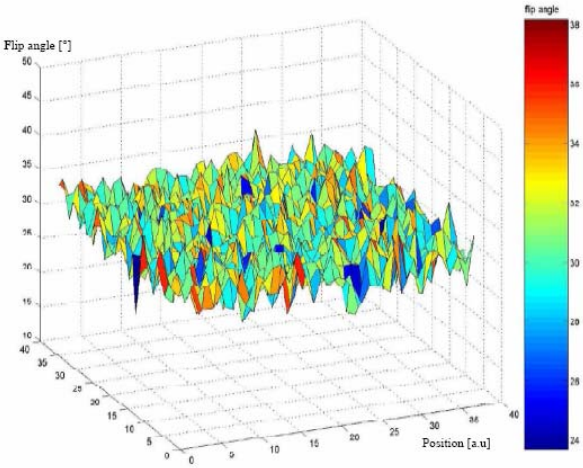

2b) Flip angle profile of a 1.5 % NaCl doped phantom at 1.5 T

MR image quality testing of k-space- and image-based parallel imaging techniques using the ACR phantom

Chien-chuan Chen[1,2], Yau-yau Wai[1,2], Ho-ling Liu[1,2]
1 Department of Diagnostic Radiology, Chang Gung Memorial Hospital, Taoyuan, Taiwan
2 Department of Medical Imaging and Radiological Sciences, Chang Gung University, Taoyuan, Taiwan

Purpose: Using ACR MRI phantom testing to evaluate the change of image quality caused by k-space- and image-based parallel imaging techniques in a 3-Tesla MRI scanner.

Method and Materials: All phantom images are acquired from a 3 Tesla Siemens Tim-Trio MRI scanner. Four sequences, namely ACR T1, ACR T2, Site T1 (IR-TSE, TR/TE/TI=2200 ms/11 ms/900 ms, ETL=5) and Site T2 (TSE, TR/TE=4280 ms/88 ms, ETL=15) , are scanned with each of the conventional, GRAPPA (iPAT=2) and modified SENSE (mSENSE, iPAT=2) modes. Images are analyzed according to standard ACR MRI QC procedures on a PC-based workstation.

Results: The results derived from the phantom images indicating that both of the tested parallel imaging techniques make no significant changes in the degree of the geometric distortion, the high contrast spatial resolution, the measured slice thickness and position accuracy, and the percent image uniformity. The signal-to-noise ratios (SNRs) obtained from all scans are lower while using parallel imaging techniques (SNR_conventional / SNR_GRAPPA = 1.18 +/- 0.08, SNR_conventional / SNR_mSENSE = 1.11 +/- 0.19). The averaged scores of low contrast object detecting test in conventional, GRAPPA, and mSENSE group are 39.3 +/- 0.5, 35.0 +/- 4.4, and 34.3 +/- 3.9, respectively. The percent signal ghosting (PSG) of GRAPPA and mSENSE images are 1.57 +/- 0.72 and 2.26 +/- 1.47 times of that measured in the conventional images. In addition, there is an obvious aliasing artifact observed in the mSENSE groups that cannot be demonstrated by the above data analysis.

Conclusion: The ACR QC test is able to detect the lower SNR, lower contrast detectability, and higher PSG caused by both k-space- and image-based parallel imaging techniques. More accurate measurement of SNR reduction and improved artifact detection require repeated phantom imaging and additional image analysis.

Quantitative proton magnetic resonance spectroscopy without water suppression

Mahir Sinan Ozdemir [1], Yves De Deene[2], Eric Achten[3], Ignace Lemahieu[1]

[1]Department of Electronics and Information Systems, Medical Image and Signal Processing (MEDISIP), Gent University, Sint-Pietersnieuwstraat 41, Gent, Belgium
[2]Department of Radiotherapy, Gent University Hospital, De Pintelaan185, Gent, Belgium
[3]Department of Radiology, Gent University Hospital, De Pintelaan 185, Gent, Belgium

Introduction: Water suppression is a common practice in proton magnetic resonance spectroscopy (^{1}H MRS) in vivo to decrease the dynamic range of the free induction signal (FID) so as to detect low concentration metabolite signals. If the goal is to use the internal water signal for the calibration of metabolite signals in order to conduct absolute quantification of metabolites, an additional measurement is needed to record the water signal. This can be sometimes impractical concerning the current clinical settings. Here, we attempt to perform absolute quantification of metabolites without water suppression in a single measurement. Method is verified by phantom experiments and in vivo measurements in the human brain.

Methods: All measurements were performed on a 1.5 Tesla whole-body MR scanner (Siemens), equipped with a head coil. All the non-water-suppressed spectra were acquired using a single voxel point-resolved spectroscopy (PRESS) localization with the following parameters: TR/TE = 1500/30 ms, voxel size = 15 mm^3, NEX=128, 1024 data points, spectral width of 1000 Hz. Gradient-induced water sidebands were removed from the spectra by correcting the phase of non-water-suppressed FID signal by using the phase of an external reference (water) signal scanned under the same experimental conditions in a separate experiment [1]. High-pass filtering of the phase of this reference FID signal (i.e., $\theta_h(t)$) imparts only the phase fluctuations caused by sidebands. The non-water suppressed FID signal of interest is then multiplied with $\exp(-\theta_h(t))$ correction term to remove sidebands. This correction scheme, by altering the cut-off frequency, enables one to alter the degree to which sidebands are removed from the spectra. A spherical phantom (500 ml) was prepared containing an aqueous solution of major brain metabolites (3 mM choline (Cho),10 mM creatine (Cre), and 12 mM N-acetylaspartate (NAA)). 0.5% NaN3 and 1 % NaCl were added to prevent bacterial invasion and to achieve coil loading, respectively. In vivo measurements were performed in the frontal gray matter of a 30 year old healthy female volunteer. Metabolite signals were extracted from the non-water-suppressed spectra by suppressing the water signal in post-processing by Singular Value Decomposition (SVD) [2]. Prior to performing quantification, signals were corrected for relaxation effects (T1, T2) and differences in number of protons per molecule contributing to each resonance.

Results: The quantified in vitro metabolite concentrations were found to be 3.05±0.27 (Cho), 10.58±0.86 (Cre) and 11.24 ±0.26 (NAA). The maximum systematic variation in the in vitro metabolite concentrations was found to be 10.8 %. The corresponding metabolites in the frontal gray matter were found to be 3.83 mM (Cho) , 4.38 mM (Cre), and 5.54 mM (NAA). Albeit Cho is in accord with the previously published literature values [3], Cre and NAA are underestimated by about 25%. This can be due to the T1 and T2 values extracted from literature to correct for the relation effects in the in vivo spectrum.

Conclusion: Our results show that absolute quantification of metabolites can be carried out without water suppression as opposed to traditional quantification schemes. This removes the need of additional experiment to record water signal and reduces the measurement time drastically (50%). The simple method proposed for sideband removal was found to be efficient. It has the advantage over the two-step gradient cycling methods [4] in terms of simplicity by avoiding any pulse sequence modification which can be difficult at some sites.

References: [1] Ozdemir M et al. ISMRM, pp 2366, 2006 [2] Zhu G et al JMR, 124 (1), 286-89, 1997
[3] Sarcielli P et al Brain,122,513-21, 1999. [4] Clayton D B et al, ISMRM, pp 1602, 1999.

A FEM Simulation study of the optimization of the imaging attributes of a Microwave radiometry system with possible functional imaging capabilities

K. T. Karathanasis, I. S. Karanasiou and N. K. Uzunoglu

National Technical University of Athens, Iroon Polutexneiou 9, Zografou Campus, Athens 15773, Greece

Abstract

A novel Microwave Radiometry Imaging System (MiRaIS) comprising an ellipsoidal conductive wall cavity and sensitive radiometric receivers, operating at low microwave frequencies (1-4GHz), has been used the past four years in various experiments for the assessment of the system as a potential intracranial imaging device [1]. Microwave Radiometry is a measurement technique which detects the natural-thermal radiation emitted by matter. The human brain being at a temperature T and having specific electromagnetic properties emits chaotic radiation throughout the whole electromagnetic spectrum. The measured receiving power quantity is proportional to the product of temperature T, of conductivity σ, and of a field factor, which is a strong function of spatial coordinates [2]. Combining experimental and theoretical data with previous human experimental results, the feasibility of brain conductivity variation imaging during reactions to external stimuli by the proposed system is continuously examined.

During the past few years extensive electromagnetic analysis of the proposed system has been performed by our group using both semi-analytical methods based on Green's function theory and a FEM simulation tool. The theoretical results show that focusing can be achieved in the brain areas of interest with a variety of dimensions of the focusing region and penetration depths related to the operation frequencies used [1]-[2], a feature which is necessary in order to possibly use the system as an intracranial complementary imaging device in practice.

With this view, current research is focused on the improvement of the system's focusing properties using matching layers and spheres made of dielectric materials and left handed materials that were placed around a double layered human head model. Another approach followed in the framework of the present research included filling the whole ellipsoidal with a lossless dielectric material in conjunction with a reduction of the ellipsoid's volume (25% smaller than original size). The simulations of the system were performed using a FEM commercial tool. The results show that combined use of left handed and dielectric materials can provide better focusing on the brain areas of interest by reducing the number and intensity of undesirable secondary foci points. Also, the use of those materials renders focusing of electromagnetic energy more sensitive to relative movements of the head around the ellipsoidal's focal point. Future research including mainly phantom experiments implementing the above ideas will illustrate the value of the present simulation study.

References

[1] Irene S. Karanasiou, and Nikolaos K. Uzunoglu, "**Single-frequency and Multiband Microwave Radiometry for feasible Brain-Conductivity Variation Imaging during Reactions to External Stimuli**", Nuclear Instruments and Methods in Physics Research A 569 (2006) 581–586.

[2] I. S. Karanasiou, N. K. Uzunoglu and C. Papageorgiou, "**Towards functional non-invasive imaging of excitable tissues inside the human body using Focused Microwave Radiometry**", *IEEE Transactions on Microwave Theory and Techniques*, vol. 52, no. 8, pp. 1898-1908, Aug. 2004.

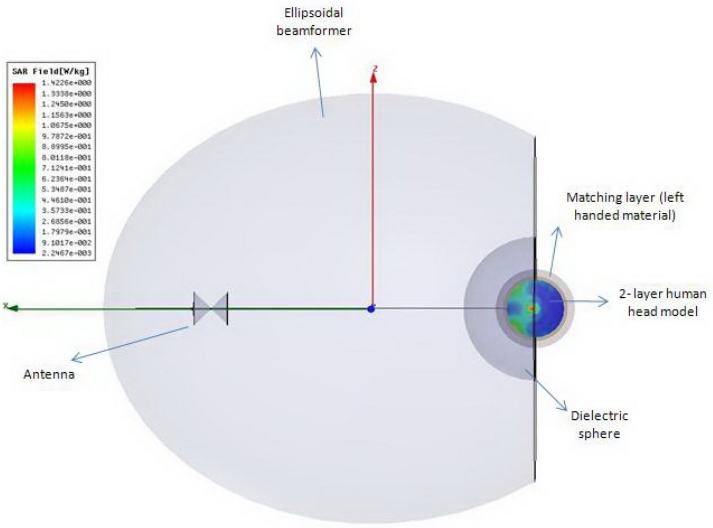

Figure. SAR distribution inside the brain (gray matter) at 1GHz.

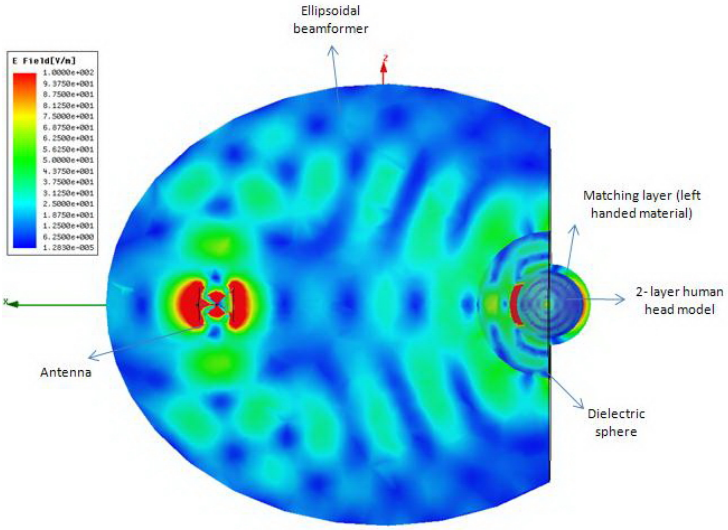

Figure. E-field distribution inside the ellispoidal and human head model at 1GHz.

Investigation on Activity from Outside the Field of View in the ClearPET™ Neuro using Monte Carlo Simulations

A. M. Fulterer[1,3], B. Gundlich [1], P. Musmann[1], S. Schneider[1,2], S. Weber[1]
(1) Zentralinstitut für Elektronik, Forschungszentrum Jülich GmbH, D-52425 Jülich, Germany
(2) Department of Mathematics and Technology, RheinAhrCampus, 53424 Remagen, Germany
(3) Institute of Material Physics, TU Graz, A-8010, Austria
Corresponding author: S. Weber, s.weber@fz-juelich.de

Small-animal positron emission tomography (PET) is a non invasive medical imaging technique that enables to image the physiological function of a given metabolically active substance in small animals with high resolution and high sensitivity. Among the recently developed small-animal PET systems is the ClearPET™ family [1] which was developed by the Crystal Clear Collaboration. Among them, the ClearPET™ Neuro was developed mainly for rat brain studies.

Not only true coincidences are detected during a PET study. Coincidences where one or both photons have undergone Compton scattering, and random coincidences from different annihilations have to be corrected for, otherwise they reduce the image quality. In rat brain studies ativity not only accumulates in the brain, but also in the bladder and heart, which are often positioned outside but close to the edge of the field of view. This activity from outside the field of view (OFOV) can result in the detection of scattered and random events. First investigations have shown that these events show up as background which varies along the axis of the scanner [2].

In this work, scattered and random events from OFOV were analysed using Monte Carlo Simulation with the MC Simulation Toolkit GEANT4 [3] for the ClearPET Neuro. The amount of detected coincidences with origin outside of the FOV was analyzed with respect to OFOV source distance, phantom or animal size, and a detailed consideration of the different parts of the gantry (e.g. animal bed, detector shielding etc.).

Scattering material inside the FOV, e.g. the animal bed, is responsible for about 20% of scattered events with a 30 mm diameter phantom. Other parts of the gantry do not contribute significantly to gantry scatter. Coincidences from simulations with OFOV activity in phantoms of different sizes are classified according to the contribution of scattered and unscattered photons from the same or different annihilations. The further the phantom reaches into the field of view, the more OFOV coincidences are detected with one or even both of the photons scattered. This is the case for true coincidences, where both photons arise from the same annihilation, as well as random coincidences, where photons from different annihilations are detected in the same coincident time window.

Using this classification on coincidences from simulations with line source in the FOV and an interfering source outside, made evident that the main source of OFOV events are scatter within the animal and the animal bed, and that shielding the object decreases the number of OFOV random events, but at the expense of more scattered events from activity inside the FOV. Thus, it is important to correct for scattered and random events from OFOV activity.

References:

1 K. Ziemons et al. The ClearPET.LSO/LuYAP phoswich scanner: a high performance small animal PET system. Page: 1728, IEEE Nuclear Science Symposium: conference record. , 2003.
2 B. Gundlich et al. Scatter Studies for Neuroimaging with ClearPET Neuro (poster), 2005.
3 S. Agostinelli et al. Geant4 - A Simulation Toolkit. Nuclear Instruments and Methods in Physics Research, A 506:250303, 2003.

On the use of high field strength and parallel imaging techniques for MRI-based polymer gel dosimetry of radio-surgical beams*

A. Moutsatsos[1)], L. Petrokokkinos[2)], I. Kantemiris[2)], O. Benekos[3)], E. Efstathopoulos[3)], P. Papagiannis[1)], V. Spevacek[4)], J. Semnicka[4)], P. Dvorak[4)] and I. Seimenis[5)]

[1)] *Medical Physics Department, Medical School, University of Athens, 75 Mikras Asias, 11527, Athens, Greece*
[2)] *Nuclear and Particle Physics Section, Physics Department, University of Athens, Panepistimioupolis, Ilisia, 157 71 Athens, Greece*
[3)] *University of Athens, Attikon University Hospital, 2nd Department of Radiology,University of Athens, 12462, Chaidari, Greece*
[4)] *Czech Technical University, Faculty of Nuclear Sciences and Physical Engineering, Department of Dosimetry and Application of Ionizing Radiation, Brehova 7 115 19, Praha 1, Czech Republic*
[5)] *"Ayios Therissos" Medical Diagnostic Center 92 Troodous Ave., P.O. Box 28405, 2033 Strovolos, Nicosia, Cyprus*

Aqueous solutions of appropriate monomers along with gelatin form a gel matrix where polymerization occurs following irradiation. Magnetic Resonance Imaging (MRI) can quantify the polymerization induced changes on the material's transverse relaxation rate (R2), and translate them to absorbed dose distributions. Polymer gel-MRI dosimetry is of acknowledged potential for dose verification in stereotactic radio-surgery techniques that employ narrow beams in order to increase dose conformity to the target lesion while sparing healthy nearby structures, since it obviates many of the problems associated with the use of conventional dosimeters. Besides its potential, polymer gel dosimetry has not been widely introduced into the clinical routine as a QA tool owing, inter alia, to the increased time of the MRI scanning session necessitated to meet the rigorous spatial resolution demands of radio-surgery dose verification. This work discusses whether this obstacle could be alleviated by exploiting the use of 3T imagers and parallel imaging techniques.

Polymer gel filled vials were irradiated in a Leksell Gamma Knife unit which employs a hemispherical configuration of 201 ^{60}Co sources, a stable primary collimator system and four final collimator helmets to form beams of 4, 8, 14 and 18 mm nominal diameter at the mechanical center of the machine. Single or double shots of these beams were programmed and delivered to the vials using the same stereotactic frame fixated to the patients' heads to achieve sub-mm, spatial dose delivery accuracy. The irradiated gel vials were scanned on a 1.5T imager with a 0.5mmx0.5mm in-plane spatial resolution and 0.75 mm slice thickness using a 32 echo, CPMG pulse sequence with 3000 ms repetition time and 40 ms inter-echo spacing (scan A). Given the interplay between increased SNR at higher field strengths, which can be translated to higher resolution images and/or faster acquisitions, and decreased SNR when parallel imaging techniques are used to speed up acquisition, the gels also underwent three scanning sessions on a 3.0 T imager; One using sensitivity encoding (SENSE) and the same spatial resolution as in scan A (scan B), one with a finer in-plane resolution than in scan A (0.3mm x 0.3mm, scan D), and one with the same high in-plane resolution as in scan D but with the implementation of SENSE (scan G).

Custom made, three dimensional processing tools were utilized to derive dose-R2 calibration data from all four scans and compare them for precision and dose resolution. Relative dosimetry results derived by scan A were benchmarked against Monte Carlo simulation calculations employing the FLUKA general purpose code and compared to corresponding results derived by the other three scans in the form of two dimensional distributions using the gamma index criterion for distance- and dose-to-agreement. Experimental results of all four scans for the beam Output Factors, a dosimetric quantity pertinent to Gamma Knife units, as well as the volume averaging effect in dosimetry of the Gamma Knife beams are also presented and compared to corresponding Monte Carlo simulation calculations.

Findings suggest that careful planning of MRI scanning based on a figure of merit that accounts for the cost in scanning time and precision for a given increase in spatial resolution, could facilitate the introduction of polymer gel dosimetry into the clinical setting as a practical QA tool for complex radio-surgery techniques.

* **Acknowledgement:** This work was supported in part by a Czech-Greece joint research and technology program (2005-2007).

Integrating multiscale active contours and region growing for microcalcifications segmentation in mammography

Nikolaos Arikidis[1], Spyros Skiadopoulos[1], Anna Karahaliou[1], Eleni Likaki[2], George Panayiotakis[1], Lena Costaridou[1]

[1] Department of Medical Physics, School of Medicine, University of Patras, 265 00 Patras, Greece
[2] Department of Radiology, School of Medicine, University of Patras, 265 00 Patras, Greece

email: costarid@upatras.gr

Accurate segmentation of microcalcifications in mammography is crucial for their automated classification into benign or malignant types, based on morphology extracted features (shape and contrast) [1,2]. Difficulty in microcalcification segmentation is due to their small size (calcifications associated with cancer are usually ≤0.5 mm in size) and to their small contrast in case of dense breast parenchyma [3]. Proposed methods for microcalcifications segmentation rely either on region homogeneity (e.g. thresholding, region growing) or on image contours (e.g. active contours [4], watersheds, radial gradients [5]) with radial gradient-based methods demonstrating improved performance.

In this work, a method that combines multiscale active contours in B-spline representation and region growing is proposed. Use of B-spline active contours alleviates the need for determining weights associated with smoothness constraints. A microcalcification centered region of interest (ROI), with the seed pixel annotated by an experienced radiologist, is decomposed into 3 dyadic scales using a B-spline redundant dyadic wavelet transform [6]. The active rays method is applied at eight orientations of the 3rd scale to define eight elements that approximate microcalcification boundaries, subsequently refined at the 2nd scale. Region growing method is applied on a processed version of the original ROI (reconstructed from the corresponding detail wavelet coefficients only), which is initialized by the annotated seed pixel. The previously defined active rays elements are used to constrain region growing and obtain the final microcalcification boundary.

The method was tested on dataset of 149 microcalcification clusters (87 benign, 62 malignant), originating from the DDSM database. An observer study was conducted to evaluate segmentation accuracy of the proposed method, on a 5-point rating scale (from 5:excellent to 1:very poor), and to compare it with the radial gradient-based method. The accuracy rating was 3.96±0.77 for the proposed method and 2.91±0.86 for the radial gradient-based method. The effect of the proposed segmentation method in the performance of automated classification of benign from malignant clusters was also investigated. A Least Square Minimum Distance classifier was employed based primarily on morphology descriptors of the individual microcalcifications and cluster distribution, achieving an area under the receiver-operating characteristic (ROC) curve 0.91 in patient-based performance.

An accurate algorithm is proposed for segmenting microcalcifications, integrating region and boundary information. Active rays allow fast computations, while their application on B-spline multiscale representation reduces the number of free parameters. The proposed method can contribute in computer-aided diagnosis in breast cancer.

References

[1] W. J. H. Veldkamp and N. Karssemeijer: Accurate segmentation and contrast measurement of microcalcifications in mammograms: A phantom study, Med. Phys., 25, 1102-1110 (1998).
[2] M. Kallergi: Computer-aided diagnosis of mammographic microcalcification clusters, Med. Phys. 31, 314-326 (2004).
[3] D. B. Kopans, Breast Imaging: Lippincott Williams, Jan 1998.
[4] I. N. Bankman, T. Nizialek, I. Simon, O. B. Gatewood, I. N. Weinberg and W. R. Brody: Segmentation algorithms for detecting microcalcifications in mammograms, IEEE Trans. Inform. Tech. Biomed. 1, 141–149 (1997).
[5] S. Paquerault, L. M. Yarusso, J. Papaioannou, Y. Jiang, and R. M. Nishikawa: Radial gradient-based segmentation of mammographic microcalcifications: Observer evaluation and effect on CAD performance, Med. Phys. 31, 2648-2657 (2004).
[6] S. Mallat, A wavelet tour of signal processing: Academic Press, 2001.

FOCUSED MICROWAVE RADIOMETRY FROM A POSSIBLE FUNCTIONAL IMAGING PERSPECTIVE: THEORETICAL OPTIMIZATION OF THE PROPERTIES OF A MICROWAVE RADIOMETRY SYSTEM

M.I.Giamalaki*, I.S.Karanasiou* and N.K.Uzunoglu*

* Microwave and Fiber Optics Laboratory, School of Electrical and Computer Engineering, National Technical University of Athens, Greece

melina@esd.ece.ntua.gr

The development of medical imaging techniques such as positron emission tomography (PET) and magnetic resonance imaging (MRI) gave researchers interested in the function of the human brain, the opportunity to examine noninvasively the neurobiological correlates of human behaviour. A non-invasive imaging system, that consists of an ellipsoidal conductive cavity and a radiometric receiver, for brain imaging applications based on the microwave radiometry technique, has been designed and constructed in our laboratory during the past few years [1]-[3]. Experimental data provide promising results concerning the system's capability of detecting temperature and conductivity variations in phantoms and biological tissues and thus, possibly opens up new prospects of contributing to the examination of brain function. The novelty of this imaging method lays in the use of the ellipsoidal as it provides convergence of the radiated electromagnetic energy from the human brain placed on one focal point on the other focus where the receiver is placed.

The focusing ability of the system in specific cortical areas with the desired spatial resolution and detection depth is of great importance for the evaluation of the system as a possible complementary clinical tool. In this context towards the enhancement of the system's focusing properties, in previous recent work carried out by our group, the receiving antenna was covered by two layers of different dielectric properties [4]. Moving on to a further stage the receiving antenna was more realistically modelled by two parallel current line sources in order to minimize artefacts deriving from the antenna modelled by a single current source. Based on the results of this theoretical electromagnetic analysis, a means for further improvement of the focusing properties of the ellipsoidal reflector is herein investigated. The main differentiating factor of our new approach is that a thin lossless dielectric layer is placed on the surface of the human head model for further focusing improvement.

Specifically, a double layered cylindrical human head model surrounded by a third dielectric cylinder is placed on one focal point of the elliptical reflector, while the receiving antenna, modelled by two parallel current line sources of infinite length and opposite sign, is surrounded by a double-layered dielectric cylinder of the same size and placed on the other focal point. The geometry of the problem is depicted in Fig.1.

For the purposes of the present research, the scope of modelling the field distribution inside an ellipsoidal conductive cavity in the presence of a human head, and especially the focusing properties of the elliptical reflector, is pursued through the implementation of a semi-analytical technique, which is based on the use of the dyadic's Green's function theory. The present paper provides details on the electromagnetic theoretical analysis of the problem and presents numerical results for the electric field distribution inside the head model when its centre is set at the first focal point where the double layered cylinder centre is placed on the other focal point and the two current sources are placed at the centre of the dielectrics, when it is placed in various positions inside the ellipse while keeping still the sources surrounded by the dielectric cylinder on the focal point, when its centre is placed on the focal point while both the current sources and the dielectric cylinder are moved and finally when it is kept still on the first focal point and the centre of the double-layered dielectric cylinder also remains on the other focal point while the sources are placed in various positions without however, altering their distance from one another. Three main operating frequencies are used, namely 0.5GHz 1GHz and 1.5GHz for the four distinct cases presented within this paper. Subsequently, several trials are conducted with a matching layer that covers the head model having various dielectric properties while its thickness varies from 1cm to 2 cm.

The above mentioned scenarios are investigated in order to assess the focuisng optimization of the system in terms of spatial accuracy and penetration depth. The latter and the spatial resolution characteristics of the discussed cases at the three operating frequencies are obtained while the method and results are also separately validated. The results show improvement of the system attributes by using the above mentioned matching material setups whereas artefacts present in previous studies deriving from the antenna modelled by a single current source, have been minimized. Ongoing research focuses on placing a thin dielectric layer consisting of left handed metamaterial, on the surface of the human head model for further focusing improvement.

References

1. I. S. Karanasiou, N. K. Uzunoglu and C. Papageorgiou, "Towards functional non-invasive imaging of excitable tissues inside the human body using Focused Microwave Radiometry", *IEEE Transactions on Microwave Theory and Techniques*, vol. 52, no. 8, pp. 1898-1908, Aug. 2004.
2. I S. Karanasiou, M.I. Giamalaki, A. Oikonomou and N. K. Uzunoglu, "Passive four frequency microwave tomography: an experimental feasibility study", IFMBE Proceedings, Vol. 11, pp. 2086-1 to 2086-5. Prague: IFMBE, 2005.
3. I.S.Karanasiou, M.I.Giamalaki, A.T.Oikonomou, G.C.Trichopoulos, N.K.Uzunoglu, "Three dimensional passive brain microwave radiometry imaging", poster presentation, 5th Conference of the German-Greek Academy for Biomedical Research, June 16-18,2006,Athens, Greece,[abstracts book], pp 26-28
4. M.I.Giamalaki, I.S.Karanasiou, N.K.Uzunoglu,"Electromagnetic Analysis & Optimization of the Focusing Properties of a Passive Microwave Imaging System", Proceedings of the 5th European Symposium on Biomedical Engineering, P.21, July 7-9, 2006, Patras, Greece.

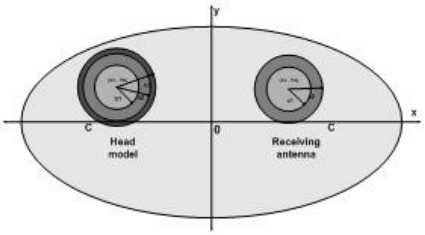

Figure 1a: The geometry of the problem

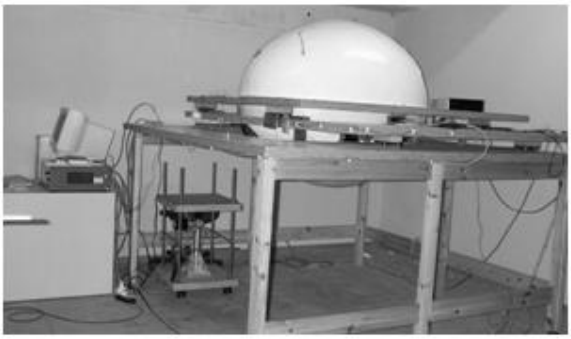

Figure 1b: The existing imaging system.

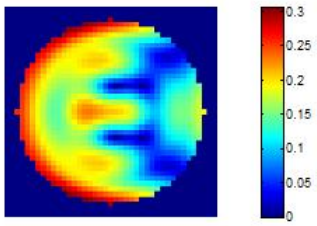

Figure 1c: Results at 0.5GHz when the centre of the head model is placed at the first focal point while the double layered cylinder centre is placed at the other focal point and the two current sources are placed at the centre of the dielectrics. The thickness of the layer that covers the head is 1cm.

Investigating the dependence of breast calcifications Signal to Noise Ratio on mammographic spectra: Monte Carlo simulation studies

H Delis [1], V Vlachopoulou [1], G Spyrou [1,2], L Costaridou [1], G Tzanakos [3] and G Panayiotakis [1]

[1] University of Patras, Faculty of Medicine, Department of Medical Physics, 265 00 Patras, Greece
[2] Academy of Athens, Biomedical Research Foundation, 115 27 Athens, Greece
[3] University of Athens, Department of Physics, 157 71 Athens, Greece

A Monte Carlo simulation model is utilized to study the influence of mammographic spectra on the Signal to Noise Ratio (SNR) of simulated inhomogeneities representing calcifications of various thicknesses, embedded inside a mathematical breast phantom.
The model includes a semicylindrical phantom, mimicking a physical phantom for mammography, with background consisting of material simulating glandular breast tissue. A step wedge arrangement with foils composed of Hydroxyapatite, which is a common calcification material, was embedded. Monte Carlo methods have been used to sample the initial x-ray photon energy from the selected mammographic spectra, and trace the photons inside the breast, simulating x-ray interactions and photon transport phenomena, taking into account all possible physical processes (Spyrou *et al.*, 1998). For the purposes of this study, only the third dimension (thickness) of calcifications was kept in realistic size, since it is the one related with the influence of the x-ray spectrum on the image, while the calcifications visibility with respect to their projection size is mainly affected by the resolving power of the imaging system.
The visualization of different calcifications thicknesses, described in terms of SNR, strongly depends on all the parameters affecting the x-ray spectrum (Delis *et al.*, 2006). Tube voltage strongly affects SNR of small and medium thickness calcifications. The common Mo/Mo spectrum demonstrates improved characteristics, with SNR differences up to 14%, with respect to Rh/Rh for the entire thickness range of calcifications studied. Increase in filter thickness decreases SNR for calcification thicknesses less than 1200 μm, while after this point increased filter thickness results in improved SNR. As far as the filter material is concerned, the thicker calcification to be visualized, the higher the k-absorption edge of the filter required, in order to achieve the maximum SNR.

References

Delis H, Spyrou G, Costaridou L, Tzanakos G and Panayiotakis G 2006 Suitability of new anode materials in mammography: Dose and Subject Contrast considerations using Monte Carlo simulation *Med. Phys.* **33** 4221-35.
Spyrou G, Tzanakos G, Bakas A and Panayiotakis G 1998 Monte Carlo generated mammograms: development and validation *Phys. Med. Biol.* **43** 3341-57.

Potential brain imaging using near field radiometry

A. Oikonomou*, I.S. Karanasiou** and N.K. Uzunoglu**
*School of Applied Mathematics and Physics
**School of Electrical and Computer Engineering
National Technical University of Athens, 9 Iroon Polytechneiou str, 15773, Zografou, Greece

aoikon@esd.ece.ntua.gr

During the past decades there has been a tremendous increase throughout the scientific community for developing methods of understanding human brain functionality. Diagnosis and treatment of diseases and malfunctions could not be developed without fully understanding how the brain works. Several methods have been proposed and investigated, such as positron emission tomography (PET) or magnetic resonance imaging (MRI). By mapping the human tissues one could potentially evaluate their function. In parallel, research effort focuses on minimizing drawbacks of existing imaging techniques including potential risks from radiation and invasive attributes of the imaging methodologies.

With this view and based on previous findings that support the possibility of using focused microwave radiometry for imaging of temperature and/or conductivity variations of subcutaneous tissues [1, 2], a new, prototype, portable and totally non invasive imaging system is herein proposed.

Towards that direction and in order to potentially add to the investigation of the mechanisms of human brain functionality we are proposing a near field radiometry imaging system for intracranial applications

This methodology is based on the fact that human tissues emit chaotic thermal type radiation at temperatures above the absolute zero at microwave frequencies. To increase resolution, sensitivity and penetration depth an optimum number of receiving antennas is placed around the head, all operating at the same frequency, 3 GHz, but with different offset phases. This way the signal received is strengthened and can then be processed for further analysis. The proposed system in conjunction with appropriate psychophysiological tests may be able to pick up brain activation through detection of conductivity differences in various cortex areas in a non-invasive totally harmless manner, providing potentially complementary information to existing standardized imaging techniques

To make the proposed device useful for clinical applications it must provide a well defined focusing detection area at the brain parts of interest. Towards this direction, several simulated trials have been performed so as to explore and validate the best configuration of the phased array antennas. Simulated trials have verified the ability of such a system to detect radiometric signals from subcutaneous tissues from a depth to up to 4 cm.[3] This is achieved by placing the antennas 2cm above the head or by placing a 1cm thick LHM in the head-patch interface. Further analysis, however, shows that when the full system is simulated LHM causes unwanted dispersion to the signal received, and thus, cannot be considered useful for the purpose required [4]. To enhance the focusing properties of the system lossless dielectric matching materials under the area of the conformal array, are used. Use of dielectrics provides a clear and concrete focal point under the area of interest, as shown in Fig1 and Fig2. The thickness of the dielectric, as well as its dielectric constant, influences the results. Simulated trials have shown that when the dielectric exceeds 2 cm thickness and/or the dielectric constant of the lossless matching media is higher that er values between 6 and 7 the focus ability of the system is strongly decreased.

Concluding, a portable, non-invasive, phased-array system of four conformal patch antennas operating at 3 GHz, could be able to detect conductivity changes of human cortical areas . To achieve this, however, careful placement, configuration and choice of dielectric materials for matching should be applied.

References

1. I. S. Karanasiou, N. K. Uzunoglu and C. Papageorgiou, “Towards functional non-invasive imaging of excitable tissues inside the human body using Focused Microwave Radiometry”, IEEE Transactions on Microwave Theory and Techniques, vol. 52, no. 8, pp. 1898-1908, Aug. 2004
2. Irene S. Karanasiou, Nikolaos K. Uzunoglu, “Single-frequency and Multiband Microwave Radiometry for feasible Brain-Conductivity Variation Imaging during Reactions to External Stimuli”, Nuclear Instruments and Methods in Physics Research A 569 (2006) 581–586
3. Oikonomou A.T, Karanasiou I.S, Uzunoglu N.K, (2006) “Conformal patch antenna for human brain imaging using near field radiometry”, 5th ESBME, Patras, Greece
4. Oikonomou A.T., Karanasiou I.S, Uzunoglu N.K. (2007), “Conformal phased array antennas for human brain imaging using near-field-radiometry” URSI 2007, Ottawa, ON, Canada

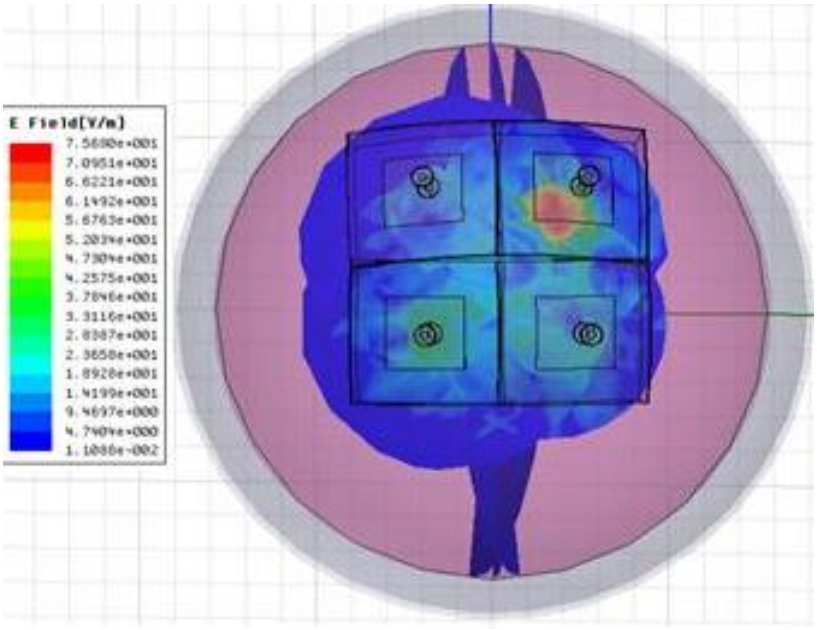
E Field[V/m]
7.5680e+001
7.0951e+001
6.6221e+001
6.1492e+001
5.6763e+001
5.2034e+001
4.7304e+001
4.2575e+001
3.7846e+001
3.3116e+001
2.8387e+001
2.3658e+001
1.8928e+001
1.4199e+001
9.4697e+000
4.7404e+000
1.1088e-002

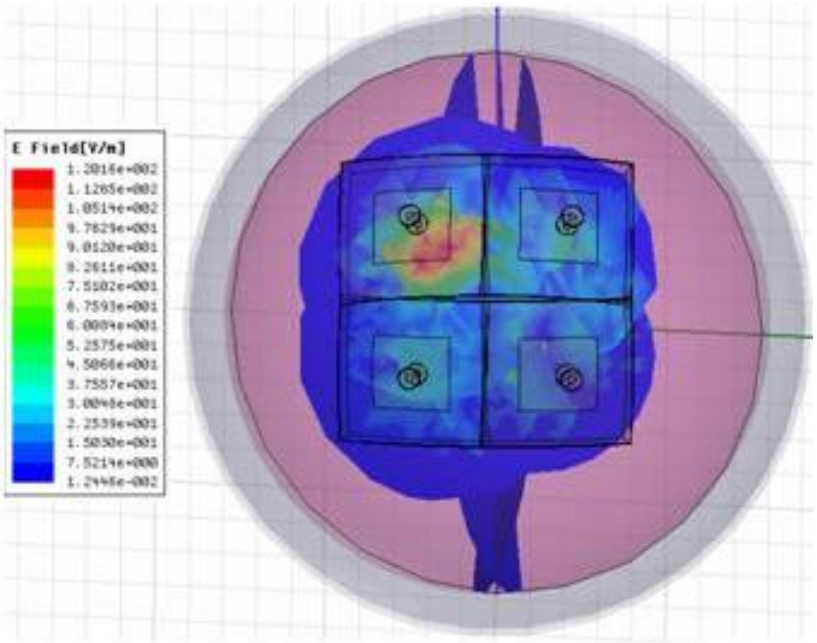
E Field[V/m]
1.2016e+002
1.1265e+002
1.0514e+002
9.7629e+001
9.0120e+001
8.2611e+001
7.5102e+001
6.7593e+001
6.0084e+001
5.2575e+001
4.5066e+001
3.7557e+001
3.0048e+001
2.2539e+001
1.5030e+001
7.5214e+000
1.2446e-002

Use of a stereo-vision system for head motion correction for PET acquisitions.

Jeroen Verhaeghe*, Xiaoyan Zhao, Stefaan Vandenberghe, Long Zhang, Steven Staelens, Yves D'Asseler and Ignace Lemahieu

Department of Electronics and Information Systems, MEDISIP, Ghent University-IBBT-IBiTech,

De Pintelaan 185 block B, B-9000 Ghent,

Abstract

Aim: Patient motion during a PET acquisition is an important source of artifacts in the reconstructed image. Different techniques already exist to perform motion correction. In this work we investigate the possibility of using a low cost stereo vision system based on two optical CCD cameras for the registration of head motion during a list-mode brain PET acquisition. A calibration procedure to align the PET and the portable stereo camera is developed and evaluated. A method is proposed to estimate the rigid body motion from the stereo images. The method uses a checkerboard target to track the head motion. From the estimated motion the PET list-mode events can be motion-corrected and a motion free image is reconstructed. To evaluate our procedure we performed a phantom study on a PET scanner.
Methods: We used a stereo-camera consisting of two CCD cameras on a stereo rig. A portable system was considered so that it could be used for different studies on various scanners. The stereo-PET camera alignment procedure makes use of a radioactive point source. The procedure consists of acquiring five short PET scans of the point source located at five different positions within the field-of-view of both the PET and stereo camera. From the reconstructed PET images and the simultaneously acquired stereo images an orthogonal transformation matrix relating the stereo coordinate system to the PET coordinate system is calculated. This involved a sub-pixel localization of the point in the PET image. After the two systems are aligned by the calibration procedure a 28 minutes PET acquisition was performed of one slice of the Hoffman brain phantom. The phantom was moved six times with intervals of 4 minutes. The motion was captured by the stereo-camera. A 7x6 checkerboard (8.4x7.2 cm^2) target was pasted onto the phantom. The motion transformation (correction) matrix can be calculated from the 30 corner points of the checkerboard before and after the motion. After calculating the corner points and the transformation matrix in the stereo images a transformation to the PET coordinate system is performed. The estimated correction transformation is applied to the end points of the measured Lines Of Response (LOR). From the corrected LORs a motion corrected image is reconstructed and is compared with the non-corrected reconstruction.
Results: The aforementioned calibration method (using the reconstructions of a point source) was accurate to within the spatial resolution of the PET scanner. This was verified by considering a PET reconstruction of the 5 point source data-sets which were transformed so that all the points were reconstructed to the same initial position. The FWHM of this reconstruction was 6.3 mm. The FWHM of the five individually reconstructed points was 6.1 +/- 0.2 mm. The Hoffman phantom results are shown in figure 1. It can be observed in the figure that the non-motion corrected reconstruction has lost almost all details while the motion corrected reconstruction shows the important details of the phantom.

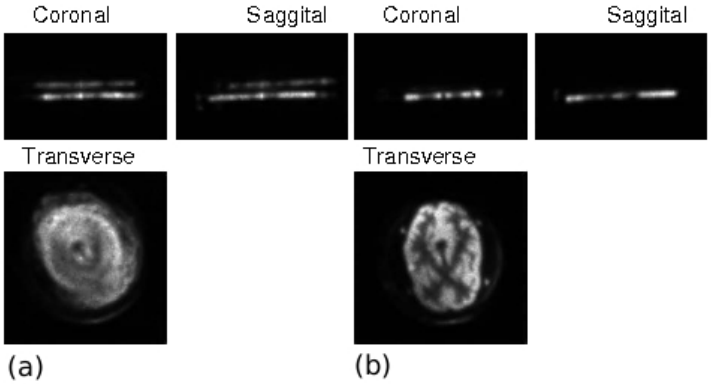

Figure 1: Non-corrected (a) and motion corrected (b) reconstructed images of the Hoffman phantom slice.

* Corresponding author. Tel.: +32 (0)9 240 46 22 ; e-mail: jeroen.verhaeghe@ugent.be

On the accuracy of a mutual information algorithm for PET-MR image registration

P. Karaiskos,[1] J.Malamitsi,[1] J. Andreou,[2] V. Prassopoulos,[3] B. Valotassiou,[3] F. Laspas,[2] C. Paraskevopoulou,[4] P. Sandilos[4] and M. Torrens[4]

[1] University of Athens, Medical School, Medical Physics Department, Athens, Greece
[2] CT – MR Department, Hygeia Hospital, Athens, Greece
[3] PET/CT Department, Hygeia Hospital, Athens, Greece
[4] Medical Physics and Radiosurgery Departments, Hygeia Hospital, Athens, Greece

Multimodality image registration and fusion has been increasingly used in radiation diagnosis and treatment planning. In these techniques three-dimensional (3D) images obtained from different imaging modalities (e.g. MRI, PET and CT) are spatially superimposed thus providing comprehensive information about the patient under study. Especially for brain lesions accurate 3D registration and overlay of MR and PET images provide important additional information by relating functional information from PET images to the detailed anatomical information available in MR images. Registration between MR and PET images can be performed using either point-based external marker techniques or automated registration techniques. For automatic registration, the method of maximization of mutual information (MMI) is a theoretically sound and increasingly accepted image registration technique in clinical practice. For MR – CT image registration this method is well tested and validated. However for the case of PET-MR, image registration is complicated by a lack of conspicuous anatomical features and a deviation from the rigid-body model. In this work the mutual information algorithm incorporated in a commercially available treatment planning software is tested. Ten patients with brain lesions underwent MR and PET/CT scanning. MR-PET registration was performed a) based on the well validated MR-CT registration technique and copying the transformation to the PET images derived from the PET/CT scan (hereon called MR/PET/CT registration method) and b) directly from the MR and PET images without taking into account the CT images (hereon called MR/PET registration method). In order to check the registration accuracy of the MR/PET method, the lesion (target) was contoured in the PET images and it was transferred to the MR images using both the above methods. The MR/PET/CT method served as the gold standard for target contouring. Target contours derived by the MR/PET method were compared with the gold standard target contours for each patient and the deviation between the two contours was used to estimate the accuracy of the PET-MR registration method. This deviation was less than 2 mm (i.e. within the spatial resolution of the PET images) for the vast majority of the cases studied. Results show that the mutual information algorithm used is able to perform the PET-MR registration reliably and accurately.

On the feasibility of real time imaging in radiotherapy using antiproton beams[1]

I. Kantemiris [*], P. Karaiskos [+], E. Georgiou [+], A. Angelopoulos [*], N. Giokaris [*]
[*]University of Athens, Physics Dpt., Division of Nuclear & El. Particle Physics, Greece
[+]University of Athens, Medical School, Medical Physics Department, Greece

The scientific interest in the use of antiproton beams for radiation therapy and imaging, which started three decades ago, was recently been renewed owing both to their advantageous dosimetric characteristics (their Relative Biological Effect, RBE, may be close to that of carbon beams) and the potential they offer for real time imaging. In this study we investigate the feasibility of real time imaging during radiotherapy using antiproton beams. The FLUKA general purpose Monte Carlo code was used at this stage to simulate a typical prostate irradiation using one beam. The spread out Bragg peak (SOBP) was formed by the energy spectrum of the antiproton beam (102 – 120 MeV). A unique feature of antiprotons is that they undergo annihilation with a nucleon at the end of their path. Each of the antiproton annihilations offers ~1.88GeV additional energy shared between the masses and kinetic energy of the produced secondary particles, and the kinetic energy of the residual nuclei formed following annihilation. Most of the secondary particles (pions and photons) escape the irradiated phantom and could therefore be utilized for real time imaging. Figure 1 presents the energy spectra of the secondary particles produced at the annihilation point upon delivery of a typical dose fraction of 2Gy to the target. Results show that real time imaging during radiation therapy with antiprotons is feasible since an adequate number of either photons or charged pions are produced. It should also be noted however that a number of neutrons with energies up to 800MeV are also produced and this could increase the shielding requirements of the installation.

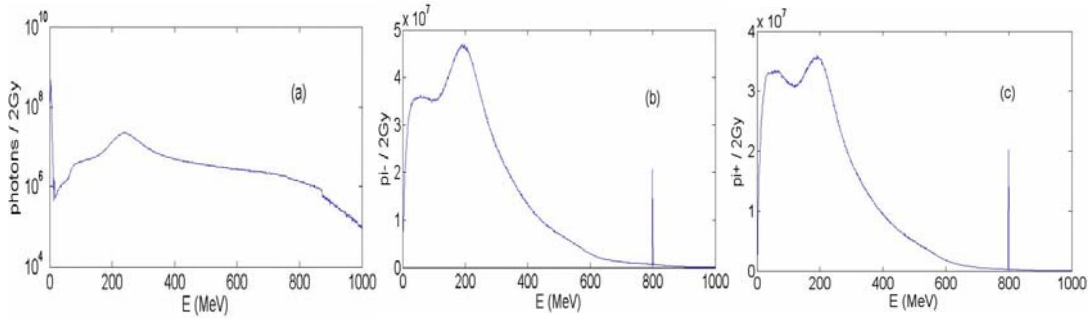

Fig. 1 Energy spectrum of the photons (a), negative (b) and positive pions (c) which are produced by the annihilation of antiprotons when the target receives 2Gy dose.

[1] This study was partly supported by a Greek-Slovak bilateral Research Agreement.

A comparison between Geant4 and EGSnrc simulation codes for SPET applications

S. Lo Meo[1], N. Lanconelli[1], F.L. Navarria[1], R. Pani[2], A. Perrotta[3]
[1]Dipartimento di Fisica, Università di Bologna, and INFN Bologna – Italy
[2]Dipartimento di Medicina Sperimentale, Università La Sapienza, and INFN – Rome – Italy
[3] INFN Bologna – Italy

1. Introduction

Monte Carlo simulation techniques are becoming very common in the medical imaging community. Several topics were addressed by Monte Carlo simulations in the Nuclear Medicine field. Among these, it is worth remarking optimization of imaging system design (including detector, collimator, and shield design), development of correction methods for improved image quantitation, evaluation of correction techniques (scatter/random/attenuation correction, partial volume effect), assessment of image reconstruction algorithms, ROC studies, pharmaco-kinetic modeling. The Electron Gamma Shower (EGS) Monte Carlo code has been widely used for many decades to model electron and photon transport over broad energy ranges. EGS has been extensively utilized in the medical field. Many applications are about radiation dosimetry, whereas others include the optimization of detection cameras. We adopted EGSnrc, the latest version of the EGS code family. GEANT4 is an object oriented toolkit for simulation of current (and next generation) High-Energy Physics detectors. It is also a showcase example of technology transfer from particle physics to other fields such as medical science. While EGS does not allow the simulation of the transport and boundary characteristics for optical photons generated by scintillating crystal, in GEANT4 a couple of optical models can be used for this purpose: GLISUR or UNIFIED model.
The purpose of this paper is to compare the performance of simulations obtained with GEANT4 and EGSnrc codes. Simulations include detection cameras composed of parallel-hole collimators with hexagonal holes in hexagonal lattices, and scintillating crystals. For GEANT4 simulations, optical photons will also be considered. Physical effects, such as the transport of electrons, fluorescence photons, together with computation requirements will be considered as figures for the comparison between the two simulation codes. In addition, the investigation of the importance of simulating the optical photons and a comparison between results obtained with and without the tracking of optical photons will be analyzed.

2. Methods

The experimental simulated setup consists of point and spherical monochromatic sources and of a detection camera composed of a parallel Lead collimator with hexagonal holes in contact with a LaBr3(Ce) scintillator. The crystal is surrounded by a thin layer of Aluminum. In the front crystal surface a very small layer of Teflon is positioned after the Aluminum. Simulations include all the physical processes available, such as Compton and Rayleigh scattering and photoelectric absorption with emission of either fluorescence photons or Auger electrons. Figures as photons fluence, spectra, spatial and energy resolution are estimated, together with the computation time needed for the various simulations. When considered, the scintillation light photons are generated as a pure Poisson process and the intrinsic resolution of the crystal was not considered. The simulated crystal was wrapped in a material acting as a Lambertian reflector (Teflon on front) or Black absorber (Aluminum). The interface was modeled as a ground finish, and the boundary processes followed the rules of the GLISUR model. The simulated crystal was coupled to the photomultiplier through a glass window. The photomultiplier surface is built as a polished quartz window, assuming an experimentally derived value for quantum efficiency. The optical properties of the materials involved in the simulations – refraction index, absorption and scattering lengths – were gathered from various sources. The GEANT4 application was run to record the spatial distribution of the detected optical light on the PM surface and energy resolution of the crystal. Figure 1 shows an example of the tracking of the optical photons inside the detection camera. Here, one 140 keV photon impinging the scintillator (LaBr) from the left generates some optical photons. Some of them travel directly through the glass window (in yellow) toward the photomultiplier (in red). Some others are reflected by the lateral surfaces or by the front side of the crystal.

3. Results

Table 1 shows an example of the spatial resolution and the efficiency calculated for a collimator with 1.5 mm holes, 0.2 mm septa and a thickness of 22 mm. Results show a very good agreement between the two simulation codes. The final version of the paper will contain a thorough comparison of simulations in different conditions (*e.g.* by activating or deactivating different physics effects, or by inspecting features such as septal penetration). In addition, the computation requirements and performance for the two codes will be estimated for several situations. Further, we will report an investigation of the importance of tracking the optical photons, so exploring the full capabilities of simulating with a single program the entire detection system, from photon sources to light photons reaching the photomultiplier.

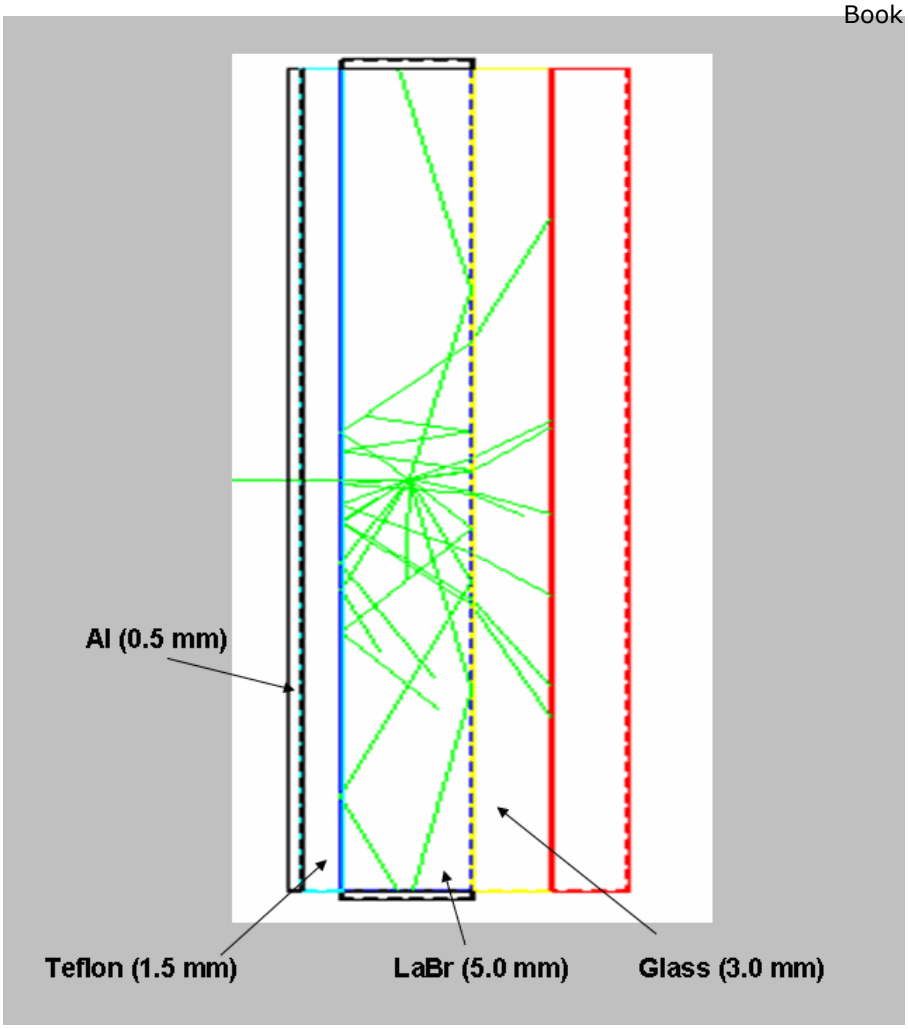

Collimator-source distance [cm]	Spatial resolution (FWHM) [cm]		Efficiency	
	EGSnrc	GEANT4	EGSnrc	GEANT4
5	0.51±0.05	0.57±0.05	$(3.2\pm0.1)\cdot10^{-4}$	$(3.2\pm0.1)\cdot10^{-4}$
10	0.83±0.05	0.80±0.05	$(3.1\pm0.1)\cdot10^{-4}$	$(3.2\pm0.1)\cdot10^{-4}$

Table 1. Comparison for a point source in air located at different distances from the collimator. Spatial resolution is defined as the FWHM of the Point Spread Function of the collimator, whereas the Efficiency is estimated as the ratio between the detected photons over the simulated photons.

Preliminary results of a Multi-Energy CT system for small animals

S. Masetti[a], M. Fiaschetti[a], M. Mariselli[b], L. Roma[c], P.L. Rossi[a], N. Lanconelli[ad], G. Baldazzi[ad]
[a] University of Bologna, Dept. of Physics, Viale Berti-Pichat 6/2, 40127 Bologna, Italy
[b] Specialization School in Health Physics, University of Bologna, Bologna, Italy
[c] S.Orsola-Malpighi University Hospital, O.U. of Radiology, via Massarenti 9, 40127 Bologna, Italy
[d] INFN Bologna, Viale Berti Pichat 6/2, 40127 Bologna, Italy

1. Abstract

A new multi-energy CT for small animals is being developed at the Physics Department of the University of Bologna. The system makes use of a set of quasi-monochromatic X-Ray beams, with energy tunable in a range from 20 to 70 keV. We characterized the beams in resolution and intensity, all over the accessible range, and we present the measured spectra. We are also presenting some preliminary results about triple-Energy radiography with contrast medium.
Triple-energy projection allows to combine a set of three quasi-monochromatic images of an object, in order to obtain a corresponding set of three single-tissue images, which are the density map of three reference materials. The triple-energy technique can be applied to the density-map reconstruction of a contrast medium, because it is able to remove completely the signal due to other tissues (i.e. the structural background noise). A valuable feature of triple-energy analysis is its ability to extract information on physico-chemical structure of the investigated tissues.
We have investigated the theoretical and experimental limits of the method, with the support of both computer simulations and theoretical analyses. For applying the multi-energy projection technique, it is necessary to know precisely the linear absorption coefficient of the materials at all the investigated energies.
To this end, we are measuring systematically the attenuation curves of many healthy and pathological tissues, in order to compile a specific data base for multi-energy application. We finally present some of our measurements.

2. Materials and methods

In the final version of the paper we'll describe the CT system, focusing on the quasi-monochromatic X-ray sources characterization. We have performed a complete set of spectrometric measurements of the beams, in order to map the most relevant parameters (the energy resolution, the intensities of the peaks, the spatial homogeneity of the flux and so on) on the entire set of configurations available. The beams at the three different energies are produced by means of a monochromator based on Highly Oriented Pyrolytic Graphite (HOPG) crystals. It has a measured mosaic spread of (0.26 ± 0.1) degrees, a thickness of 0.1 cm and a surface area of 2.8 × 6.0 cm^2. The digital detector consists of two CCDs coupled with a structured CsI scintillator. Each CCD is composed of 3072 × 128 pixels with a pixel pitch equal to 48 μm. Thus, the active area of each detector turned to be about 150 × 6 mm^2. Figure 1 shows a picture of the CT system presented in this paper.

2.1. The triple-energy radiography reconstructs the contrast medium density map

Triple-energy radiography is an important technique, able to provide accurate estimations about the investigated materials. These information are determined by acquiring images of the analyzed object at three different energies. Suitable algorithms have been developed, in order to reconstruct the density-map of an object, starting from the acquired images. We have performed some Monte Carlo simulations and a set of experimental measurements in order to validate theoretical predictions: results show that triple-energy drastically reduces the projection errors (from 10 to 60 times smaller to dual-energy one), making it negligible with respect to the statistical noise. Some applications of triple-energy imaging will be presented.

2.2. *In vivo* imaging and earlier cancer diagnosis with multi-energy techniques

The ultimate aim of this study is to get an *in vivo* imaging of the cancer growth and metastasis development in different tumor types on mice. To this end, we are systematically measuring the attenuation curves of many healthy and pathological tissues, in order to compile a specific data base for in vivo multi-energy algorithm application. The mass absorption coefficient μ(E) of samples, as a function of energy, has been measured in the range of clinical interest (15 KeV to 100 KeV). Tumoral tissues are supplied by the Laboratory of Immunology and Biology of Metastasis (Dept of Experimental Pathology of the University of Bologna). The Laboratory team is experienced of in vivo models for the study of human and murine tumors grown on mice. The models applied can be classified in three categories:

1) Human tumors in immunodepressed mice;
2) Mouse tumors in inbred mice and
3) Autochthonous tumors in transgenic/knockout mice.

The first model has the advantage of a great number of cell lines available from every type of human tumor, *e.g.* breast, lung, colorectal and so on. All these tumors are characterized by being very fast tumors and having metastasis growth. Experiments usually take a time ranging from 2 to 4 weeks. Spontaneous tumor development synthesizes the entire natural history, from early neoplastic lesions to malignancy.
In the final version of the paper we will present our experimental set and some of more significant measurements on tissues.

Effect of Geometric Models of Convergence Rate of Iterative Image Reconstructions

Chih-Chieh Liu[1], Ching-Han Hsu[1,3], Ing-Tsung Hsiao[2], Kurt M Lin[3]

[1]Department of Biomedical Engineering and Environmental Sciences, National Tsing Hua University

[2]Department of Medical Imaging and Radiological Sciences, Chang Gung University

[3]Division of Medical Engineering Research, National Health Research Institutes

Abstract

Statistical methods for PET image reconstruction are capable of modeling Poisson data noise, and many physical effects to improve quantitation. Geometric model in statistical methods defines the transformation between image and sinogram domains based on scanner geometry. The convergence rate of each iterative algorithm derived from a statistical model depends on the design of geometric model. This paper examines the convergence rates of three popular PET geometric models: interpolative, area-based, and solid-angle. The iterative algorithm used in this study is the Maximum Likelihood Expectation-Maximization (MLEM) algorithm. To evaluate the performance of the 3 different geometric models, the projection data are obtained from both GATE simulation and real Inveon animal PET scanner. From the plots of log-likelihood curves, the results from solid-angle model consistently reach the stable value at early iterations. It means that the MLEM algorithm with the solid-angle model will converge faster than the other two models. In addition, the image results generated by the solid-angle model exhibit better contrast recovery. Therefore, from our preliminary results, the solid-angle model generates better performance as a favorable geometric model for iterative image reconstruction in PET.

An Accurate and Efficient System Model of Iterative Image Reconstruction in High-Resolution Pinhole SPECT for Small Animal Research

Po-Chia Huang[1], Ching-Han Hsu[1,3], Ing-Tsung Hsiao[2], Kurt M Lin[3]
[1]Department of Biomedical Engineering and Environmental Sciences, National Tsing Hua University
[2]Department of Medical Imaging and Radiological Sciences, Chang Gung University
[3]Division of Medical Engineering Research, National Health Research Institutes

Abstract

Accurate modeling of the data formation and detection process in pinhole SPECT is essential for optimizing resolution. In this work, the authors develop an accurate system model in which pinhole finite aperture and depth-dependent geometric sensitivity are explicitly included. To achieve high-resolution pinhole SPECT, the pixel size is usually set in the range of sub-millimeter so that the total number of image pixels increase accordingly. As the pixel number is growing, the system model becomes more complicated. It is inevitably that a system matrix that models a variety of favorable physical factors will become extremely sophisticated. An efficient implementation for such an accurate system model is proposed in this research. We first use the geometric symmetries to determine the required entries in the matrix. Due to the sparseness of the matrix, only non-zero terms are stored. A novel center-to-radius addressing mechanism is also developed to effectively describe the relation between a pixel and its corresponding detectors at every projection angle. The proposed addressing mechanism is suitable for multi-threaded computing. Finally, the accuracy and effectiveness of the proposed system model is evaluated in a dual Xeon with dual cores workstation.

A Fast OS-Type Bayesian Reconstruction with an Edge-Preserving Median Prior

Hsuan-Ming Huang[1,2], Ing-Tsung Hsiao[2, 3*]

[1]University of Missouri-Columbia, Missouri, USA

[2]Chang Gung University, Taoyuan, Taiwan

[3]Molecular Imaging Center, CGMH, Taoyuan, Taiwan

In emission tomography, Bayesian tomographic maximum a *posteriori* (MAP) reconstructions, which consist of log-likelihood term and prior (or penalty) term, can improve problems of ill-conditioning and apply spatial properties to the solution through the weight of penalty. Among priors, two typical properties are smoothing and edge-preserving (with locally monotonic). The easiest and the most popular prior used in nuclear medicine is the quadratic smoothing prior, which attracts the intensity of each pixel to that of its neighborhoods. This action leads to noise reduction, but it may result in over-smoothness on each region. To avoid this effect, a feasible alternative is to use edge-preserving prior. We have proposed an edge-preserving median prior (MP) implemented by a preconditioned conjugate gradient (PCG) reconstruction algorithm (PCG-MP). The MP is not only capable of preserving edges but also imposing local uniformity. Furthermore, the MP reconstruction method is not empirical and is analyzable.

However, PCG-MP is difficult to use and to adjust the hyper-parameters based on our previous studies. In addition, in order to stabilize the result, imposing positivity-constraint in PCG is necessary, and this leads to computation burdens. In this paper, our goal is to develop an easier MP reconstruction method for PET and SPECT. A separable paraboloidal surrogate (SPS) transformation was applied to MP, and combined with a fast convergent OS-type algorithm (COSEM). Based on the preliminary studies, the new algorithm, MAPCOSEM-MP, showed similar edge-preserving performance as in previous studies. We also found that the control of the hyper-parameters is easier in MAPCSOEM-MP as compared to PCG-MP. To evaluate further the performance of MAPCOSEM-MP, we also conducted bias-variance studies using two digital phantoms with different conditions and then compare with MAPCOSEM-MM (membrane prior). The preliminary results of MAPCOSEM-MP show better bias-variance tradeoff and SNRs in larger ROIs while are compatible to those of MAPCOSEM-MM in smaller ROIs. Further studies are needed to evaluate its efficiency in reconstructing real data. For future work, we will conduct the MAPCOSEM-MP reconstruction and evaluate its performance using real PET data, i.e. animal PET data.

Image guidance quality assurance of a G4 CyberKnife® robotic stereotactic radiosurgery system

Pantelis Evaggelos[1], Antypas Christos[1], Petrokokkinos Loukas[2], Verigos Kosmas[1], Doukaki Kleanthi[1], Nikolaos Salvaras[1] and Tzouras Argyris[1]

1. Medical Physics Department, CyberKnife Center, Iatropolis – Magnitiki Tomografia Clinic and Diagnostic center, Ethnikis Antistaseos 54-56, Chalandri, 152 31, Athens, Greece
2. University of Athens, Physics Department, Nuclear and Particle Physics Section, 15771, Athens, Greece

Purpose: To quality control the image properties of the acquired x-rays using the Target Locating System (TLS) and to evaluate the accuracy and reproducibility of the patient position and orientation calculated by the 6 dimension (6D) image analysis software of the TLS of a fourth generation CyberKnife® image guided robotic stereotactic radiosurgery system (Accuray™ Inc., Sunnyvale, USA).
Materials & Methods: The ETR-1 multi purpose test tool (Scanditronix, Wellhöfer, Germany) together with a 1mm thick aluminum leaf were situated at the isocenter of the system facing the tested x-ray camera. X-rays were acquired using typical in clinical practice tube parameters, i.e 120kV and 10mAs. The image properties (geometrical distortion, contrast and spatial resolution) were measured using appropriate features on ETR tool.
An anthropomorphic head and neck phantom was used to test the accuracy and reproducibility of the positions and orientations calculated by the TLS 6D image analysis software. The head phantom was attached on the treatment couch and situated at the isocenter. The head phantom was moved and tilted at different positions inside the field of view of the system. A new pair of x-rays was acquired and the image analysis software of the system calculates the new position and orientation of the phantom. At each point 3 acquisitions were performed and the average position and orientation of the phantom was calculated. Comparison between the average measured and the actual head phantom position and orientation give the accuracy and the relative standard deviation in percent the reproducibility of the TLS software outcome. The described procedure was followed for the Fiducial, 6D Skull and Xsight tracking methods available with the TLS system, using respectively the five fiducials, the skull and the cervical spine of the phantom.
Results & Conclusions: The acquired x-rays using the TLS were found to depict the shapes of the imaging objects without any geometrical distortion, while at the same time able to resolve differences in the features of the imaging objects with a critical frequency of 1.8lp/mm and 2lp/mm for detector A and B, respectively. The image analysis software of the TLS was found to measure with an uncertainty lower than 0.2mm and 0.2^{o} the position and orientation of the phantom for Fiducial, 6D Skull and Xsight tracking algorithms, respectively. Reproducibility of the calculated positions and orientations was found less than 1% for the tracking locating algorithms studied.
The above findings render the TLS system capable of accurately positioning the patient to treatment position and monitoring patients movement during treatment delivery, based either on the bony structure of the skull and the spine or on fiducials.

Reducing of the respiratory motion artifacts in PET cardiology: A simulation study

K. E. Gorji[1], H. Rajabi[2], H. Zaidi[3], E. Hajizadeh[4]

1- Department of Medical Physics, Tarbiat Modares University
2- Department of Medical Physics, Tarbiat Modares University
3- Division of Nuclear Medicine Geneva University Hospital- Switzerland
4- Department of Biostatistics, Tarbiat Modares University

Introduction: There are several technical features that make PET an ideal device for the noninvasive evaluation of cardiac physiology. Organ motion due to respiration is a major challenge in diagnostic imaging, especially in cardiac PET imaging. These motions reduce image quality by spreading the radiotracer activity over an increased volume, distorting apparent lesion size and shape and reducing both signal and signal-to-noise ratio levels

Material and methods: 4D average male torso (2 cm diaphragmatic motion) produced by NCAT phantom was used for simulations. Emission sinograms generated by Eidolon PET simulator were reconstructed using iterative algorithm using STIR. The respiratory motion correction (RMC) applied to data sets using an automatic algorithm. Cross section views, activity profiles, contrast-to-noise ratios and left ventricle myocardium widths of corrected and non-corrected images were compared to investigate the effect of applied correction.

Results: Comparison of respiratory motion corrected and non corrected images showed that the algorithm properly restores the left ventricle myocardium width, activity profile and improvements contrast-to-noise ratios in all cases. Comparing the Q_m shows that the applied correction effected phases of number 7,8 and 9 of cardiac cycle more than the other 13 phases.

Discussions: Blurring and ghosting of each image depends on the speed of diaphragm during that respiratory phase. This simulation study demonstrates that respiratory motion correction has good overall effect on PET cardiac images and can reduces errors originating from diaphragmatic motion and deformation. Using an automatic algorithm capable correcting respiratory motion using full signal may be very useful to prevent lengthening overall scan time to obtain same motionless lesion signal levels

Key words:
PET, Cardiology, Respiratory motion, Eidolon, Monte Carlo.

Fast Iterative Reconstructions: Simulation and Application for Animal CT

Hsuan-Ming Huang[1,2], Ing-Tsung Hsiao[2, 3*], Meei-Ling Jan [4]
[1]University of Missouri-Columbia, Missouri, USA
[2]Chang Gung University, Taoyuan, Taiwan
[3]Molecular Imaging Center, CGMH, Taoyuan, Taiwan
[4]INER, Taoyuan, Taiwan

Iterative reconstruction algorithms for computed tomography (CT) are capable of modeling Poisson data noise, detector response and have more flexibility in different system geometries. In addition, iterative reconstruction methods can reduce sampling artifacts in wide-angle cone-beam CT, or limited field-of-view data. In particular, they have been shown to outperform the analytical methods in low-count data. However, iterative reconstruction methods are usually slow and require high computational load. Under the need for a fast iterative reconstruction method for CT, Kamphuis and Beekman (1998) extended the original convex algorithm to ordered subsets convex (OSC) algorithm by applying the ordered-subset projection at each sub-iteration. They have shown increased speed and studied the performance of OSC. We are interested in reconstructing wide-angle cone-beam (and helical) CT data from an animal CT scanner in INER, Taiwan. Although OSC is a relatively fast algorithm, it needs one forward projection and two backward projections per iteration. Unlike convex algorithm, the gradient algorithm only requires one forward projection and one backprojection per iteration. Here, in order to reduce computation load as in OSC, we applied ordered subsets of projection data to the gradient algorithm with some modification in the step parameter. The new algorithm is called the ordered subset gradient (OSG) algorithm. In addition to the OSG algorithm, we also implemented an OS algorithm proposed by Erdogan and Fessler (1999), called OSTR, which also required one forward and one backprojection per iteration.

We studied the three fast iterative reconstruction methods using both simulated cone-beam and helical CT data, and real animal CT data, and evaluate their performance in terms of log-likelihood values, contrast recovery, and root-mean squared errors (RMSE). The preliminary results show that, for a 128x128x247 image matrix, and 120x128x128 helical projection data, the reconstruction time per iteration for OSC, OSG, and OSTR are 2.7, 1.9, and 1.91 (min), respectively. The log-likelihood values illustrate compatible speed for 3 reconstructions, but OSC displayed decreased log-likelihood values after 10 iterations. The RMSE values after 20 iteration are OSTR(0.125)<OSC(0.138)<OSG(0.165). Thus, from the preliminary results, we conclude that OSTR performs better than both OSC and OSG, in terms of speed, and image quality (RMSE), while OSG shows its potential if step parameter is adjusted correctly. Future work will include their performance evaluation in terms of animal imaging, and optimization of the step parameter in OSG.

Characterization of the univariate and multivariate techniques on the Analysis of Simulated and fMRI Datasets with Visual Task

Liang-Kung Chen[1,2,3], Chia-Lin Chen[4], Jason JS. Lee[4], Yung-Hui Huang[4], Kun-Mu Lu[1], Yeu-Sheng Tyan[5] and Tung-Hsin Wu[5,*]

[1] Department of Radiology, Shin Kong Wu Ho-Su Memorial Hospital
[2] College of Medicine, Fu Jen Catholic University
[3] Department of Radiological Technology, Yuan Pei University
[4] Department of Biomedical Imaging and Radiological Sciences, National Yang Ming University
[5] Department of Medical Imaging and Radiological Sciences, Chung Shan Medical University
*Corresponding author: Tung-Hsin Wu (E-mail address: tung@csmu.edu.tw)
Corresponding address：No. 110, Sec. 1, Chien-Kuo N. Road, South District, Taichung 402, Taiwan, R.O.C.

Abstract—

Functional magnetic resonance images (fMRI) provide high-resolution datasets which allow researchers to obtain accurate delineation and sensitive detection of brain physiological activation areas involved in cognitive processes. This is a valuable tool for studies ranging from brain diseases (e.g. Alzheimer, Parkinson) to study normal brain function in aging. However, the small relative size of the change in image intensity and the existence of possible artifacts have presented a challenge to attempt to optimize identification of activated brain regions. Current analytical techniques applied to fMRI data may be generally divided into two parts: univariate and multivariate techniques. It is therefore our attempt to evaluate and inter-compare their respective algorithms on simulated and fMRI visual task data sets. In this study, the two representative univariate approaches, including the correlation and the specified-resolution wavelet analytical methods, and three multivariate-based independent component analysis (ICA) approaches; including the Infomax ICA, the Fast ICA, and the JADE ICA are used for the purposes. Two simulated spatial sources with different time courses and noise levels and one fMRI dataset with visual task were employed for inter-comparisons. Strategies for quantifying the performance of these techniques, the correlation analysis and receiver operating characteristics (ROC) are used to evaluate their respective accuracies on estimated time-courses and spatial layouts from the simulated and the fMRI visual task dataset. Although those model-based univariate methods are easy to implement and are effective in analyzing data with simple paradigms, they are not applicable in situations in which pattern of neural response are complicated and when fMRI response is unknown. Therefore, both simulated and experimental results demonstrate that the multivariate techniques generally outperformed the univariate techniques when applied to fMRI studies. Of three different ICA approaches, Fast ICA performs satisfactory well on temporal and spatial accuracy, which might be due to the “batch” mode in updating the unmixing matrix, which doesn’t require the choice of a learning rate, which makes Fast ICA approach performed better in our experiment. However, Infomax ICA with “adaptive” mode seems to be preferable only if fast adaptivity in a changing environment is required. Each of the methods has their own contributions and unwanted drawbacks, and all we can do is to comprehend the underlying assumptions and theories of each method in depth, and try to choose the appropriate techniques for our experiment. In our study, it shows that the Fast ICA seems to be a more suitable choice for our task.

Three-dimensional imaging for dose distribution and mapping in intraoral and panoramic radiographies

Hsiu-Ling Chen[1], Yung-Hui Huang[2], Tung-Hsin Wu[3], Shih-Yuan Wang[2], Ching-Ching Yang[2], Jason J.S. Lee[2,*]

[1)] *Dept. of Dental Medicine, Mackay Memorial Hospital, Taipei, Taiwan.*
[2)] *Dept. of Biomedical Imaging and Radiological Sciences, National Yang-Ming University, Taipei, Taiwan*
[3)] *Dept. of Medical Imaging and Radiological Sciences, Chung Shan Medical University, Taichung, Taiwan*

In current medical imaging applications, high quality images not only provide much diagnostic value for anatomic delineation but also offer functional information for treatment direction. However, this approach would potentially subscribe higher radiation dose in dental radiographies, and such as, has been putatively associated with low-birth-weight during pregnancy, which affects the hypothalamus-pituitary-thyroid axis or thereby directly affects the reproductive organs.

To better understand dose distribution from dental radiographies, several highly variable factors should be concerned, such as operating parameters (tube voltage, exposure time, and filter thickness, etc.) and types of the study (intraoral films, panoramic tomography). The aim of this study was to apply high resolution 3-D image mapping technique to evaluate radiation doses from the following aspects: (1) verifying operating parameters of dental x-ray units, (2) measuring the leakage radiations and (3) mapping dose with 3-D radiographic imaging to evaluate dose distribution in head and neck regions.

In this study, the leakage radiation and output from dental x-ray radiographies were measured by utilizing a Barracuda multi-functional detector. For measuring radiation dose from staff and patient, a Rando phantom and Thermoluminescent Dosimeter (TLD-100H) were used. All the measured doses were further processed via an AMIRA software and 3-D mapped with intraoral and panoramic radiographies. The results were then compared with current radiation regulations. From the study results, we found that (1) leakage radiation from x-ray units was about 21.31 ± 15.24 mR/h (<100 mR/h), (2) error of the actual tube voltage for the 60 kVp setting was from 0.2% to 6.5%, with an average of 2.5% (<7%), (3) error of the exposure time for a 0.5~1.5 sec setting was within 0.7% to 8.5%, with an average of 7.3% (< 10%) error as well.

Our 3-D dose mapping demonstrated that dose values were relatively lower in soft tissues and higher in bone surfaces compared with other investigations. Multiple causes could contribute to these variations, including irradiation geometry, image equipment and type of technique applied, etc. From the results, we also observed that larger accumulated doses presented in certain critical organs, such as salivary gland, thyroid gland and bone marrow. It is worthy of paying more attention to these findings and their successive biological effects are encouraged for further exploration.

Topic: Image Visualization and Processing
Presentation: Poster Contribution

***Corresponding Author**

Jason JS Lee, Ph.D.

Department of Biomedical Imaging and Radiological Sciences, National Yang-Ming University,

No. 155, Sec.2, Li-Nong St., Taipei 112, Taiwan

Tel: 886-2-2826-7134

Fax: 886-2-2822-4860

E-mail: jslee@ym.edu.tw

Integration of PET-CT and cone-beam CT for image-guided radiotherapy for high image quality and registration accuracy

Chia-Hao Liang[1], Jason JS. Lee[1], and Tung-Hsin Wu[2,*]

[1] Department of Biomedical Imaging and Radiological Sciences, National Yang Ming University, Taipei, Taiwan.
[2] Department of Medical Imaging and Radiological Sciences, Chung Shan Medical University, Taichung, Taiwan.

Abstract—

Purpose: Treatment position setup errors often introduce temporal variations in the position of target relative to the planned external radiation beams. The linear accelerators equipped with the on board X-ray cone-beam computed tomography (CBCT) imaging system for image-guided radiotherapy (IGRT) can provide excellent verification on position setup error to reduce the errors. In current hybrid positron emission tomography-computed tomography (PET-CT) systems, high quality CT images not only increase diagnostic value by providing anatomic delineation of hyper- and hypo-metabolic tissues, but also shorten the acquisition time for attenuation correction (AC) compared with standard PET imaging. The purpose of our study is to optimize the CT acquisition protocols and integrate PET-CT and high quality CBCT mounted on linear accelerators for image-guided radiotherapy on lifting the image quality and decreasing position setup error.

Material and methods: The tube current, tube voltage, and rotational speed of the gantry were modified on CT for optimizing AC in PET-CT and the parameters of CBCT in IGRT were also changed for increasing the image quality on the tube current, tube voltage, and radiation pulse length. The delicately hybrid PET-CT was combined with high quality CBCT for IGRT for improving the accuracy in the position of target using a sophisticatedly fused technology. The reproducibility and repositioning accuracy of both bone and gray value registration algorithms between the PET-CT and CBCT were also evaluated with head and neck of Rando Phantom.

Results: The optimization of CT in AC and CBCT in contrast was practical in our work. The registration accuracy between images of PET-CT and those of CBCT was within CBCT voxel size (0.75 x 0.75 x 1.00 mm) in translational dimensions and within 0.8 degrees in rotational dimensions. The results of the phantom study revealed that the bone registration algorithm was more delicately accurate than gray value registration algorithm.

Conclusion: Registration between PET-CT and CBCT for IGRT is a state-of-the-art registration technology which provides much more information and accurate tumor contour while implementing a radio-therapeutic task. The novelty technology and the optimization of CT and CBCT may have a potential to become more clinical in the future.

***Corresponding Author**

Tung-Hsin Wu, Ph.D.

Department of Medical Imaging and Radiological Sciences, Chung Shan Medical University,

No. 110, Sec. 1, Chien-Kuo N. Road, South District, Taichung 402, Taiwan, ROC

Tel: 886-4-24730022 ext. 17215

Fax: 886-4-24730022 ext. 17210

E-mail: tung@csmu.edu.tw

Monitoring of Bone Regeneration Process by means of Texture Analysis

Kokkinou E.[1], Boniatis I.[1], Costaridou L.[1], Saridis A.[2], Panagiotopoulos E.[2], Panayiotakis G.[1]
[1]University of Patras, School of Medicine, Department of Medical Physics, 265 00 Patras, Greece
[2] University of Patras, School of Medicine, Department of Orthopaedics, 265 00 Patras, Greece

When bone is gradually distracted, the reparative process, initiated by an osteotomy or fracture, which can result in the formation of new bone, is referred to as “regeneration” by Ilizarov. Our research aims to investigate whether texture analysis can assess quantitatively-monitor the growth progress regeneration of the calf bone. The research was motivated by the fact that no other monitoring method has previously been developed and/or applied.

For this purpose, a sample of 13 patients, all bearing common orthopedic lesions in the calf area, was used. All of the patients had undergone operation for calf bone lengthening by application of the Ilizarov method, while a number of radiographs, taken at successive time intervals after the operation, were available for each of them. After radiographs digitization, a Region Of Interest (ROI), corresponding to the gap in which bone regeneration was expected to occur, was determined on each radiograph, employing proper available software. Within this ROI, three sub-ROIs were accurately selected: one at the upper, a second in the center and a third one at the lower aspect of the gap. Each patient’s X-ray films were subjected to texture analysis techniques. Accordingly, a number of texture features, evaluating aspects of image pixel intensities fluctuations were generated, employing custom developed algorithms. In addition, a texture features-based regression model providing a quantitative estimation of texture feature values (dependent variable) as a function of time (independent variable), was introduced for the monitoring of the regeneration process.

The values of texture features, generated from sub-ROIs corresponding to successive time intervals after the performance of the operation, were found to increase. This finding complies with relevant clinical data, concerning the formation of new bone and the subsequent increased absorption of X-ray radiation due to bone calcification. This absorption increment was reflected by the increased intensities (brightness) of the pixels comprising the studied ROIs. A regression model, described by a cubic polynomial equation, fitted data adequately ($r^2 = 0.9$). The results of the present study indicate the potential capacity of texture analysis regarding the assessment of bone regeneration process. Texture features can be considered as markers of the rhythm of bone regeneration. The proposed regression model provided a quantitative description the regeneration process. The suggested method may contribute to the monitoring of bone regeneration process under circumstances of clinical routine.

Characterization of a new polymer gel for radiosurgery dosimetry using Magnetic Resonance Imaging*

Petrokokkinos Loukas[1], Kozicki Marek[2], Pantelis Evaggelos[3], Seimenis Ioannis[4], Pantelis Karaiskos[5], Antypas Christos[3], Fijuth Jacek[6], Sakelliou Loukas[1]

1. University of Athens, Physics Department, Nuclear and Particle Physics Section, 15771, Athens, Greece
2. Technical University of Lodz, Faculty of Textile Engineering and Marketing, Institute of Architecture of Textiles, Department of Textile Finishing, 90-543, Lodz, Poland
3. Iatropolis – Magnitiki Tomografia Clinic and Diagnostic center, CyberKnife Center, Medical Physics Department, Ethnikis Antistaseos 54-56, Chalandri, 152 31, Athens, Greece
4. Medical Diagnostic Center Ayios Therissos, 92 Troodous Ave., Strovolos, Nicosia, Cyprus
5. University of Athens, Medical School, Medical Physics Department, 75 Mikras Asias, 115 27 Athens, Greece
6. N. Copernicus Hospital, Teleradiotherapy Department, 62 Pabianicka, 93–513, Lodz, Poland

A modification of a known polymer gel dosimeter formulation (VIPAR) was pursued to eliminate deoxygenation; a manufacturing procedure step which affects dosimetric material reproducibility in terms of dose sensitivity and obviates the routine clinical application of gel dosimetry due to its laborious and time consuming nature and the need for dedicated infrastructure.

Aiming at a wide dose response range combined with adequate dose sensitivity, to facilitate the dose verification of demanding radiosurgery applications employing narrow beams of steep dose gradients, we concluded at the new formulation (VIPARnd) consisting of 8% N-Vinylpyrrolidone, 7.5% gelatine, 4% N,N'-methylenebisacrylamide with the addition of 0.0008% Copper Sulfate and 0.007% Ascorbic Acid as oxygen scavengers.

For an initial characterization of the new gel in terms of dose – R_2 response dose resolution and precision, we prepared 55 gel filled glass vials of small volume that were irradiated at doses ranging from 1 Gy to 65 Gy using a calibrated Cobalt-60 source beam. After 24 hours, each tube was NMR measured employing a 32 echoes CPMG sequence to measure the spin–spin relaxation rate ($R_2=1/T_2$) at each dose. The new gel dosimeter was found to respond linearly to doses up to 50 Gy, while the full dose response range was found to exceed the maximum delivered dose of 65 Gy.

In order to attest the potential of the new gel in radiosurgery applications, one gel filled vial was irradiated using circular CyberKnife radiation fields of 60 and 10 mm diameter. The irradiated gel vial was MR scanned 2, 14 and 25 days post irradiation using a dual echo TSE sequence for time efficiency. Using custom-made processing tools, dose – R_2 response data were derived from the largest diameter field in each scan to verify temporal stability. Relative dosimetry data for the remaining fields were utilized to investigate "edge effect" phenomena that could affect the potential of the new gel to resolve the penumbra region of the fields.

Overall, results suggest that the characteristics of the new gel formulation combined with the inherent three dimensional character of the method could facilitate dosimetry of radiosurgical applications provided that it is coupled with appropriate MRI parameters to arrive at acceptable relative uncertainties for adequate image spatial resolution, in practicable scanning times.

*__Acknowledgement:__ Financial support of the Polish Ministry of Science and Higher Education (grant no. N205 048 32/293) is appreciated.

This work was supported in part by a Greece-Poland joint research and technology program (2005-2007).

VISUALLY LOSLESS MEDICAL IMAGE COMPRESSION THRESHOLD BASED ON WAVELET ACTIVITY MEASURES

V. Georgiev, L. Costaridou and G. Panayiotakis

Department of Medical Physics, School of Medicine, University of Patras, Patras 26500, Greece

The increasing need for efficient image storage and transmission in hospitals imposes heavy requirements on the design of picture archiving and communication systems. Thus, with the evolution of teleradiology, the use of lossy compression techniques is a requirement for reducing image volume and speeding up communication. However, greater compression is obtained at the expense of image quality. Efforts have been devoted to evaluate the subtle difference between images, using visual or numerical methods. Many studies had tried to build a visual threshold or acceptance level (visually/diagnostically lossless threshold) of lossy image compression. The golden standard for evaluation of compression algorithms is based on ROC analysis of observer performance. This method has a high accuracy but it is time consuming. This introduces the need for automated numerical measures, which are able to predict the diagnostics accuracy rather than subjective quality measures. An ideal image quality measure should be able to mimic the human observer. The traditional mean square error (MSE) and peak signal to noise ratio (PSNR) error measures are mainly focused on the pixel by pixel difference between the original and the compressed images. Such metrics are improper for subjective image quality assessment, since the human perception is very sensitive to specific correlations between adjacent pixels.

The objective of this study is to present a method for a new wavelet based image activity measure (WIAMs) [1, 2] of image quality, used for automated computer evaluation of lossy compressed medical images. Initially the method was validated using computer-generated test patterns of different activity, with respect to spatial frequency and the relationship between frequency/contrast content and scale was derived. Following, the propose measures were applied on a set of 40 mammograms with microcalcifications. Mammograms have been compressed up to 100 compression ratio, with a step of 5 using 2 different medical image wavelet-based compression algorithms [3, 4]. The WIAMs coefficients corresponding for scales 1-4 were derived for each compressed image. Results indicate a diagnostically lossless compression of 30:1, based on WIAMs' degradation in scale 3 and 4, which is in agreement with a previous observer based study for the same set of images [5].

The proposed method is fast and easy to use, and seems more accurate for a visually/diagnostically lossless threshold determination of a lossy image compression algorithm, compared to the traditional metrics. Nevertheless the additional automated picture activity measures have to be investigated.

References

[1] Costaridou L., Sakellaropoulos P., Stefanoyiannis A., Ungureanu E. and Panayiotakis G. (2001): "Quantifying Image Quality at Brest Periphery vs. Mammary Gland in Mammography Using Wavelet Analysis", The British Journal of Radiology, Vol. 74, pp. 913-919.

[2] Georgiev V., Costaridou L. and Panayiotakis G. (2005): "A Wavelet-based Activity Method in Performance Evaluation of Medical Image Complession Algorithms", HPC-Europa, Science and Supercomputing in Europe, Report 2005, pp 219-223.

[3] Pegasus Imaging Corporation: http://www.pegasusimaging.com/pictools.htm

[4] MeVis Technology: http://www.mevis-technology.de/index.html

[5] Kocsis O., Costaridou L., Varaki L., Likaki E., Kalogeropoulou C., Skiadopoulos S. and Panayiotakis G. (2003): "Visually Lossless Threshold Detection in Wavelet Compressed Mammograms", European Radiology, Vol. 13, pp. 2390-2396.

Study of the optical properties of both continuous and pixelated scintillation crystals

A. Polychronopoulou[1], D. Thanasas[1], N. Giokaris[1,2], A. Karabarbounis[1,2], D. Maintas[3], C.N. Papanicolas[1,2] and E. Stiliaris[1,2]

(1) Physics Department, National & Kapodistrian University of Athens
(2) Institute of Accelerating Systems & Applications (IASA)
(3) Institute of Isotopic Studies, Athens

Abstract

The principal goal of this study is to characterize the light diffusion in scintillation crystals and to figure out the basic differences in the optical behaviour of the pixelated crystals compared to continuous. The light distribution for a given number of initial optical photons is expressed as a function of the depth in the crystal, where the initial optical photons are produced, the size of the initial volume the optical photons occupy before starting the transmission and the geometrical properties of the optical medium that guides the light to the photomultiplier surface, such as the size of the pixel in the case of a pixelated crystal.

The light distribution in both continuous and pixelated crystals is considered. Monte Carlo runs based on the optical simulation package DETECT2000 have been performed. DETECT2000 is a program dedicated to modeling the optical properties of scintillators taking into account Snell's law and the optical properties of the various surfaces such as the index of refraction and the reflection coefficient. A pixelated scintillation crystal has been modeled in this Monte Carlo study in accordance with the available CsI(Tl) scintillation crystal (with 1x1 mm^2 pixel size) which is used in the small field γ-Camera of our Laboratory. Direct comparison of the obtained theoretical results with experimental approaches is therefore possible.

The results indicate that in the case of continuous crystal there is an apparent correlation of the Depth of Interaction (DOI) and the width of the exiting light distribution. In the case of pixelated crystals, the width of the light distribution seems to be independent of the DOI when the source is located deep in the crystal but there is a strong dependence as the source approaches the PSPMT's entrance window. This correlation of the DOI and the light distribution is not affected by the transverse dimensions of the continuous crystal. In the case of the pixelated crystals, this correlation is strongly depended on the crystal's aspect ratio, such as the pixel size to crystal thickness.

A Correction Method of the Spatial Distortion in Planar Images from Gamma Camera Systems

D. Thanasas[1], A. Polychronopoulou[1], N. Giokaris[1,2], A. Karabarbounis[1,2], D. Maintas[3], C.N. Papanicolas[1,2] and E. Stiliaris[1,2]

(1) Physics Department, National & Kapodistrian University of Athens
(2) Institute of Accelerating Systems & Applications (IASA)
(3) Institute of Isotopic Studies, Athens

The aim of this work is to demonstrate a correction method of the spatial distortion usually obtained in planar images of γ-Camera systems with multiwired anodes. In our study, the γ-Camera system consists of a 3" diameter circular envelope Position Sensitive Photomultiplier Tube (PSPMT) with a 16X+16Y crossed wire anode (Model R2486, Hamamatsu), a 46 mm in diameter and 4 mm thick CsI(Tl) pixelated scintillation crystal and a 27 mm thick parallel hexagonal hole collimator.

The correction method is based on the fact that the distorted pixels of the centers of the pixelated crystal are very well distinguishable at a planar image using a small laboratory ^{60}Co source without the collimator. The correction method utilizes therefore the error signal produced by the difference of the well known nominal position with the experimentally observed position in the planar image. The algorithm, based mainly on interpolation methods, has been developed in FORTRAN and using the HIGZ (High level Interface to Graphics and Zebra) package of the CERN program library allows the easy extraction of the corrected image.

This correction method has been successfully applied to several images obtained with phantoms with small capillaries (1.1 mm outer diameter) filled with water solution of ^{99m}Tc. Results will be presented also for 3D SPECT image of a rotating phantom by collecting a small set of planar projections.

Labelling of bevacizumab with Technetium-99m: initial *in vitro* and *in vivo* studies

P. Bouziotis[1], E. Gourni[1], A. L. Harris[2], G. Loudos[3], N. Sakellios[3], S. Xanthopoulos[1], S. Archimandritis[1], A. D. Varvarigou[1]

[1]N.C.S.R. "Demokritos", Aghia Paraskevi, Athens, GREECE;
[2]Molecular Oncology Laboratory, University of Oxford, Oxford, UNITED KINGDOM, [3]NIMgroup, Biomedical Simulations and Imaging Applications Lab, School of Electrical and Computer Engineering, National Technical University of Athens, Athens, GREECE.

Abstract:

Aim: Monoclonal antibodies have demonstrated their feasibility as drugs, either as “naked” antibodies or, using the power of their specificity, as a way to deliver cytotoxic moieties or radioisotopes to selected sites of action. Target antigens uniquely expressed on neovasculature can provide an effective target for Mabs. One such target is Vascular Endothelial Growth Factor (VEGF). Researchers have shown that anti-VEGF agents may work by causing regression of existing microvessels and inhibition of vessel growth and neovascularization. Bevacizumab (Avastin®) is a therapeutic antibody that is believed to work by targeting and inhibiting the function of VEGF. Avastin® is the first U.S. FDA approved therapy designed to inhibit angiogenesis. The aim of this study is the development of a novel radiotracer, ^{99m}Tc-bevacizumab, which enables noninvasive imaging of VEGF. **Materials and methods:** Labeling of the thiol-modified antibody was performed by radionuclide exchange with a preformed technetium kit. The immunoreactivity of the ^{99m}Tc-labelled antibody was assessed in each case. Biodistribution studies were performed in normal Swiss mice at 1, 2, 4 and 24 h p.i. Athymic SCID mice were inoculated subcutaneously in the right front leg with U87 MG human glioblastoma cells (10^7 cells/animal). Dynamic gamma-camera imaging was performed on an experimental gamma camera. **Results:** Labeling of the antibody with Technetium-99m was quantitative at 37°C and 60 min, while the immunoreactivity of the labeled antibody varied from 20-50%, depending on the method of thiol modification. ^{99m}Tc-bevacizumab exhibited fast *in vivo* kinetics, with the the tumors being clearly delineated from the first 15 min p.i. The uptake of ^{99m}Tc-bevacizumab was specific, as demonstrated by the effective *in vivo* blocking with unlabeled bevacizumab. **Conclusions:** The encouraging results obtained warrant the need for further investigation into the labeling of bevacizumab with technetium-99m and other short-lived gamma- and positron-emitting isotopes, for selective and highly-specific tumor imaging.

Reducing High Energy Contamination in SPECT using a Rotating Slat Collimator

Roel Van Holen, Stefaan Vandenberghe, Steven Staelens, Erwann Rault, Jan De Beenhouwer and Ignace Lemahieu
Department of Electronics and Information Systems, Ghent University, Belgium

I. Introduction

Quantitative SPECT imaging is limited by many factors, including collimator blurring, scatter and attenuation. Next to these effects, penetration of High-Energy (HE) photons through the collimator has been recognized as an important factor limiting accurate quantification. Even small peaks of high energy give large contamination in the main energy window. Rotating Slat (RS) collimators typically offer a 30- to 40-fold increase in geometric detection efficiency while HE penetration is expected to remain similar. The aim of this study is to show that SPECT for isotopes with high energy peaks could benefit from the use of a rotating slat collimator by significantly reducing the effect of HE contamination.

II. Methods

A simulation study was performed for I-123 which has, besides the main energy peak at 159 keV, high energy emissions at 346 keV, 440 keV, 505 keV, 529 keV and 539 keV. A point source in a 20 cm diameter sphere filled with water was simulated at 10 cm distance from the collimator for both an RS and a PH collimator. The collimators had equal septal thickness, height and gap/hole pitch of respectively 0.3 mm, 40 mm and 1.8 mm resulting in a collimator resolution of 5 mm@10 cm. A modified version of Geant4 Application for Tomographic Emission (GATE) was used in order to track the history of each emitted photon. After detection in the photopeak window, the photons were categorized in 4 classes: (1) penetration, (2) collimator scatter, (3) object scatter and (4) geometric. Geometric photons are non-penetrated photons which did not undergo any interaction before detection in the crystal. Class 2 and class 3 photons underwent scatter but no penetration in respectively the collimator and the object while penetrated photons are the photons which penetrated the collimator, regardless of whether they scattered or not.
To investigate the influence on the resolution, Point Spread Functions (PSF) are obtained from the raw projection data and the FWHM is calculated from these PSFs .

III. Results

Results show that the RS collimator is able to significantly reduce the relative contribution of penetrated photons in the photopeak energy window while maintaining approximately the same relative scatter contribution (Fig. 1). The total contribution of penetrated photons (considering all emission energies) is reduced from 32.4% to 3.8%. Since the penetration from the main energy peak is only reduced by a factor of 2.3, the large decrease of total penetration contamination is mainly mediated by suppressed HE penetration. The PSF are shown in Fig. 2. The FWHM is 8,7 mm and 5,6 mm respectivily for the PH-PSF and the RS-PSF.

IV. Discussion and conclusion

Due to the higher sensitivity for geometric photons of an RS collimator, high energy contamination due to septal penetration can be significantly reduced for isotopes like I-123, which has high energy emission peaks. This can lead to improved quantification for all isotopes which suffer from HE septal penetration (e.g. I-131, In-111). Furthermore, for isotopes that need a medium energy collimator, we could still use a low energy RS collimator due to the 2.3-fold decrease of main energy photon penetration. This would result in a better spatial resolution. The impact on image quality requires further investigation, but the FWHMs of the PSFs already indicate that a better quantification will be possible using the RS collimator.

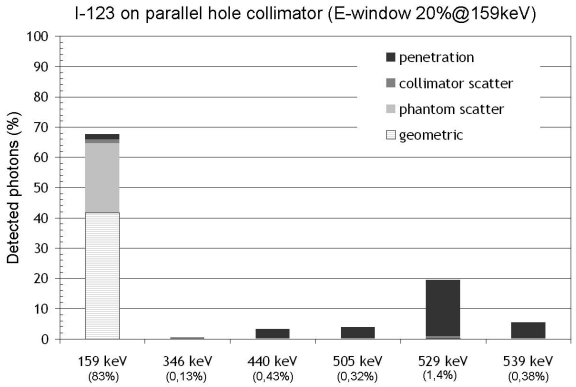

(a)

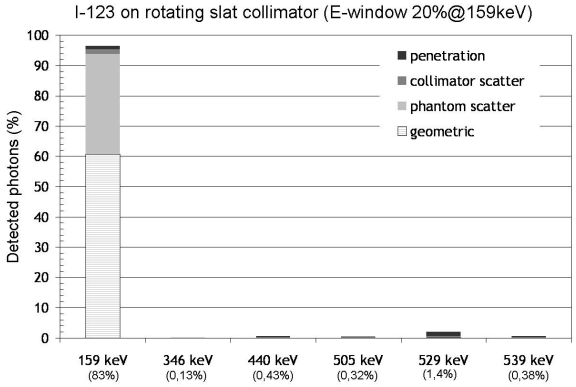

(b)

Fig. 1. The relative contributions from the different emission energy peaks to the photopeak window for the PH (a) and the RS (b) collimator. The probability of emission for every peak is also indicated.

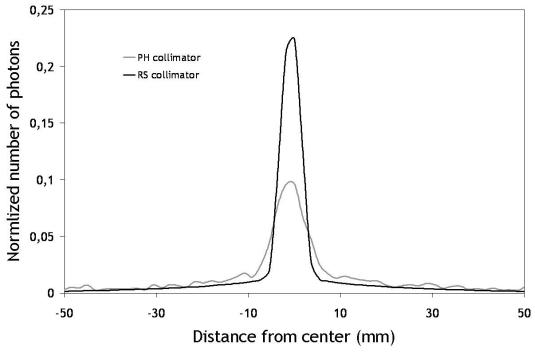

Fig. 2. The PSF for I-123 on a the PH and the RS collimator.

Synogram correction technique for non-parallel projection SPECT imaging

V. Y. Pedash, A. Gektin, A. Dyomin
Institute for scintillation materials NAS of Ukraine, Kharkov, Ukraine

During last decade the problem of breast cancer diagnosis at early stage of development becomes more and more important task. The ability of conventional SPECT systems to detect small cancer in human breast is generally limited by two factors. The first one is connected with radiopharmaceuticals. The ratio of uptake in cancer to the one in normal tissue is not high enough to detect lesions smaller then 10 mm. The second limiting factor is anatomical. The region of the most probable cancer location is inconvenient for visualization. In order to get higher resolution one needs to put detection heads as close to breast as possible, but in such case that's impossible to built system using parallel projection. Some works with non-parallel projection scheme have been reported recently. The resolution of such systems especially in the region of interest are higher then that of conventional cameras, but its very hard to make 3D reconstruction because of incomplete data and high background which is caused by core and lungs. In this work a sort of synogram correction algorithm for initial projection filtering was evolved. After such a filtration of initial data, the reconstructed images are suffered from high Poison noise, but contain more useful data about studied region then images reconstructed from unfiltered projections

Calibration of Pinhole MicroSPECT Using a Single Point Source

Zhou Rong, Ma Tianyu, Liu Yaqiang, Wu Zhaoxia, Wang Shi, Jin Yongjie
Department of Engineer Physics, Tsinghua University, Beijing, 100084, China

1 Objectives

We are developing a MicroSPECT system used for small animal imaging. The system consists of two or multiple single-pinhole gamma camera heads located in a ring. Knowing the exact geometry of the system is essential to the system's imaging performance. Our work is to develop feasible calibration method to accurately obtain system's geometrical parameters.

2 Methods

The geometrical parameters to be determined include focal length f, tilt angle Φ, twist angle Ψ, location of axis of ratation (AOR) (x_0, y_0), location of pinhole center (x_c, y_c, z_c), relative angle ρ and shift along AOR Δz of two heads(Fig. 1 and 2).

Based on published literatures, we proposed two improved calibration methods which only use a single point source. And we proved that the geometry of both single-head and multi-head systems are able to be uniquely determined by method A, while only that of muti-head ones by method B. Method A requires two circular scans with a point source in different transverse planes. The point source has to be located the same distance away from AOR in two scans, which can be easily guaranteed in practical. And the distance between the two transverse planes has to be known in advance, which can be exactly given for most actual systems. Method B assumes that Φ(or f) and y_c are determined in the previous calibration method and vary very slowly over time, which is true for the real system. Therefore one circular scan of a point source can sufficiently calibrate the rest parameters.

The system is calibrated in the following steps: 1) derive the function $F_{\mathrm{p}}(S, \theta)$ with system geometry parameters set S and projection location at arbitrary projection angle θ; 2) acquire the projections $\vec{p}(\theta_i)$ of the point source according the requirement of the proposed methods.; 3) minimize objective function $F_{\mathrm{obj}} = \sum_i \|F_{\mathrm{P}}(S, \theta_i) - \vec{p}(\theta_i)\|^2$ to obtain the estimated value of S as calibration results.

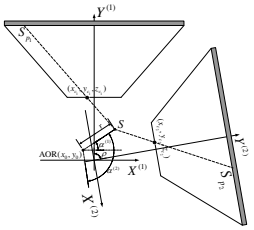

Fig. 1: Imaging geometry of two-head single pinhole MicroSPECT

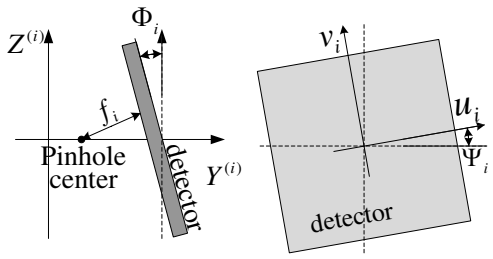

Fig. 2: Tilt(left) and twist(right) of detector in i-th head

3 Results

We modeled a dual-head MicroSPECT system with 4 sets of geometrical parameters in a Monte Carlo program, GATE. The projections of a point source were acquired. The geometrical parameters were calibrated and compared with their true values.

The results shows that reasonable calibration error is given by both method A and B. In method A, the observed maximum absolute error is 0.43 mm for f, and are less than 0.3 mm for y_c, z_c and Δz, and for the rest length values are less than 0.1 mm. For angle values, the maximum absolute errors are 0.21°, 0.03°, and 0.47° for Φ, Ψ, and ρ respectively. In method B with y_c and Φ of each head given exactly, the observed maximum absolute error is 0.42 mm for f, and are no more than 0.1 mm for the rest length values. For angle values ,the maximum absolute errors are 0.03° and 0.47° for Ψ and ρ respectively.

4 Conclusions

In this work, we developed two calibration methods for determining the geometry of pinhole MicroSPECT systems. Both methods use only a single point source. Method A requires two circular scans at different transverse planes with distance between each other known. Method B requires one circlular scan and y_c and Φ(or f) of each head given.

Both requirements is feasible in practical systems. Simulation studies show reasonable calibration error with both methods. Method B provides better results thanks to given y_c and Φ values of each head. The relative larger error of f is believed to be caused by depth of interaction (DOI) of gamma photons inside the crystal. Relative stronger correlations between y_c, Φ, z_c and Δz are observed. Further studies include evaluating the impaction of calibration error on reconstruction performance and applying the proposed methods on an actual system.

Table 1: Calibration results of each head. result A is calibrated by two circle scan, and result B is calibrated by one circle scan with y_c and Φ given. The calibration results are rounded off to 2 decimal places.

sets	head		x_0 mm	y_0 mm	x_c mm	y_c mm	z_c mm	f mm	Φ deg	Ψ deg
1	1	true value	0.5	0.5	0	20	0	50.5	0	0
		result A	0.39	-0.49	-0.09	20.08	-0.09	50.87	0.05	-0.03
		result B	0.48	0.53	-0.01	—	-0.03	50.85	—	-0.01
	2	true value	0.5	-0.5	0	20	0	50.5	0	0
		result A	0.49	-0.39	-0.01	20.21	-0.24	50.95	0.16	-0.00
		result B	0.53	-0.48	0.03	—	-0.02	50.85	—	-0.01
2	1	true value	0	0	0.5	20	-0.5	50.5	0	0
		result A	-0.01	0.02	0.48	20.10	-0.73	50.93	0.21	-0.03
		result B	0.00	0.00	0.49	—	-0.46	50.93	—	-0.03
	2	true value	0	0	0	20	0	50.5	0	0
		result A	0.02	0.01	0.01	20.10	-0.26	50.93	0.19	-0.01
		result B	0.00	-0.00	0.00	—	-0.02	50.92	—	-0.02
3	1	true value	0	0	0	20	0	50.5	0	0
		result A	0.03	0.02	0.02	20.12	0.002	50.91	-0.02	0.00
		result B	0.04	-0.02	0.03	—	-0.01	50.92	—	-0.00
	2	true value	0	0	0	20	0	50.5	0	0
		result A	0.02	-0.03	0.01	20.01	0.24	50.93	0.17	0.01
		result B	-0.02	-0.04	-0.02	—	0.00	50.92	—	0.02
4	1	true value	0	0	0	20	0	50.5	0	5
		result A	0.02	0.10	0.01	20.21	0.06	50.93	-0.06	5.00
		result B	-0.07	0.10	-0.06	—	-0.03	50.90	—	5.00
	2	true value	0	0	0	20	0	50.5	0	5
		result A	0.01	-0.02	0.07	20.08	-0.28	50.90	0.20	5.00
		result B	0.10	0.07	0.08	—	0.00	50.92	—	5.00

Table 2: Calibration results of the coupling of two heads. result A is calibrated by two circle scan, and result B is calibrated by one circle scan with y_c and Φ given. The calibration results are rounded off to 2 decimal places.

Sets	ρ / deg true value: 90		Δz / mm true value: -2	
	result A	result B	result A	result B
1	89.53	89.53	-1.85	-2.00
2	89.54	89.54	-2.00	-1.93
3	89.54	89.54	-1.75	-1.99
4	89.54	89.53	-1.65	-2.02

References

[1] D. Beque, J. Nuyts, G. Bormans, P. Suetens, P. Dupont, Characterization of pinhole spect acquisition geometry, IEEE TRANSACTIONS ON MEDICAL IMAGING 22 (5) (2003) 599–612.

[2] Y. C. Wang, B. M. W. Tsui, Pinhole spect with different data acquisition geometries: Usefulness of unified projection operators in homogeneous coordinates, IEEE TRANSACTIONS ON MEDICAL IMAGING 26 (3) (2007) 298–308.

Ectomography – tomographic technique for mobile imaging systems

I. Valastyán[a,b], D. Bone[c], L-Å Brodin[a], H. Elmqvist[d], A. Kerek[a], J. Molnár[b], D. Novák[b], and T. Ribbe[d]

[a]Royal Institute of Technology, Stockholm, Sweden
[b]Institute of Nuclear Research of the Hungarian Academy of Sciences, Debrecen, Hungary
[c]Karolinska University Hospital, Stockholm, Sweden
[d]Karolinska Institute, Stockholm, Sweden

Early diagnosis of acute myocardial infarction is important for rapid restoration of perfusion. A mobile gamma camera system, the CARDIOTOM™, that is based on a tomographic technique, ectomography is an ideal tool for making such an early diagnosis. Ectomography is a limited view angle method, using a slant hole collimator and a stationary scintillator, to produce projection images.

The new updated CARDIOTOM™ system has been used for over a year at the Karolinska University Hospital in Stockholm. The present performance of the camera meets the requirements necessary for a system for acute heart examinations:

- it is mobile and easy to position close to the heart of the patient for bedside examination
- the flexibility of the camera permits simultaneous use of life-supporting equipment
- data acquisition and the fully 3D iterative reconstruction of the system provide images within 10 minutes from the start of the examination, that means before the patient leaves the emergency room
- the sensitivity, spatial resolution and other performance parameters are similar to stationary SPECT systems

In the present report the hardware and software of the new CARDIOTOM ™ system and validation of its performance are described. Clinical results as well as gated images of a moving heart phantom are presented. Since the ectomographic technique can be used to advantage for other types of examinations, future systems dedicated to other organs will be discussed.

The description of a software platform for nuclear medical image representation, visualization and reconstruction that is implemented in the CARDIOTOM™ system is submitted as a separate contribution to the conference.

Unified software platform for nuclear medical image representation, visualization and reconstruction

I. Valastyán[a,b], D. Bone[c], A. Kerek[a] J. Molnár[b], D. Novák[b]

[a]Royal Institute of Technology, Stockholm, Sweden
[b]Institute of Nuclear Research of the Hungarian Academy of Sciences, Debrecen, Hungary
[c]Karolinska University Hospital, Stockholm, Sweden

A unified software platform has been developed in order to store, process, visualize and reconstruct nuclear medical imaging data sets, especially data acquired by the CARDIOTOM™ mobile tomographic gamma camera system. The platform consists of two toolkits. The unified base toolkit (M-SDK) includes the general pixel and voxel based image representation, geometry and visualization classes. The MCARDIOTOM toolkit, based on the M-SDK, contains the data acquisition modules of the CARDIOTOM™ camera and the optionally connected ECG unit. This toolkit also contains the unified image reconstruction library as well as the applications needed for the CARDIOTOM™ camera calibration, quality control, data acquisition and image presentation.

The platform is implemented in C++, the graphical user interfaces use the QT software library, while the visualization is based on OpenGL.

The M-SDK toolkit contains 6 modules, the CORE contains the timing and base secure memory access classes, the GEOMETRY implements the general 2D and 3D objects, (e.g. point, line, plane, rectangle, triangle, cube) and their related methods (e.g. point-object distance or cross point calculation of an object and a predefined line). The VOXELSTORAGE module implements the different pixel or voxel representation classes (like curve, slice, volume, dynamic slice and dynamic volume) and the axis information which describe the positions of the voxels in the 3D space. The SURFACE module calculates the surface information from a volume or a dynamic volume. The GLVIS module handles the OpenGL based visualization. This module realizes the displaying of primitive items, like slices, curves, histograms, cursors, markers, text on an OpenGL canvas. All item drawing classes are derived from an abstract canvas item which ones can be superposing on the canvas. The MQWIDGETS module provides some useful predefined and configurable canvas layouts (e.g. histogram viewer, single slice viewer, multi slice viewer, orthogonal slice viewer of a volume, dynamic slice viewer). The number and type of canvas items in these viewers can be configured dynamically; items can be added or removed as required.

The MCARDIOTOM toolkit contains the unified iterative image reconstruction module as well as the camera dependent data acquisition, quality control and file input/output modules and application dialogues. The image reconstruction module contains unified abstract classes, methods and tools for a general camera independent iterative image reconstruction algorithm, where the abstract camera model contains all necessary functions for the camera independent image reconstruction. The camera dependent geometrical data are implemented in inherited classes and these have been used during the system matrix calculation and reconstruction processes. The applications provide easy handling of the camera system.

Modeling imaging performance and low contrast detectability in digital mammography.

Spyropoulou V.[1], Kalivas N.[1,2], Gaitanis A.[1,2], Michail C.[1], Panayiotakis G.[1], Kandarakis I.[2]

[1] *Department of Medical Physics, Medical School, University of Patras, 26 500 Patras, Greece*
[2] *Department of Medical Instruments Technology, Technological Educational Institution of Athens, Ag. Spyridonos, Egaleo, 122 10 Athens, Greece*, e-mail: kandarakis@teiath.gr.

Digital x-ray mammography is a modern method for the early detection of breast cancer. The quality of a mammography image depends on various factors, the detector structure and performance being of primary importance. The aim of this work was to develop an analytical model simulating the imaging performance of a new commercially available digital mammography detector. This was achieved within the framework of the linear cascaded systems (LCS) theory. System analysis has allowed the estimation of important image quality metrics such as the Modulation Transfer Function (MTF), the Noise Power Spectrum (NPS) and the Detective Quantum Efficiency (DQE). The detector was an indirect detection system consisting of a large area, 100μm thick, CsI:TI scintillator coupled to an active matrix array of amorphous silicon (a-Si:H) photodiodes combined with thin film transistors (TFT). Pixel size was 100μm, while the active pixel dimension was 70μm. MTF and DQE data were calculated for air kerma conditions of 25, 53, 67 μGy using a 28 kVp Mo-Mo x-ray spectrum. The theoretical results were compared with published experimental data. The deviation between the theoretical and experimental MTF curves was less than 4%, while the DQE differences were found at an acceptable level. The model was also used to estimate system's capability to detect low contrast objects in the breast. It was estimated that, in the breast gland, low contrast structures larger than 170μm can be adequately identified by the above system.

A theoretical model for single-crystal scintillators in the diagnostic energy range.

Petropoulou A.[1], Kalivas N.[1,2], Kandarakis I.[2], Valais I[1,2]. and Panayiotakis G.[1]

[1] *Department of Medical Physics, Medical School, University of Patras, 26 500 Patras, Greece*
[2] *Department of Medical Instruments Technology, Technological Educational Institution of Athens, Ag. Spyridonos, Egaleo, 122 10 Athens, Greece*, e-mail: kandarakis@teiath.gr.

The aim of this study was to develop a theoretical model to examine emission features of single-crystal scintillators under x-ray excitation. The results will be useful in designing hybrid tomographic imaging systems based on a common gamma-ray and x-ray detector (PET/CT or SPECT/CT). The theoretical model can estimates the depth of x-ray absorption within the crystal, the generation and the propagation of the optical photons inside crystal scintillator. The shape of the x-ray spectrum, the site of the optical photon production, its emission angle and the reflection at the crystal scintillator inner surface were taken into account. The model was used to simulate the emission efficiency of a GSO:Ce crystal of finite dimensions: 10x10x10mm. Gd_2SiO_5:Ce (or GSO) is a non-hygroscopic scintillator, with very short decay time, which is used in positron emission tomography (PET) systems. The model was validated against GSO experimental data in the energy range between 110-140kV, employed in x-ray computed tomography (CT) applications. Satisfactory agreement between model and experimental data was obtained for specific values of the optical absorption coefficient $k=0.09746mm^{-1}$. The latter was estimated by taking into account optical transmission data. The variation that came up between model and experimental data was about 1.25%. Furthermore, the efficiency of GSO crystal was theoretically evaluated for various thicknesses of 5, 10, 15, 20, 25mm. The GSO crystal's efficiency was found optimum at 140kV and for 10mm thickness. In conclusion, a theoretical model to predict the efficiency of single crystal scintillators was developed. The model may be used to determine optimum crystal dimensions for use in hybrid imaging systems.

Investigation of two heavy element scintillators by Monte-Carlo methods

Konstantinidis A.[1], Liaparinos P.[1], Panayiotakis G.[1], Kandarakis I.[2]

[1] *Department of Medical Physics, Medical School, University of Patras, 26 500 Patras, Greece*
[2] *Department of Medical Instruments Technology, Technological Educational Institution of Athens, Ag. Spyridonos, Egaleo, 122 10 Athens, Greece*, e-mail: kandarakis@teiath.gr.

The aim of this study was to estimate the influence of K-characteristic radiation on the performance of x-ray scintillating screens containing two heavy elements (90/10 and 50/50 LYSO ($Lu_{1.8}Y_{0.2}SiO_5$ and $LuYSiO_5$ respectively), CsI and $YTaO_4$) by Monte Carlo methods. K-characteristic radiation is produced within materials of at least one heavy (high atomic number) element (e.g. Lu, Y, Cs, I, Ta). This radiation may either be reabsorbed or it may escape the scintillator. In both cases the imaging performance of the scintillator may be affected resulting either in spatial resolution degradation or in emission efficiency decrease. All the aforementioned ~~above~~ scintillators have two heavy elements, thus the K-characteristic radiation of the high-Z element can produce secondary K-characteristic photons on the low-Z element, resulting in further degradation. Scintillator performance was described in terms of the: (a) Probability of generation and absorption of a K-characteristic photon (PKR) and (b) Spatial distribution of K-characteristic radiation at various layers within ~~of~~ the scintillator material. A custom validated Monte Carlo model was used, in order to simulate the transport of K-characteristic radiation within the above scintillator materials. Results showed that, depending on screen thickness (20-100 mg/cm^2) and incident photon energy (20-80 keV) the scintillator's emission efficiency may be significantly reduced and affect spatial or energy resolution.

Comparative evaluation of scintillators under x-ray imaging conditions

Ioannis G. Valais [1,2], Christos Michail[1], Stratos David[1], Anastasios Konstantinidis[1], Dionysis Cavouras[2], Costas D. Nomicos[3], George S. Panayiotakis[1] and Ioannis S. Kandarakis[2]*

[1] Department of Medical Physics, Medical School, University of Patras, 265 00 Patras, Greece
[2] Department of Medical Instruments Technology, Technological Educational Institution of Athens, Ag. Spyridonos, Aigaleo, 122 10 Athens, Greece, e-mail: kandarakis@teiath.gr

The present study is a comparative investigation of the luminescence properties of $(Lu,Y)_2SiO_5$:Ce (LYSO: Ce), Lu_2SiO_5 (LSO: Ce), Gd_2SiO_5: Ce (GSO: Ce) and ($Bi_4Ge_3O_{12}$) BGO single crystal scintillators under x-ray excitation. Results will be of value in designing dual modality tomographic systems (PET/CT, SPECT/CT) based on a common scintillator crystal. All scintillating crystals have dimensions of 10x10x10 cm^3 are non-hygroscopic exhibiting high radiation absorption efficiency in the energy range used in medical imaging applications. The comparative investigation was performed by determining the absolute luminescence efficiency (emitted light flux over incident x-ray exposure) in the range of x-ray energies employed in: (i) general x-ray imaging (40-140 kV, using a W/A x-ray spectrum) and (ii) x-ray mammography imaging (22-49 kV, using a Mo/Mo x-ray spectrum). Additionally, light emission spectra of crystals at various x-ray energies were measured, in order to determine the spectral compatibility to optical photon detectors incorporated in medical imaging systems and the overall efficiency (effective efficiency) of a scintillator-optical detector combination. The light emission performance of LYSO:Ce and LSO:Ce scintillators studied was found very high for x-ray imaging.

Evaluating optical spectral matching of phosphor-photodetector combinations

Kalivas N[1,2], Valais I[2,3]., Costaridou L[2], Kandarakis I[3], Cavouras D[3], Panayiotakis G[2]

[1]*Greek Atomic Energy Commission P.O. BOX 60092, 153 10 Agia Paraskevi, Greece*
[2] *Department of Medical Physics, Medical School, University of Patras, 26 500 Patras, Greece*
[3] *Department of Medical Instruments Technology, Technological Educational Institution of Athens, Ag. Spyridonos, Egaleo, 122 10 Athens, Greece*, e-mail: kandarakis@teiath.gr.

Abstract

Phosphor materials are used in medical X-ray imaging combined with various photodetectors suitable for conventional and digital radiography and fluoroscopy. A prerequisite for these combinations is good optical spectral matching [1], which results in patient dose minimization. In the present work, a recently introduced factor [2], named OGTE, which accounts for optical gain signal-to-noise ratio transfer efficiency, is utilized for the evaluation of various phosphor-photodetector combinations. The phosphor materials studied were Y_2O_3:Eu^{3+}, YVO_4:Eu^{3+}, Gd_2O_2S:Tb, La_2O_2S:Tb, Y_2O_2S:Tb $LaCl_3$:Ce, CdS(In), CdS(In, Te), CdS(Te) HiLight^{TM}.

The optical photon spectrum of the phosphor materials studied was either determined experimentally, or obtained from literature. These phosphors were examined in conjuction with various photodetectors (mainly CMOS and CCD based photodetectors, as well as GaAs and Si) which optical response functions were obtained from literature. No ideal film, providing a perfect OGTE value (OGTE=1) for all phosphors studied, was found. All photocathodes studied exhibited an OGTE value over 0.60 for every phosphor material. Considering digital imaging detectors, numerous combinations exhibited OGTE value above 0.80, contributing to patient dose minimization.

References

1. Giakoumakis GE (1991) Matching factors for various light-source photodetector combinations. Appl Phys A 52:7-9
2. Kalivas N, Costaridou L, Kandarakis I, Cavouras D, Nomicos CD, and Panayiotakis G (2004) Optical gain signal-to-noise ratio transfer efficiency as an index for ranking of phosphor-photodetector combinations used in X-ray medical imaging. Appl Phys A 78:915-919

The influence of software filtering in digital mammography image quality

Spyropoulou V.[1], Michail C.[1], Kandarakis I.[2] , Valais I[1,2], Dimitropoulos N[3]., ,Panayiotakis G.[1]

[1] Department of Medical Physics, Medical School, University of Patras, 26 500 Patras, Greece
[2] Department of Medical Instruments Technology, Technological Educational Institution of Athens,
[3]"Euromedica" Medical Center, Medical Imaging Dept, Vas. Sofias avenue
Ag. Spyridonos, Egaleo, 122 10 Athens, Greece, e-mail: kandarakis@teiath.gr.

Breast cancer is one of the most frequently diagnosed cancers among women. Several techniques have been developed to help in the early detection of breast cancer such as conventional and digital x-ray mammography, positron and single-photon emission mammography, etc. A key advantage in digital mammography is that images can be manipulated as simple computer image files. Thus non-dedicated commercially available image manipulation software can be employed to process and store the images. The image processing tools of the Photoshop (CS 2) software usually incorporate digital filters which may be used to reduce image noise, enhance contrast and increase spatial resolution. However, improving an image quality parameter may result in degradation of another. The aim of this work was to investigate the influence of three sharpening filters, named hereafter sharpen, sharpen more and sharpen edges on image resolution and noise. Image resolution was assessed by means of the Modulation Transfer Function (MTF). MTF was experimentally determined by the Square Wave Response Function (SWRF) method using a Nuclear Associates resolution test pattern (typ-53, Nuclear Associates). The MTF test pattern was irradiated by x-rays on a General Electric Senographe DMR Plus mammographic unit using a Mo/Mo x-ray spectrum at 28 kVp and 10mAs. The x-ray beam was additionally filtered by Perspex slabs of various thicknesses (1, 2, 4 cm) to simulate spectrum alteration by various breasts. The three sharpening filters were then applied on ~~in~~ the raw image data. The MTF was determined via the Coltman formula applied on ~~at~~ the digital images (both raw and filtered) of the bar pattern.. The noise was estimated by means of the coefficient of variation in an area of 100 pixels. It was found that the image filtered by the sharpen edges filter demonstrated higher MTF values for spatial frequencies above 3 cycles/mm. The corresponding coefficient of variation was found 0.864%. In the frequency range between 1 and 3 cycles/mm, the sharpen more filter was found to give higher MTF values. However, the image filtered by the sharpen more filter appeared to be more noisy corresponding to a coefficient of variation of 2.46%. The image filtered by the sharpen filter was poorer in resolution and moderate in noise with a coefficient of variation of 1.38%.In conclusion it was found that the correct use of commercial non-dedicated software on digital mammograms may improve some aspects of image quality.

Optimize ^{18}F-FDG Positive Tumor Volume Delineation in microPET – correlate with autoradiography and histopathology results.

Lin, Kun-Ju[1]; Hsiao, Ing-Tsung[2], Hong, Ji Hong[3]; Lin Chung-Fu[2], Wey, Shiaw-Pyng[2]

[1] Department of Nuclear Medicine, Chang Gung Memorial Hospital, Taiwan

[2] Department of Medical Imaging and Radiological Sciences, Chang Gung University, Taiwan

[3]Department of Radiation Oncology, Chang Gung Memorial Hospital, Taiwan

Background: Recent advanced in microPET scanners enables non-invasive approach to study mouse model of human disease, providing a novel tool to monitor tumor response to therapy over time using metabolic activity within the targets. The lesion size and the localization of the tumor contour play an important role in these investigations. The aim of this study was to apply different methods for tumor volume delineation and compared the resulting volumes and quantification of metabolic activity to histopathology and autoradiography results. **Methods**: Tumor cells (TRAMP-C1) were injected to the thigh of C57BL/6J mice and grew to 5~10 mm before experiments. Twenty FDG microPET scans were performed and tumor sections were acquired immediately after the scan. Quantitative autoradiography was measured and the intensity was converted to kBq/mL for comparison. Simulated PET section images were generated from the quantitative autoradiography after applying a smooth Gaussian filter. Tumor volume determined by isocontour of 30% maximum intensity (I_{30}), a fixed intensity ($I_{0.2}$), and combination function of mean tumor and muscular background intensities (I_{mb}) were used for comparison (Fig 1). The resulting tumor volume and total metabolic activity within the targets were compared to the manual drawing (I_m) method with the help of histopathology and autoradiography results. **Results**: 11/20 tumors showed homogenous distribution of F-18 FDG radioactivity. Among them, the mean intensity of simulated PET images were similar to the microPET results ($r^2 = 0.89$). The metabolic activity and tumor volume determined by $I_{0.2}$, and I_{mb} correlate well to the I_m, whereas the I_{30} did not. Inhomogeneous F-18 FDG accumulation and tumor necrosis was demonstrated in the other 9 tumors. In these cases, the I_{mb} method gives the closest measurement as compared to I_m results. **Conclusion**: Different isocontour methods result in different tumor volume measurement especially for those inhomogenous tumor lesions. Isocontour determined by delicate function derived from mean tumor and background intensities can be used for longitudinal monitoring tumor growth.

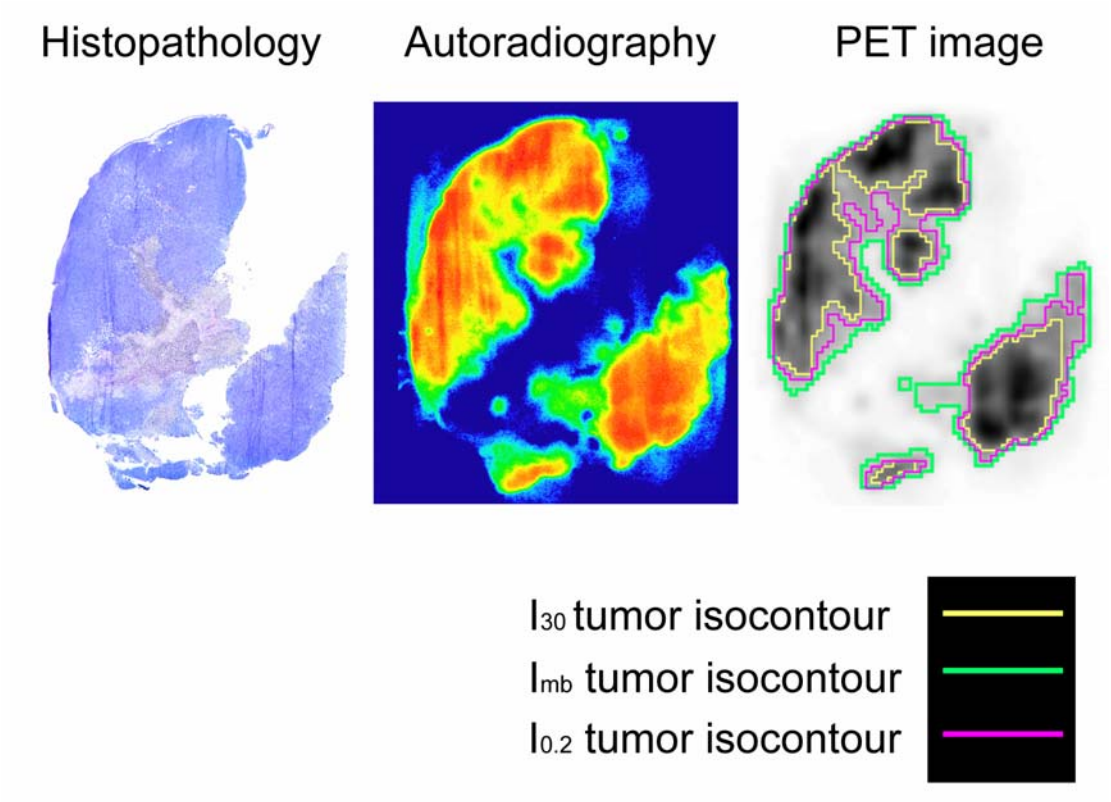
Histopathology
Autoradiography
PET image
I_{30} tumor isocontour
I_{mb} tumor isocontour
$I_{0.2}$ tumor isocontour

QUANTIFYING HETEROGENEITY OF LESION UPTAKE IN DYNAMIC CONTRAST ENHANCED MRI FOR BREAST CANCER DIAGNOSIS

KARAHALIOU A.[1], VASSIOU K.[2], SKIADOPOULOS S.[1], KANAVOU D.[3], YIAKOYMELOS A.[1], COSTARIDOU L.[1]

[1]Department of Medical Physics, School of Medicine, University of Patras, 26500 Patras, Greece
[2]Department of Anatomy, School of Medicine, University of Thessaly, 41222 Larissa, Greece
[3]Department of Radiology, School of Medicine, University of Thessaly, 41222 Larissa, Greece

costarid@upatras.gr

Dynamic Contrast-Enhanced Magnetic Resonance Imaging (DCE-MRI) is a significant complement to mammography, increasingly used for the detection and diagnosis of breast cancer. Nevertheless, its specificity in distinguishing malignant from benign lesions is highly varied, mainly due to lack of standardized criteria in the assessment of contrast kinetics [1]. In clinical practice, assessment of contrast kinetics is based on the selection of a region of interest (ROI) within the lesion, providing average kinetics. Pixel-based methods have been developed to map more accurately contrast uptake [2-5]. Texture analysis on postcontrast images has been proposed to quantify heterogeneity of contrast uptake and discriminate benign from malignant lesions [6]. In this study, to quantify heterogeneity, texture analysis is performed on three individual kinetic feature maps and used for lesion characterization.

A total of 55 women with 57 histologically verified breast lesions (27 benign, 30 malignant) were included in the study. A coronal 3D T1-weighted spoiled gradient echo sequence was acquired before and five times after intravenous administration of 0.2mmol/kg of gadopenate dimeglumine. For each lesion, the most representative slice was selected by an experienced radiologist. On a selected slice contrast kinetic curves were calculated pixel-wise and subsequently fitted with a bilinear model [5]. From each modeled curve three parameters were calculated (wash out, time to peak enhancement and peak enhancement), yielding three individual kinetic feature maps. Kinetic maps were used to define an HSV colour space as well as to quantify uptake heterogeneity. Texture analysis was applied on individual kinetic feature maps and restricted to a region delineated by the lesion contrast uptake boundary on the HSV colored image. Boundary delineation was obtained by means of thresholding and morphological operations applied on the gradient of an HSV ROI containing the lesion. 32 first and second order statistics features [7] were extracted from each individual kinetic feature maps. The discriminating ability of the three texture feature sets was investigated using a Probabilistic Neural Network classifier. An additional classification scheme was implemented by combining classification outputs of the most discriminating feature sets, with a majority voting rule. Receiver Operating Characteristics (ROC) analysis was employed to evaluate performance of the individual feature sets and of the combined scheme.

Among individual feature sets the best performance was achieved by features extracted from the wash out map providing an area under ROC curve of 0.90 ± 0.04. The combined scheme outperformed statistically significant individual feature sets ($p<0.05$), achieving an area under ROC curve of 0.98 ± 0.01.

Texture analysis can efficiently quantify heterogeneity of contrast uptake in breast lesions and may contribute to computer assisted tissue characterization.

This work is supported by the Karatheodory Programme (C.183) of the University of Patras, Greece.

1. S.C. Rankin, “MRI of the breast”, *Br. J. Radiol.*, 73:806-818, 2000.
2. H. Degani, V. Gusis, D. Weinstein, S. Fields, and S. Strano, “Mapping pathophysiological features of breast tumors by MRI at high spatial resolution”, *Nature Medicine*, 3:780-782, 1997.
3. A.T. Agoston, B.L. Daniel, R.J. Herfkens, D.M. Ikeda, R.L. Birdwell, S.G. Heiss, and A.M. Sawyer- Glover, “Intensity-modulated parametric mapping for simultaneous display of rapid dynamic and high spatial-resolution breast MR imaging data”, *RadioGraphics*, 21:217-226, 2001.
4. F. Pediconi, C. Catalano, F. Venditti, M. Ercolani, L. Carotenuto, S. Padula et al. “Color-coded automated signal intensity curves for detection and characterization of breast lesions: preliminary evaluation of a new software package for integrated magnetic resonance-based breast imaging”, *Invest. Radiol.*, 40:448-457, 2005.
5. Mehnert, E. Bengtsson, K. McMahon, D.Kennedy, S.Wilson, and S. Crozier “Visualisation of the pattern of contrast enhancement in dynamic breast MRI”, *in Proc. APRS Workshop in Digital Image Computing*, WDIC2005, B. Lovell, A. Maeder (eds.), February 2005, Brisbane, Australia.
6. P. Gibbs and L.W. Turnbull, “Textural analysis of Contrast-Enhanced MR Images of the Breast”, *Magn. Reson. Med*., 50:92-98, 2003.
7. R.M. Haralick, K. Shanmugam, I. Dinstein, “Textural features for image classification”, *IEEE Trans. Syst. Man. Cybern.*, SMC-3:610-621, 1973.

Tumor-bearing mice imaging by using a high-throughput positron imager system with planar tomography reconstruction

Meei-Ling Jan [1,*] , Yu-Ching Ni[1], Chen-Yu Liu[1], Zhi-Kun Lin[1], Mei-Hsiu Liau[1], T. Yamashita[3], Norihisa Tsurumi [2], Sammy Chen[3], Lie-Hang Shen[1]

[1] Institute of Nuclear Energy Research, Longtan 325, Taiwan, ROC
[2] Electron Tube Division, Hamamatsu Photonics K.K., Japan
[3] Central Research Laboratory, Hamamatsu Photonics K.K., Japan

Purpose: We have developed a planar tomography method to reconstruct 3D images from 2D acquired data. The reconstruction method was performed on tumor-bearing mice imaging by using a high throughput positron imager system. It is proved that the two-layer positioned mice imaging could at least double the throughput rate. Image quality and semi-quantitation of tumors were compared with those of one-layer positioned mice imaging. Effect of Detector-to-detector distance on the image quality was evaluated also.

Methods: A positron imager system PPIS-4800 (Hamamatsu Photonics K.K., Japan) with two large planar detector heads (120.8 mm x 186.8 mm) was used for acquiring animal projection data. The PPIS-4800 was designed to provide high resolution, and high throughput measurement capability for small animal experiments. To break through limitations of focal plane imaging, a planar tomography reconstruction was performed to provide quasi-tomographic images.

Male BALB/cJ mice were subcutaneously inoculated with colon carcinoma cells in the right legs. The mice were scanned by PPIS-4800 with wide- coincidence mode after 10 days of tumor cell inoculation. The mice injected with F-18-FDG (~ 3.7×10^6 Bq) were placed at z=0 cm for scan to evaluate the effect of detector-to-detector distance, and for the experiments of one-layer positioned mice imaging. As for two-layer positioned mice imaging, two mice placed on the z=0 cm plane, and z=-5 cm plane were scanned simultaneously.

Results: The results of quasi-tomographic images reveal that scanned mice could be placed on the off focal plane without blurring the images. It also shows the scan time was 5 times shorten without sacrificing the image quality if only the 300 mm detector-to-detector distance (DD) decreased to 120 mm. Quasi-tomographic images clearly show slices with only a mouse on each even for the two-layer positioned mice were scanned simultaneously. That means to double the scanned mice at a time is possible.

Conclusion: Using planar tomography to obtain quasi-tomographic images is able to speed up the throughput rate of a dual-head positron imager by decreasing the detector-to-detector distance and by doubling the number of scanned mice.

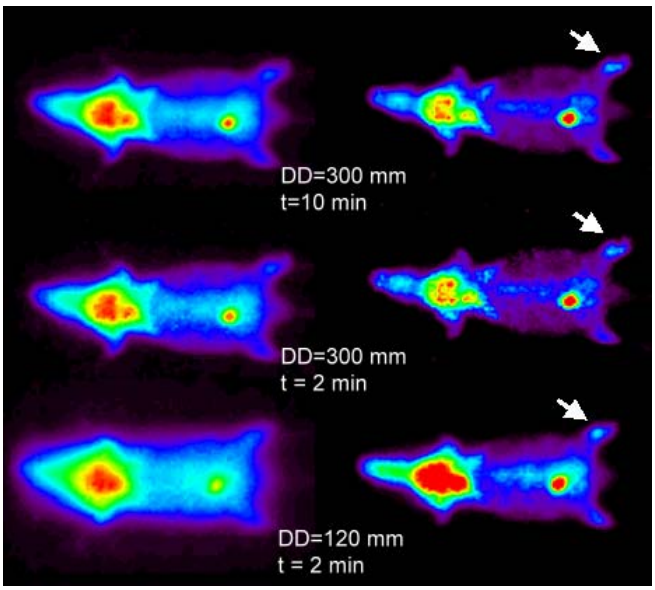

Fig. 1: (Left) original focal plane images, (Right) planar tomographic images of tumor-bearing mice imaging. The bottom right image shows good quality although the scan time was decreased.

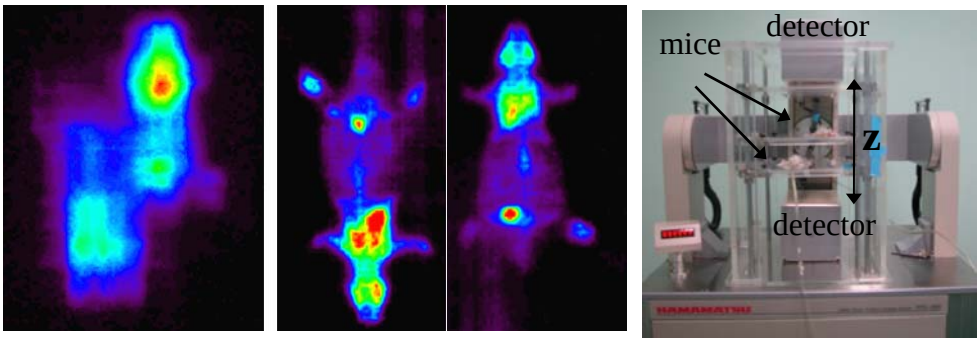

Fig. 2: Results of two-layer positioned mice imaging, (left) original focal plane images, (middle) planar tomographic images. One mouse was placed on z=0 cm plane, and the other mouse was placed on z=-5 cm plane as the photo shows (right). Two mice were scanned simultaneously.

Name of participant: Meei-Ling Jan
Affiliation: Radiation application Center, Institute of Nuclear Energy Research
Address: No. 1000, Wenhua Rd., Jiaan Village, Longtan Township
Taoyuan County, 32546, Taiwan, ROC
Title:Associated Researcher
Oral or Poster Contribution: Poster

Changes of regional cerebral flow when playing a 3D platform video game using voxel-by-voxel analysis

Bang-Hung Yang[1,2], Yuan-Hwa Chou[3,4] , Jyh-Cheng Chen[2,5],Tung-Ping Su[3,4], Shyh-Jen Wang[1,3*]

[1]Department of Nuclear Medicine, Taipei Veterans General Hospital, Taiwan.

[2] Departments of Biomedical Imaging and Radiological Sciences, National Yang-Ming University Taipei, Taiwan.

[3]National Yang-Ming University Medical School, Taipei, Taiwan.

[4]Department of Psychiatry, Taipei Veterans General Hospital, Taipei, Taiwan

[5]Taipei City Hospital, Department of Education and Research, Taipei, Taiwan

Abstract

Objective: Video game playing is one of the most popular pastimes in modern life, which involves stimuli, and needs various cognitive functions. There have been only a few studies examining the biological effects of video games on brain activity, especially in 3D platform video game. The Tc-99m ethyl cysteinate dimer (ECD) has high in vitro stability and rapid in vivo blood clearance. Tc-99m ECD is reliable tracer for use in quantifying regional cerebral flow. The purpose of this study was to evaluate the changes of playing video game on regional cerebral flow using ECD brain SPECT study. **Material and Methods:** There were twenty-four healthy volunteers in this study (fourteen males, mean age, 24.7 ±5.2y; ten female, 24.1±4.9y).Subjects were not included in until they had been interviewed by psychiatric doctor. In the first examination, each subject would take a rest in quiet and dimly environment for twenty minutes before ^{99m}Tc ECD injection. And then each subject would play the video game “Super Mario 64” on Nintendo 64 device for thirty minutes before ^{99m}Tc ECD injection in the second examination. SPECT imaging was performed at 30 minutes after injection of 740 MBq of ^{99m}Tc-ECD according to routine regional cerebral flow (rCBF) protocol in clinical. Two examinations were performed on each individual at least about 1 week apart. Images were then transformed into standard stereotactic space. All scans were statistically analyzed using statistical parametric mapping 2 (SPM 2) in cluster-level and statistical model of paired t-test was applied to compare the variation of rCBF distribution between first and second scans from each individual. The variations of rCBF distribution were significant if the Z-score was higher than 3.48 and the voxel size bigger than 100. **Results:** According to the result of paired t-test on SPM 2, there were significant changes on rCBF between two examinations of each individual. We found that the distribution of rCBF decreased in left superior frontal gyrus, Brodmann area 8 and 9. Increasing area was in bilateral cerebrum occipital lobe Brodmann area 18 and 19, left cerebrum gray matter of precuneus Brodmann area 31, and right cerebrum fusiform gyrus of temporal lobe Brodmann area 20, after each subject playing video game. **Conclusion:** Resting frontal, temporal, and occipital rCBF is significantly changed with the stimulation from playing video game.

Key words: video game; ^{99m}Tc-ECD SPECT; voxel-by-voxel; rCBF

Development of an LYSO Based Gamma Camera for Positron and Scinti-mammography

H. C. Liang[1,2], M. L. Jan[1,*], W. C. Lin[1], S. F. Yu[1], J. L. Su[2], L. H. Shen[1]
[1] Institute of Nuclear Energy Research, Physics Division, Longtan, Taiwan ROC
[2] Department of Biomedical Engineering, Chung-Yuan Christian University, Taoyuan, Taiwan ROC

Purpose: For construction of a prototype mammography scanner for both positron emission and scinti-mammography, a gamma head with an effective area of at least 8×8 cm^2 is required. In this research a gamma head with larger and successive detective area was developed and constructed by combination of multiple PSPMTs with light sharing techniques applied.

Methods: The gamma camera was composed of LYSO fine pixels and H8500 PSPMTs (HAMAMATSU). Borosilicate glasses of 2 and 3 mm were chosen as light guides for the scintillation light spreading in the crossover regions. Crystal pixels of size 1.5, 1.8 and 2.0 mm were tested to find out the minimum distinguishable size. Then according to the results, a larger crystal matrix was built. The performances in high and low gamma bands of the installed camera were measured. The influences of crossover regions and light guides on the imaging will be evaluated, especially the light loss behaviors. And also the feasibility for single photon imaging will be verified, because of the drawbacks from the ^{176}Lu spontaneous radiations of the scintillation material itself.

Results: According to the test results of practical pixel size and useful area, a crystal matrix composed of 2.0 mm pixels and actual dimension 90×90 mm^2 was built. The analyzed mean performances of the gamma camera are listed in table 1. These indices show its good capability of pixel identification in positron and single photon imaging. The results of light loss analysis show that the light loss fraction from region 1 (PMT effective area) to region 2 (2-PMTs junction area) and region 3 (4-PMTs junction area) are 37% and 61% respectively. The results of more precise light loss analysis are arranged in table 2. Refer to the table, the loss fraction in region 3 of almost 50% means the light sharing of 2 mm glass is not wide enough. During the analysis of light loss behavior, it was found that a model composed of Gaussian functions can similarly describe the distribution of the loss fraction. Therefore a compensator based on the set of Gaussian model was built and thus flood images of more uniform and better pixel identification were obtained. In the background measurements, a 10M counts acquisition was made, and a specific count rate of 40 cps/cm^3 was obtained. When an energy window (122keV±25%) was applied, the background count rate became 5 cps/cm^3 remaining. In the single photon collimated (a parallel-hole collimator of 2mm aperture and 15mm high) imaging tests, the weak source (7×0.5cm^2, 200μCi/cm^2) resulted an average signal count rate of over 3 times higher than that of backgrounds. And thus a meaningful single photon collimated image did show.

Conclusion: Although light sharing techniques make the larger and successive imaging area realize, they physically degrade imager performances, especially in the crossover region. Even so this area extended camera still shows good imaging abilities in both high and low gamma energy bands. And even under the influences of ^{176}Lu nature background, it shows a meaningful count rate in collimated conditions. It is concluded that this LYSO based gamma camera is potential for both positron emission and

scinti-mammography applications.

Table 1. Mean imaging performances

Gamma energy (keV)	511	122
Pixel width (mm, FWHM)	0.87 ± 0.22	1.32 ± 0.25
Peak-to-valley ratio	4.7 ± 1.6	3.4 ± 1.5
Energy resolution (%)	16.3 ± 3.8	30.5 ± 5.5
Uniformity (%)	67 ± 11	57 ± 8

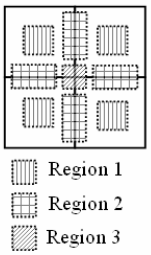

Table 2. Energy loss fraction (%) compared to the rims of region 1

Gamma energy (keV)	511	122
Rims of region 2	7	8
Center of region 2	24	26
Whole region 2	13	14
Whole region 3	47	47

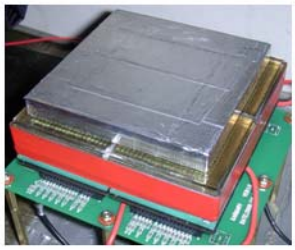

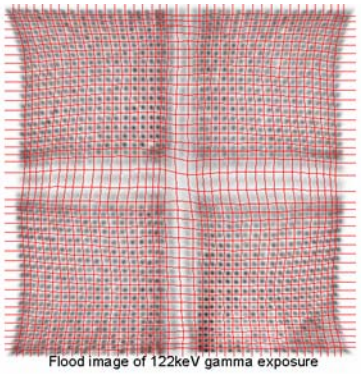

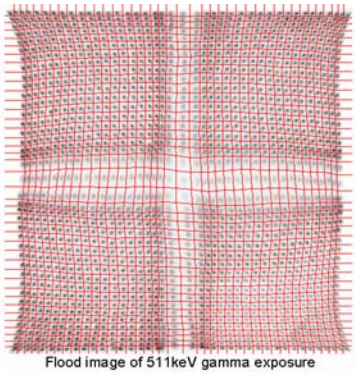

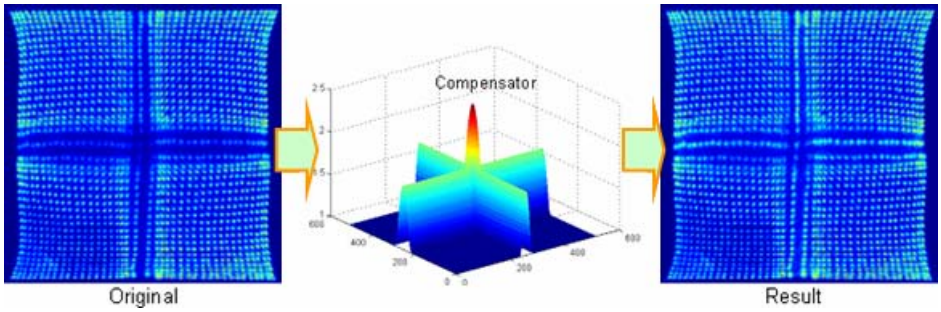

Name of participant: Meei-Ling Jan

Affiliation: Radiation application Center, Institute of Nuclear Energy Research

Address: No. 1000, Wenhua Rd., Jiaan Village, Longtan Township

Taoyuan County, 32546, Taiwan, ROC

Title:Associated Researcher

Oral or Poster Contribution: Poster

A Quantitative Method for Monitoring Pulmonary Fibrosis Rats by Micro-CT 3D Images

U.T. Fang, M.L. Jan*, C.H. Yeh, H.C. Lu, H.T. Tsai, L.T. Huang, L.H. Shen
Institute of Nuclear Energy Research, Longtan 325, Taiwan, ROC

Purpose: We developed a 3D quantitative method to monitor the process of lung injury for small animal model.

Methods: 32 Sprague-Dawley rats divided into four groups were given aqueous solution of Paraquat via oral single dosage. The study of tracing pulmonary-fibrosis injury of rats were performed by using a home-made cone-beam micro-CT. The system has 2 lp/mm spatial resolution. The voxel volume and image size are 100×100 ×100 μm^3 and 512×512×512, respectively. X-ray source operating at 45 kV and 0.6 mA were performed for animal scans.

The first step of image analysis is to define the thoracic cavity through ribs automatically. Adequate parameters were chosen to exclude the ribs from the selected regions, and then to analyze the volume histogram inside the ribcages. The 3D quantitative technique is to segment air and soft tissue, and to quantify the volume variance of lung's air proportion.

Results: After monitoring the rats for 28 days, the air-volume ratios of rats' lung reduce average 21%, 33%, and 43% for low, middle, and high dosage groups respectively. Further details of the effect of dosage and the staging of the lung lesions will be discussed.

Conclusion: Using micro-CT images with the proposal quantitative method to monitor pulmonary-fibrosis injury of rat model could be achieved. It could offer more objective results and also decrease individual differences.

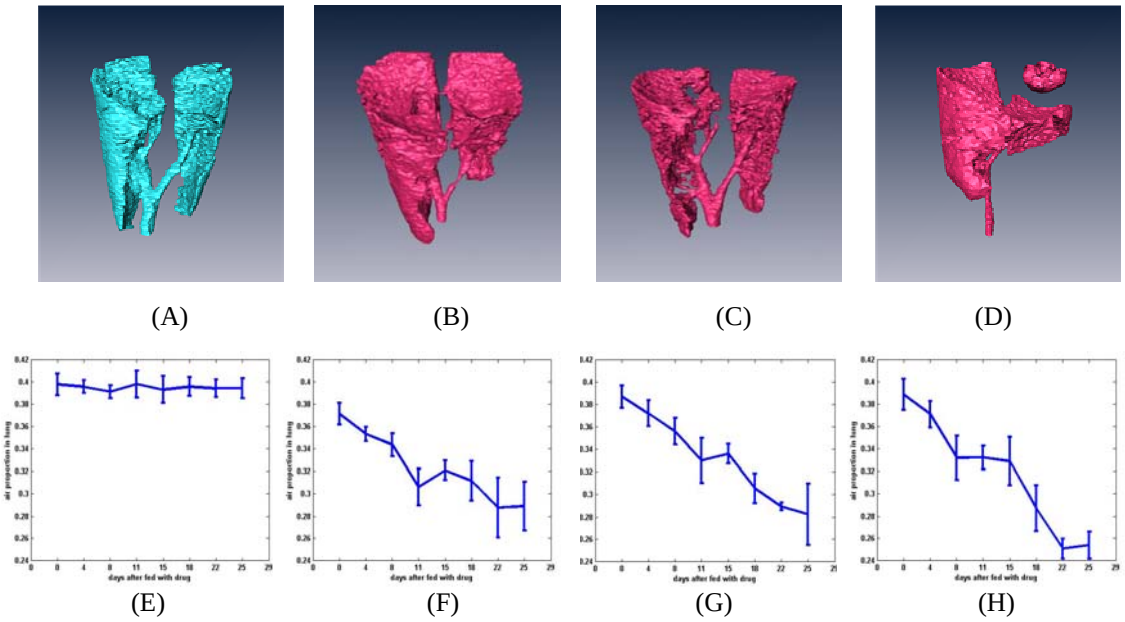

(A) (B) (C) (D)

(E) (F) (G) (H)

Figure: (A), (B), (C), (D) show the 3D lung structure of typical rats under none, low, meddle, and high dosage of Paraquat administration, respectively. (E), (F), (G), (H) show the corresponding quantitative results.

Name of participant: Meei-Ling Jan
Affiliation: Radiation application Center, Institute of Nuclear Energy Research
Address: No. 1000, Wenhua Rd., Jiaan Village, Longtan Township
Taoyuan County, 32546, Taiwan, ROC
Title:Associated Researcher
Oral or Poster Contribution: Poster

Improving the reconstruction of Yttrium-90 Bremsstrahlung images using Monte Carlo based reconstruction

Erwann Rault, Stefaan Vandenberghe, Steven Staelens, and Ignace Lemahieu

ELIS Department, MEDISIP, Ghent University-IBBT-IBiTech, De Pintelaan 185 Block B, B-9000 Ghent, Belgium

Yttrium-90 (Y90) is a promising isotope for radionuclide therapy. Its beta- emission allows for an optimized dose deposition but its lack of gamma emission is complicating the task of imaging for a personalized dosimetry. Bremsstrahlung of the emitted electrons generates however a continuous spectrum of gamma rays that can be used for imaging. A previous study, focused on the history of the photons arriving on the detector, showed the importance of using a low energy window (50-150keV) for limiting the proportion of contamination in the image. This work aims to improve the reconstruction of Y90 bremsstrahlung images using Monte Carlo modelling.

Methods: Bremsstrahlung emission of Y90 was simulated with the GATE (GEANT4 Application for Tomographic Emission) package. Instead of following the electrons emitted by the Y90 source (less than 10% of them will emit a bremsstrahlung photon), the position of the emission and the energy of the bremsstrahlung photons were recorded using a modified version of GATE. A new fast generator of bremsstrahlung photons was implemented in GATE using this new kernel.

The first step of the reconstruction is focused on correcting the sinogram of the scatter in the phantom. Regarding the continuous energy distribution of the photons emitted from bremsstrahlung, the use of energy windows (as usually done in SPECT) seems difficult. Therefore, a method based on the tails of the distribution outside the object was chosen.

A system matrix of the bremsstrahlung photons from Y90 on a SPECT Philips Axis camera with a ME collimator has been simulated in Gate. Penetration in the collimator, detector blurring and extrinsic resolution were incorporated in the MLEM algorithm within both forward and back projections.

Images of a Jaszczak phantom were reconstructed with this method and compared to images made with a simple MLEM algorithm. The comparison was based on two parameters: the contrast recovery and the noise.

Results and Discussions: Results (Fig.1) show a reasonable accordance between the generation of bremsstrahlung photons with the kernel and with the simulation of the Y90 beta emission. The small deviations in the PSF ($< 5\%$) and in the spectrum ($< 9\%$) can be explained by the distribution angle of the electrons which is not included in our fast simulations.

The results obtained with the background substraction and the Monte Carlo reconstruction technique (Fig.2) showed an improvement of 72% in contrast compared to the results obtained with a simple MLEM algorithm. The noise is also significantly reduced (from previously 0.667 to 0.404).

Conclusions: In this study, we showed an accurate technique for reconstructing bremsstrahlung images. This method, based on a scatter removal by fitting to the tails of the distribution outside the object, and a resolution modeling of the camera, can improve the contrast of 72% while reducing the noise of 39%.

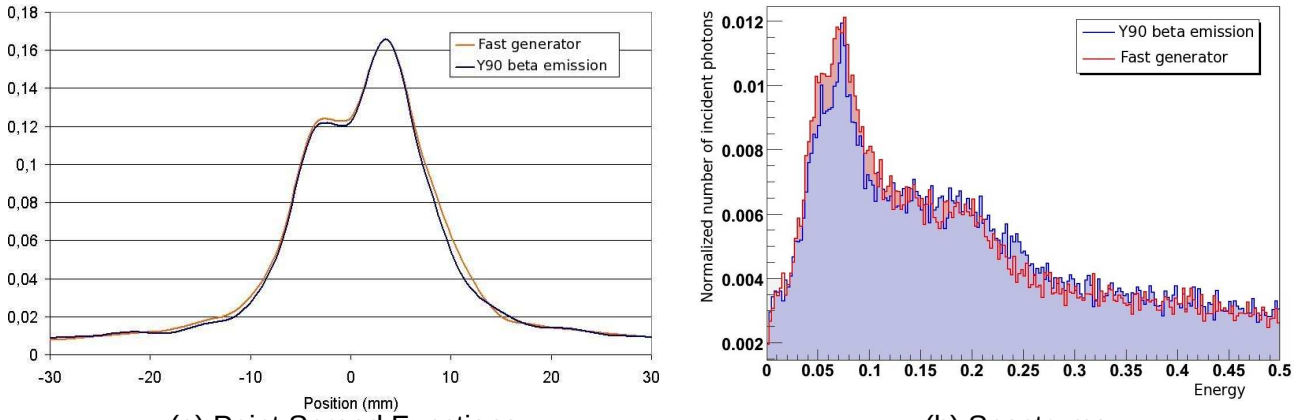

(a) Point Spread Functions (b) Spectrums

***Fig.1**: Comparison of the Point Spread Functions (a) and the Spectrums (b) obtained with the fast generator of Bremsstrahlung photons and the simulation of the Y90 beta emission.*

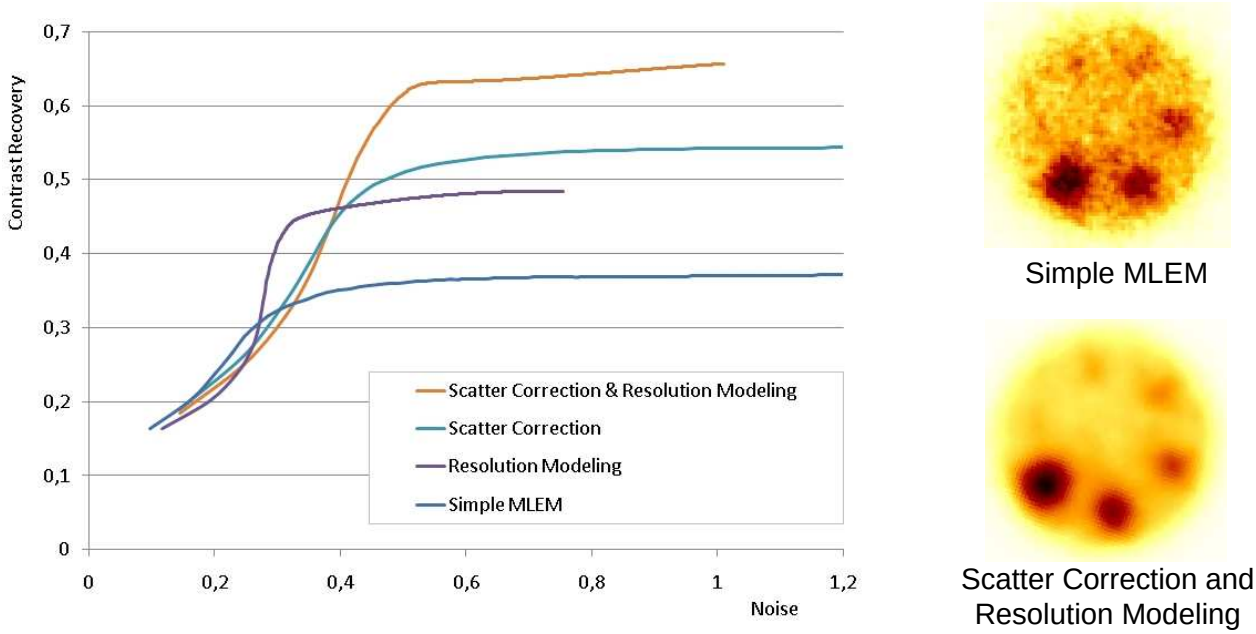

***Fig.2**: Comparison of the Contrast Recovery Curves obtained with the different reconstruction techniques investigated in this study. The images of the jaczszak phantom are shown on the right.*

Improvement of quantitative micro-PET images of the rat brains using 3D deconvolution methods

Fan-Pin Tseng, Meei-Ling Jan, Yu-Ting Fang, Zhi-Kun Lin, Lie-Hang Shen
Institute of Nuclear Energy Research, Longtan 325, Taiwan, ROC

Small-animal micro-PET scanning is increasingly used in murine models of human diseases for the ability to conduct both functional and molecular imaging *in vivo* without sacrificing animals. Usually body weights of small animals, such as rats and mice, are ~300g and ~25 g respectively, therefore higher spatial resolution is required for small animal imaging. The spatial resolution of micro-PET is between 1.0 mm ~ 2.0 mm currently, which is far from the investigators' expectation - the order of autoradiography. In this work, image restoration was used to improve spatial resolution of the microPET images, and to recover the quantitation of rat brain radioactivity-uptake ratios on images.

The microPET images of rats brains with 2-deoxy-2-[18F] fluoro-D-glucose (^{18}F-FDG) uptake abnormal were applied to verify the performances of the three dimensional deconvolution methods. The Sprague-Dawley rats after surgery were injected with 0.2 mCi of ^{18}F-FDG via tail vein and were scanned by Siemens Concorde microPET R4. 3D MAP algorithm was selected to reconstruct images from singrams. The three dimensional degraded function of microPET R4 was simulated by experience. Several directed methods and iterative restoration algorithms, such as Inverse Filter, Wiener Filter, Constrained Least Squares Filter, and Lucy Richardson, were used together with the degraded function to de-blur the rat brain images. *Ex vivo* autoradiography of rat brain were measured with a FUJIFILM FLA-5000 IP Reader. The results of autoradiography is to confirm the uptake of ^{18}F-FDG in the regions of left brain and the right brain were significantly different after surgery. The regions of interest (ROIs) of left inferior colliculus and right inferior colliculus were drawn on the recovered and original microPET images. Then the radioactivity-uptake ratios of left inferior colliculus divided by right inferior colliculus were calculated.

After deconvolution processing, the rat brain images are with better contrast and spatial resolution. The average recovery coefficient after deconvolution is improved 25% compared with that of original images.

From the comparison of deconvolution methods applied on the ^{18}F-FDG rat brain microPET image, the Lucy Richardson algorithm shows the best result than other methods, though the computing speed is the slowest. It is concluded also the recovered effects by iterative methods are better than the directed method with

carefully selected stop criterion.

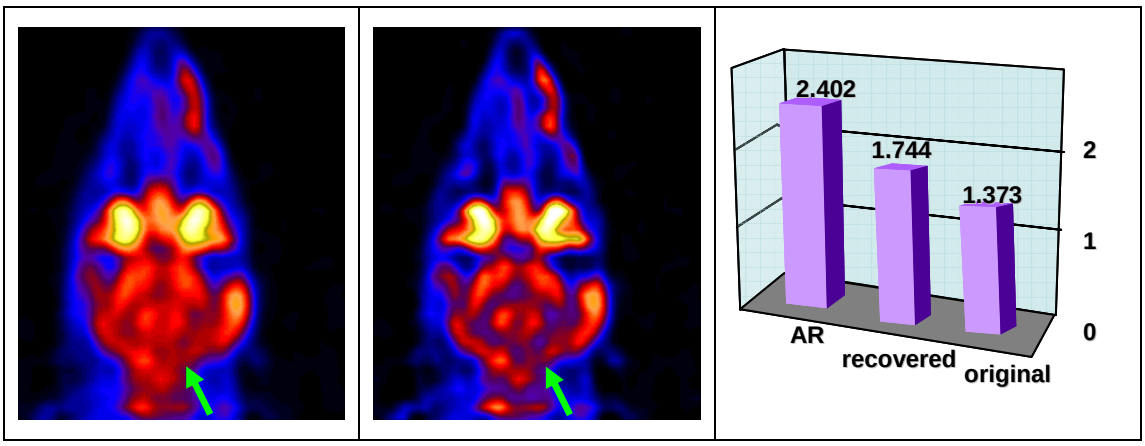

Figure.1. A typical original rat brain image (Coronal view)
Figure.2. A typical Restored rat brain image by three dimensional Wiener Filter (Coronal view)
Figure.3. The radioactivity-uptake ratios of left inferior colliculus to right inferior colliculus from AR (autoradiography), original and recovered images.

Name of participant: Meei-Ling Jan
Affiliation: Radiation application Center, Institute of Nuclear Energy Research
Address: No. 1000, Wenhua Rd., Jiaan Village, Longtan Township
Taoyuan County, 32546, Taiwan, ROC
Title:Associated Researcher
Oral or Poster Contribution: Poster

POST-INJECTION TRANSMISSION IMAGING FOR ATTENUATION CORRECTION ON A MICROPET SCANNER

Jonathan P. J. Carney and Brian J. Lopresti

P.E.T. Facility, Department of Radiology, University of Pittsburgh,
Pittsburgh, Pennsylvania 15260, U.S.A.

In most non-human primate MicroPET neuroimaging studies at our institution, short-lived radiopharmaceuticals labeled with C-11 are used, such that Co-57 singles-based transmission imaging for the purposes of attenuation correction is performed prior to the injection of the positron-emission-tomography (PET) radiopharmaceutical. However, in cocaine addiction studies assessing cognitive task performance, for example, longer-lived F-18 labeled fluorodeoxyglucose (FDG) is used, and is injected prior to the task being performed, and therefore the subsequent imaging session. The use of FDG imaging here is desirable as it provides a record of glucose utilization in the brain during the task without the need for scanning during the task itself. One consequence, however, is that transmission imaging cannot be performed prior to injection, which is seen to lead to significant artifacts in the reconstructed transmission images, the origin of which is attributed to corruption of the true transmission signal by the signal originating in the object (i.e. the injected activity that is taken up). This is problematic as the resulting artifacts preclude segmentation of the transmission images to replace the observed soft tissue and bone attenuation values with their correct 511 keV values – a necessary step for performing attenuation correction of the emission PET data. Though there are levels of injected activity that can be used without adverse affect, these injected activities are more typical of small animal studies, and are exceeded by the activities injected in non-human primate studies.

On the MicroPET scanner, transmission imaging is accomplished by inserting a Co-57 point source into the point source holder, which moves in a corkscrew motion during the transmission acquisition. The level of scatter in significant, such that the resulting transmission images are not quantitative (scatter correction is not performed). However, it is generally possible to perform a reasonable segmentation of the image into bone, soft tissue, and air. The nature of the above-mentioned artifact is such that the segmentation can no longer be reliably performed, motivating the need to correct the transmission acquisition for the corrupting effect of the object activity. In order to estimate this contribution, an additional transmission acquisition is performed without the point source in place. This acquisition must be decay corrected to the time of the actual transmission acquisition before being subtracted from it to get an estimate of the true transmission data (i.e. those that would be obtained in the absence of injected activity in the object). In a phantom experiment the artifact has been replicated and removed in this way for the range of relevant injected activities and higher (up to 2 mCi in the brain), and the method has subsequently been applied successfully to animal studies. We conclude that the appropriate subtraction of a transmission scan without the point source present is adequate to correct this problem, resulting in images that can be segmented for attenuation correction in the usual way. An alternative approach would be to use conventional CT images of the object for attenuation correction in the case that they are available. The CT acquisition would not be sensitive to the injected activity due to the high flux involved. Furthermore, as CT images are quantitative, the segmentation step would not be necessary as a direct transformation to 511 keV values could be implemented, as for clinical PET/CT scanners.

Firsts Results of a New High Resolution PET System for Small Animals using large continuous Scintillating Crystals

J.M. Benlloch (1), V. Carrilero (1), J.V. Catret (2), R. Colom (3), C. Correcher(2), M. Delgado (4), E. Gorospe (4), R. Gadea (3), A.J. González (1), V. Herrero(3), Ch. Lerche (1), C. Mora (1), F.J. Mora(3), C. Morera(2), A. Munar (5), A. Orero (1), N. Pavón (1), M.A. Pozo(4), A. Ros(1), F. Sánchez(1), A. Sebastià(3), A. Soriano(1), L. Urrutia (4), L.F. Vidal (1).

(1) Instituto de Física Corpuscular, Nuevos Edificios de Investigación, Paterna E46071, València, España.
(2) OncoVision company, C/ Benjamin Franklin 12, Edificio CEEI modulo 16, Tecnologic Park of Valencia, 46980 Paterna (València), Spain.
(3) Universitat Politècnica de València, Camino de Vera s/n, 46022 Valencia, Spain.
(4) Instituto Pluridisciplinar, Universidad Complutense de Madrid, Avda. Juan XXIII 1, 28040 Madrid, Spain
(5) Universitat Jaume I, Avda. Vicente Sos Banyat s/n, 12071, Castelló, Spain

We present the first results of a new high resolution PET system for small animal studies. The PET system is based (Figure 1) in a new approach using single large continuous scintillating crystals (LYSO) together with position sensitive photomultipliers (Hammatsu H8500). Enhanced spatial resolution is obtained due to gamma ray depth of interaction detection by means of a modified resistive network, that allows the online analog computation of the depth of interaction as a function of the pulse light width. Spatial resolutions of 1.2 mm are achieved at the center of the FOV (1.7 mm at 2 cm) with a FOV of 80mm (transverse) by 40mm (axial). Energy resolution is 14% with a sensitivity of 4.5%. The use of a small number (8) of large scintillating continuous crystals (50x50 mm^2 area) allows the construction of a highly compact, simple and reliable system. Data readout and control has been implemented through the wide available USB port interface.

Detector design, performance results and calibration procedures (Figure 2), together with first images from *in vivo* trials of mice coronal brain (FDG) and image fusion with MRI for mice with brain ischemia (Figure 3), obtained from a network of collaborating hospitals and research centers will be presented.

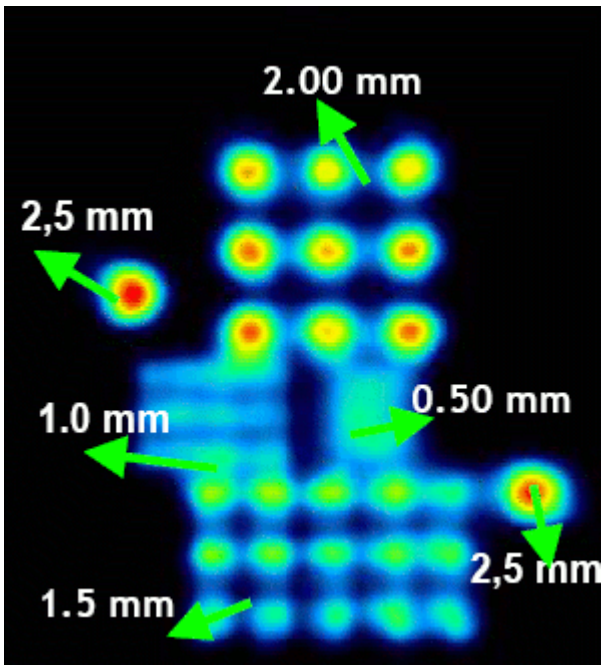
2.00 mm
2,5 mm
1.0 mm
0.50 mm
2,5 mm
1.5 mm

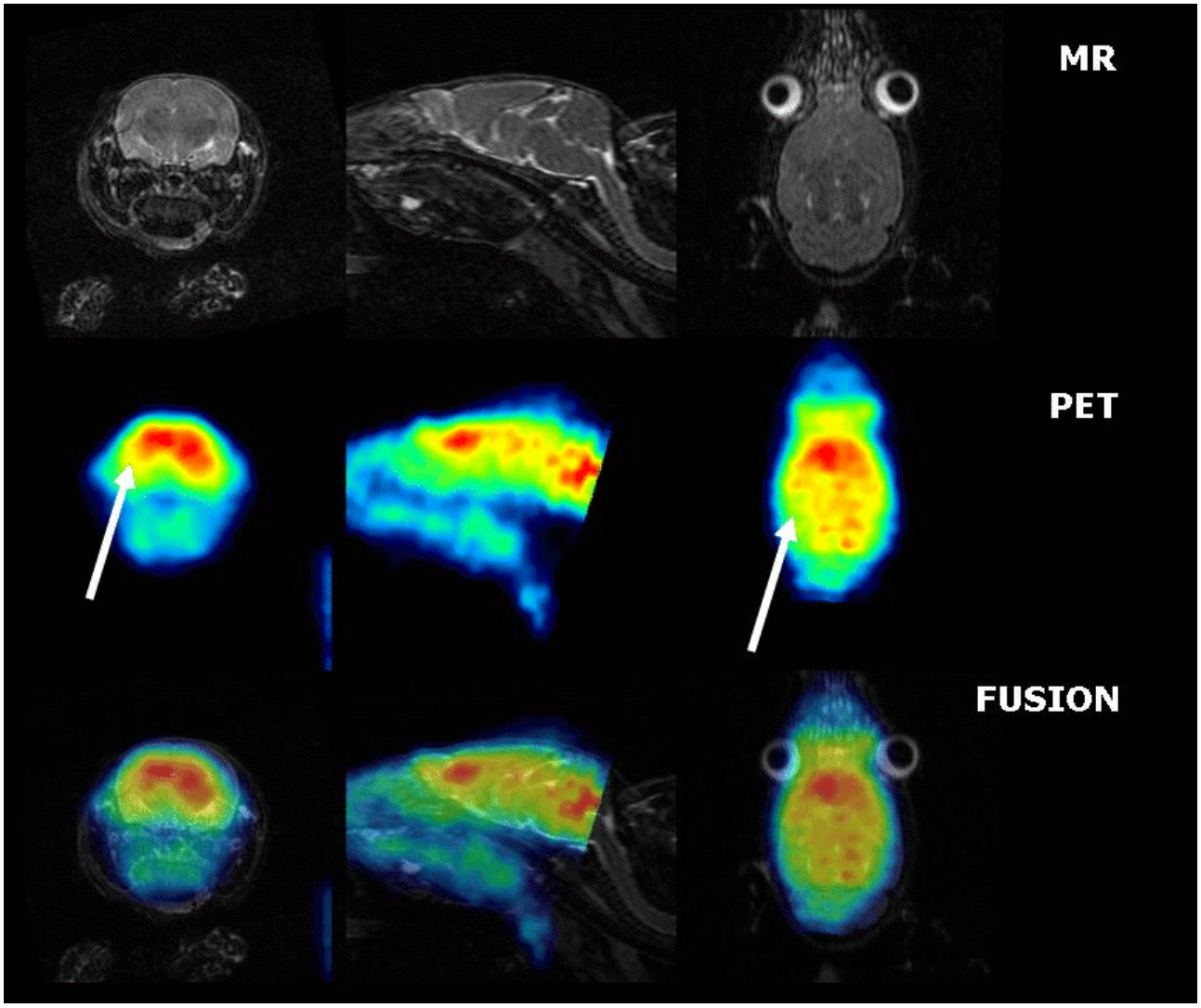
MR
PET
FUSION

Influence of tumor mean atomic number and density on CT attenuation corrected PET: Phantom studies

Houzard Cl[1], Maintas C,[1] Cachin F[2], Mognetti Th[3], Galy G[1], Slosman D[4], Maubland J[2], Itti R[1], Maintas D.[1,5]

[1]Centre de Médecine Nucléaire, GroupeHosptitalierLyon Est, 59Boulevard Pinel 69500Bron France
[2]Nuclear Medicine Dept, Centre jean Perrin, Clermont Ferrand, France

[3]Service de Médecine Nucléaire,Centre Anticanéreux Leon Berard, Lyon, France

[4]Institute of Nuclear Medicine, Clinique Générale Beaulieu, Geneva Switserland

[5]Institute of Radioisotopic Studies Athens Medical Center,Distomou 5-7Maroussi Greece

The use of external positron emitting sources or single photon emitting sources at energies similar to annihilation photons seems to give acceptable results permitting the quantification of PET data. The attenuation correction based on CT data generates artefacts around metallic prostheses, after use of contrast media and in the pulmonary region near calcifications and on dense lesions. In the present phantom study we investigated the density influence of simulated lesions on attenuation correction based on CT transmission data. A cylindrical phantom of 21 cm diameter and 20 cm height, with two compartments, was used. The lower one with cylinders of 4.0 to 10.0 mm to evaluate the resolution of the system and the upper one with 3 pairs of cylindrical vials of 2.6cm diameter and 4.5 cm height, positioned in a distance of 7 cm from the axis of the cylinder in a way to form an hexagon. The first pair of vials was completed with alcohol solution (d= 0.8 g), the second one with water (d= 1.0 g) and the third one with a KJ solution (d= 1.2g). The phantom's lower part was filled with water and the upper with water or polystyrene spheres plus water containing 18-FDG. In one vial of each pair equal activities of 18-FDG were added, giving a ratio of 3 with the environment water or water plus polystyrene. An initial acquisition by spiral CT was followed by one bed acquisition of emission and external source transmission data. After reconstruction by using filtered back projection for CT, iterative OSEM algorithms for PET and scaling and segmentation attenuation correction procedures, proposed by the constructors, we measured on transversal slices the activities of the 6 vials by drawing similar ROIs over the vials and one ROI in the centre of the slices to estimate the background activity. The activities on NAC images for all the 3 tomographs are inversely depended on the density of the liquids due to more intense absorption by the denser material. On CT attenuation corrected slices, in the two first tomographs, the estimated activity in denser material of specific activity 1.2g and elevated atomic number is much higher than the expected due to incorrect attenuation correction procedure. In the third tomograph the CTAC has not the same correctional effect.

Feasibility of iodine contrast enhanced CT-scan during a 18F-fluorodeoxyglucose (18FDG) Positron Emission Tomography (PET-CT) study

C.Houzard [1 2], C.Tychyj [1], I.Morelec [1], F.Ricard [1], P.Got [1], F.Cotton [1], F.Giammarile [1] D.Maintas [3]

[1] PAM d'imagerie Centre hospitalier Lyon-Sud, Lyon,
[2] EA 3738 Lyon,
[3] Institute of Isotopic Studies & PET/CT Unit Athens Medical Centre, Athens.

OBJECTIVE: The aim of this prospective study is to evaluate the feasibility in current clinical practice of contrast enhanced CT-scan for diagnosis purpose, performed during 18FDG PET-CT study with a PET/CT tomograph witch is not affected by the height atomic number and elevated density in previous phantom studies.
METHOD: 25 patients (8 males and 17 females, mean age 46 ±17 years), underwent FDG imaging for lymphoma staging. Studies were performed after i.v. administration of 5.2 MBq/kg of 18FDG (mean blood glucose level 6 ±1.17) using a GEMINI PET-CT camera (PHILIPS MEDICAL SYSTEMS). The TEP scan was performed immediately after the usual low dose CT (lCT). A second CT scan was consequently acquired by using classical diagnostic CT parameters (dCT) and iodinated contrast (100 ml of Iobitridol 350). For each patient, all CT attenuation correction (CTAC) PET images were visually compared. Density in Hounsfield units and maximum Standarized Uptake Value (SUVmax) were then measured on brain (grey matter, white matter), peripheral lung, aorta, muscle, liver, spleen, cortical and medullar bone, and up to 5 specific lymphoma localisations, for a total of 294 measurments.
RESULTS: Visual analysis was similar for the 2 modalities, without discordant interpretation for the pathologic sites. SUVmax means and standard deviation of each organ for lCTAC and dCTAC were comparable. The equation of the fitted multiple linear regression model was: dCT=0.0748191 + 1.17024*lCT with adjusted R-squared statistic of 98.7126% ($p<0.01$).
CONCLUSION: These first results allow the use of injected CT scan, before the PET scan acquisition since objective measures and visual analysis show no difference in lymphoma staging with this PET-CT scan. A great benefit is therefore obtained on diagnostic, logistic and radioprotection purposes.

The metabolic activity of high density tissue in PET is influenced by CT attenuation correction? A phantom simulation study.

C.Maintas[1], Cl.Houzard[2], Th.Mognetti[3], G.Galy[2], D.Slosman[4], J.Maubland[5], R.Itti[2], D.Maintas[1]

[1]Institute of Isotopic Studies, Athens Medical Centre, Greece
[2]Centre de Médecine Nucléaire, Groupe Hosptitalier Lyon Est, 59 Boulevard Pinel 69500 Bron, France
[3]Service de Médecine Nucléaire,Centre Anticanéreux Leon Berard, Lyon, France
[4]Institute of Nuclear Medicine, Clinique Générale Beaulieu, Geneva Switserland
[5]Nuclear Medicine Dept, Centre Jean Perrin, Clermont Ferrand, France

Objectives: To study the influence of tissue's atomic number (Z) and density on CT attenuation correction PET data.
Methods: We used a cylindrical phantom containing 3+3 vials filled with KI and CaCl2 solutions at densities of 1,1, 1,05 and 1,025gr/ml. Equal activities of 18F-FDG added in each vial simulating lesions of different densities and mean atomic number. The environing compartment was filled with "radioactive" water plus polystyrene spheres simulating pulmonary parenchyma with a vial/environment activity ratio of 2 to5. The experiments were performed with three 3 PET/CT scanners of different manufacturers. On transverse slices of the phantom were estimated the activity in counts/pixel on the non- attenuation corrected (NAC) and CT attenuation corrected images (CTAC) along with the density in Hounsfield units on CT images. Image reconstruction and attenuation correction performed using the algorithms proposed by the manufacturers.
Results: With vial/environment ratio 2 on NAC images discrimination between vial and background was difficult due to low contrast. On CTAC images of the first 2 scanners the contrast was increased proportionally with Z and density. With ratio 5 we observed hyperactivity regarding the vials with more elevated Z number denser vials content. This observation was confirmed quantitatively by the histograms expressing the mean activity/pixel of the vials. For the third PET/CT scanner, there was no hyperactivity regarding the denser and of higher Z number vials.
Conclusions: Performing CT attenuation correction of PET data, the density and atomic number of the lesions influence the correctional effect in a way that denser tissue leads to an overcorrection compared to the expected and non corrected ones. The importance of careful studying of non corrected images is revealed if we want to avoid misinterpreting metabolic behavior of more dense lesions. Moreover, the use of CT transmission data does not offer us an fully acceptable attenuation correction with the nowadays PET/CT systems for the correct quantification of PET data. Standardized Uptake Value used as a means for this quantification is strongly influenced by the density and atomic number of tissues and lesions.

Impact of Statistical Region Growing on the Recovery of Standard Uptake Values (SUV) for Small Lesions by using Fourier-Transform-Interpolation, Deconvolution and Statistical Region Growing ("FIDES") to determine SUV.

T. Weitzel[1], T. Krause[1], M. Hofmann[1]

[1]Clinic for Nuclear Medicine, Molecular Imaging and Therapy Group (MIT-Bern,CH), Inselspital, Freiburgstrasse 10, 3010 Bern.

Aim:

The Determination of SUV critically depends on determining the exact volume correlating to a measured activity. In case of small lesions the overall activity can still be measured but the determination of the corresponding volume suffers from both, the limited spatial resolution of the measurement and reconstruction process as well as the sampling artefacts which degrade the determination of a certain volume of interest.

Using highly selective markers like Ga-68-DOTATOC/NOC, PET scans yield high contrast "hot spot" imaging, allowing the detection of very small tumours. The determination of SUV is in this case strongly limited by the partial volume effect.

It was already shown that the determination of SUV can be improved by using a combination of Fourier-transform-interpolation and deconvolution to enhance spatial resolution in order to reduce the partial volume effect. The method of determining a volume according to the measured activity using region growing plays a important role in the process.

The impact of different criteria for statistical region growing on the measurement is discussed.

Methods:

The software is developed in IDL 6.2 (Interactive Data Language) on a Windows XP platform. A modular software approach allows quick parameterization and reconfiguration of the algorithms to evaluate and compare a range of methods. The mathematical interpolation and deconvolution algorithms were adopted to the PET imaging realm using physical boundary conditions to further improve the results. A range of criteria for statistical region growing was tested.

Datasets from phantoms filled with 68-Ga-DOTATOC (recovery calibration) and from patients undergoing Ga-68 DOTATOC PET/CT (Biograph, Siemens, Erlangen) were evaluated.

Results

Statistical region growing criteria taking into account overall properties of the selected region like variance perform better than conventional methods based on local parameters.

Use of "**FIDES**" for improvement of resolution was shown to be feasible using phantom and patient data. In "hot spot images" a full recovery of the signal could be reached for objects with an diameter down to the FWHM of the PET-System.

Clinical studies have to show whether the improved images can be verified by pathological workup.

Contrast improvement of anatomical and metabolic features in PET imaging by using principal component analysis of dynamic PET Data to generate multimodal images.

T. Weitzel[1], T. Krause[1], M. Hofmann[1]

[1]Clinic for Nuclear Medicine, Molecular Imaging and Therapy Group (MIT-Bern,CH), Inselspital, Freiburgstrasse 10, 3010 Bern.

Aim:
Modern PET imaging generates a lot more data than is commonly used to calculate images.
Using dynamic PET results in a 4 dimensional dataset covering a certain measurement volume over time. There exists a variety of methods to analyze the time dependence of activity according to models incorporating metabolic features of certain tissue in order to identify tissues or classify tissue properties.
As opposed to those complex models we evaluated a fast method to enhance image contrast in order to visualize anatomic and metabolic features with maximal contrast without the constriction to any metabolic model. In this context the method aims on image contrast and not on quantitative aspects.

The method uses a 4 dimensional PET dataset covering a certain measurement volume over time.
In a first step the data volume is expanded by interpolation and spatial resolution is enhanced by deconvolution. In a second step a principal components analysis over the time dimension is performed. The first few of the resulting principal components are used as modes to generate a multimodal fused image.

The projection of the modes to colour scales has to take into account basic properties of the human physiology how to interpret colours. By using a suitable projection of the modes to colours we generate an image which clearly shows certain different tissues in different colours.

Methods:

The software is developed in IDL 6.2 (Interactive Data Language) on a Windows XP platform. A modular software approach allows quick parameterization and reconfiguration of the algorithms to evaluate and compare a range of methods. The mathematical interpolation and deconvolution algorithms were adopted to the PET imaging realm using physical boundary conditions to further improve the results.

Results
The calculated images clearly show anatomic features not visible in a conventional image. Furthermore the calculated images show some contrast according to metabolic properties not visible in a conventional image.

The method will have to be extended to calculate pca on a database of multiple PET studies to standardize the results.

A clinical study will have to show whether the improved images have an useful impact on diagnostic routine.

ITBS07 SPONSORS

We gratefully acknowledge the sponsorship of the following Laboratories, Institutions and Companies:

S&B Industrial Minerals S.A.

Greek Ministry of National Education and Religious Affairs